



**Maximum Optimal Asset Utilization in Overhead
Transmission and Low Voltage Distribution Networks**

Saifal Talpur

A thesis submitted to
Auckland University of Technology
in fulfillment of the requirements for the degree of

Doctor of Philosophy (PhD)

September 2020

Supervisor: Professor Tek Tjing Lie

Second Supervisor: Dr. Ramon Zamora

Third Supervisor: Assoc. Prof. Nirmal Kumar Nair

School of Engineering, Computer and Mathematical Sciences

Preface

This thesis has been prepared at School of Engineering, Computer and Mathematical Sciences, Auckland University of Technology, New Zealand to fulfil the requirements for the degree of Doctor of Philosophy (PhD). The work has been carried out during the period from July 2016 to September 2020 under the supervision of Prof. Tek Tjing Lie, Dr. Ramon Zamora and Associate Prof. Nirmal Nair.

The thesis aimed at obtaining the maximum asset utilization in the overhead transmission and the low voltage distribution networks. The research work carried out in this thesis is divided in two parts to consider assets in the transmission and distribution networks. The first part of the thesis deals with overhead transmission lines while the second part is related to distribution transformers. The work carried out in both parts is mentioned in the form of published manuscripts. The link between the work presented in each manuscript and its relevance to the main idea of the thesis is explicitly mentioned at the beginning of each chapter. Each chapter furthermore is dedicated to describing the work presented in the published manuscripts.

Acknowledgments

A PhD journey is full of sacrifices and thus needs support from the loved ones. First of all, I am very grateful to Almighty for providing me the wisdom and patience to complete this piece of work. I acknowledge the support, I received from my PhD supervisors Prof. Tek Tjing Lie, Dr. Ramon Zamora and Associate Prof. Nirmal Nair. In addition, I also acknowledge the moral and emotional support from my parents and siblings throughout my entire PhD journey. Finally, I am grateful to my laboratory colleagues and friends for making my PhD journey wonderful.

Abstract

The growing trend towards renewable energy and e-mobility is behind the congestion in the overhead transmission and low voltage distribution networks. An effective approach towards minimizing the congestion in both networks is to operate the assets to their maximum but optimal utilization. An excessive but reliable electricity flow can minimize congestion, avoid load shedding and maintain reliability in the electricity network.

In the transmission network, congestion across overhead transmission lines is obtained when loading them at their maximum rating, calculated under the assumed and worst weather conditions, thus resulting in bottlenecks and ultimately the limited line flows. The congestion in the distribution network is seen across distribution transformers, mainly in result of growing electric vehicles (EVs) charging load. Distribution transformers when rated under the worst weather conditions may exhibit underutilised loading capacity towards fulfilling the loading demand from EVs.

Asset management in both networks moreover requires the ability of existing assets to transfer the required electricity flow at the minimum cost while attaining the maximum life by operating them to their maximum optimal physical limit. The concept of ‘maximum optimal asset utilization’ is related to operating the existing assets to their maximum but efficient loading capacity to maintain reliability and security with obtaining the minimized congestion and extended asset lifetime. It further assures that the asset operation complies with the design standards as well as addresses both electrical and thermal constraints.

This thesis thus provides ‘maximum optimal asset utilization’ solution to transmission and distribution system operators to manage the asset loading in order to obtain maximum, reliable and efficient capacity utilization. The scope of the thesis is furthermore divided in two parts, where, the first part deals with maximum utilization of overhead transmission lines (OHLs) in the high voltage (HV) transmission network. To obtain the maximum optimal loading across OHLs, the hot-spots were identified with the help of the proposed technique to achieve the reliable line loading.

The second part concentrates on obtaining the maximum capacity utilization across distribution transformers in the low voltage (LV) distribution network. The results indicated that the test DT achieved 25.9% more life with proposed technique under coordinated BEV charging and 51% more life under uncoordinated BEV charging.

Contents

Preface	ii
Acknowledgements	ii
Abstract	iii
Declaration	v
Chapter 1: Introduction	1
1.1 Background	1
1.2 Thesis outline	4
1.3 Thesis contribution	10
1.4 Manuscripts in one thesis.....	11
1.5 References	12
Chapter 2: Weather dependent critical line span identification	15
2.1 Introduction to Manuscript 1	15
2.2 Manuscript 1	16
Chapter 3: Weather dependent electro-thermal line rating	49
3.1 Introduction to Manuscript 2	49
3.2 Manuscript 2	49
Chapter 4: Battery storage-weather dependent transformer rating	83
4.1 Introduction to Manuscript 3	83
4.2 Manuscript 3	83
Chapter 5: Demand response with smart charging in the LV network	110
5.1 Introduction to Manuscript 4	110
5.2 Manuscript 4	110
Chapter 6: Conclusions and future work	126
6.1 Conclusions	126
6.2 Future work	129

Declaration

I hereby declare that the work presented in this thesis is solely based on my own research. The content of this PhD work is original, except where the work is referenced. I also declare that this work has not been submitted in whole or in part for the purpose of degree or qualification at any degree-awarding institute. I declare that this thesis is my own work and contains nothing as an outcome of work done in internal and/or external collaboration.

.....

Saifal Talpur

September, 2020

Chapter 1

1.1 Background

Complex and rapidly growing advancements in generation, transmission and distribution of electricity are changing the way assets are managed. Asset management is necessary to control and manage both direct and inverse power flows from assets with generation and consumption capability. The asset management responsible for transmission and distribution of electricity needs to consider the requirements from both the utility and from the consumer's sides. The unpredictable nature of weather-influenced changes in generation, transmission and distribution of electricity are raising concerns for asset managers to operate and manage their assets in order to obtain reliable and efficient flow of electricity. A cost-effective, optimum and reliable electricity flow can be obtained under maximum capacity utilization of transmission and distribution assets. Additionally, rising electricity demand from distributed energy resources (DERs), deferral in the upgrading of transmission and distribution network assets and growing integration of electric vehicles (EVs) are some major reasons behind operating the assets to their full capacity. By doing so, congestion is removed and reliability is maintained.

Asset management covers a wide cluster of asset analysis, asset planning and asset management. In result of excess renewable energy, e-mobility, digitalization, deregulated electricity market and rising socio-economic challenges have forced transmission and distribution system operators towards the requirement of efficient asset management. From this perspective, utilities need techniques, which can bring optimal asset life cycling while allowing assets to their maximum capacity utilization. Overhead transmission lines in regions of excess renewable energy may face congestion as most of them are not designed to transmit excess electricity that is beyond their design limits. Construction of new overhead lines or replacement of existing lines with high temperature-high current carrying overhead lines are financially and socio-economically infeasible options. In order to avoid congestion and allow renewable energy in the transmission network, the techniques feasible from technical, financial, and socio-economic perspectives, like dynamic line ratings have to be implemented. Dynamic line ratings can be beneficial due to their linear relationship with wind energy. Hence, the larger the wind speed, the more electricity can be transmitted under higher conductor cooling. In result, an efficient asset management is possible to benefit both utilities and consumers.

As dynamic line ratings depend on unpredictable weather, an instantaneous variation in line ratings can thus cause changing line flows. For reliable, manageable and controllable electricity flows, line ratings can be classified in short-term and long-term loading conditions. Under short-term or emergency loading, a line may be allowed to transfer additional electricity provided it does not violate the safety margins. Similarly, under long-term loading, a line is allowed to transmit excess electricity until it reaches the allowable temperature limit to avoid violation in ground clearance limit. Furthermore, dynamic line rating under long-term loading cannot be considered as a feasible approach as it may jeopardize the physical limits, particularly of old overhead lines. As, dynamic line rating is weather dependent, the ambient parameters like ambient temperature, wind speed, wind direction (to the axis of conductor) and solar radiations may affect the line ratings, which can then differ from the design limits. The design limits of overhead lines are moreover based on considering the worst ambient situations, which involve the highest ambient temperature, the lowest wind speed and the highest solar radiation in the geographical location of an overhead line. The current carrying line limits are calculated by taking the ratio between actual current and maximum line current. Actual current represents the amount of current based on actual line loading, whereas, maximum line current represents the amount of current at fixed maximum line temperature (for instance, 80°C) and actual or worst weather conditions (depending on the type of limits to be implemented, i.e. dynamic or static). Mathematically, the higher the maximum current, the lesser the line loading becomes and vice versa. At fixed physical dimensions, the actual weather conditions improves the maximum line current limit in comparison to the worst weather conditions, further, resulting in two conclusions, 1) increased capacity margin and 2) sag within limits towards allowing an excess electricity flow, hence minimizing the congestion. Additionally, under the dynamic loading state, the usage of actual weather conditions can also decrease the rate of change of line temperature, resulting in additional time for the system operator and higher line flows for a longer time under the nominal sag and temperature limits.

The overhead line is modelled as a pi-equivalent circuit, where line inductance and capacitance contribute to voltage changes, while resistance influences line temperature. Across medium and long lines, capacitance effect cannot be disregarded towards influencing the line voltage. Similarly, across short lines, resistance based voltage drop is negligible but temperature dependent voltage drop can be significant. Besides, in short lines, due to linear relation between line resistance and power losses, joule effect is found

substantial. The mutual coupling between line's electrical and thermal parameters is known as electro-thermal effect and is investigated in [1]-[5]. This impedance control based technique can be used to reduce congestion in the transmission network. Additionally, line impedance contributes towards affecting the power transfer capability of a transmission line, i.e., lower impedance leads to higher power transfer capability and vice versa as referred in [6] and [7].

When an overhead line passes through various geographical regions, a number of line spans face diverse weather conditions, which may cause uneven line sag. Therefore, to derive reliable line loading, dynamic line rating must be calculated across each line span during each loading interval. This will result in allowable loading range and permissible line sag. The calculated results will then help in identifying the critical line spans or spans responsible to determine the loading for the entire line. It is important to mention that critical span is space and time dependent, meaning that a critical span or set of critical spans change with location and time and varies in numbers as well. Refs. [8] and [9] have investigated the optimal number and placement of sensors required to monitor line sag across critical spans under dynamic line loading. The studies in [10]-[12] have carried out critical span identification without examining the line terrain conditions. Additionally, in [10]-[14], static weather conditions were considered across every line span in the test overhead lines. The spans violating the ground clearance or spans with highest line sag at uniform line loading were taken as critical spans.

Thermal rating associated with dynamic weather conditions can also improve the loading capacity of the distribution transformers. In line with that, this thesis also investigated dynamic thermal rating across distribution transformers. Based on the concept of dynamic ratings, weather-cooling impact can alleviate thermal stress, leading to increased transformer loading across distribution transformer. On contrary, weather-heating impact can increase thermal stress, leading to reduced transformer loading to maintain life and limit voltage drops. The growing demand in electric vehicles is a major reason towards increased loading across distribution transformers.

To investigate the impact of EV loading, a number of charging scenarios were evaluated in the thesis. The obtained results indicated a huge influence on life of distribution transformer, where, transformer loading in result of simultaneous charging demand from each residential house during peak hours was found as a worst-case scenario. For longevity, simultaneous EV charging is not recommended across distribution transformers, particularly during peak loading hours. Besides, the impact on loss of life,

the excess EV loading may also cause severe voltage drop. As, EV loading is transient in nature; winding and oil temperature inside a distribution transformer may vary cyclically and non-cyclically and are furthermore addressed in the thesis.

In addition to exploiting the dynamic thermal ratings, the potential of battery energy storage system and demand response technique is also considered in this thesis under simulation based experiments. Besides, reduced loading across distribution transformer, BESS installation in a LV network can also bring a significant reduction in the unit cost, for instance by around 16.7% per house/day as proved in a case study demonstrated in [15]. Additional benefits a BESS can provide are peak load reduction in the MV/LV substation [16], reinforcement deferral of a 10 kV cable in the distribution network [17] and contribution towards balanced voltage, which is furthermore affected by distributed generators (DGs) [18].

Demand response (DR) is a load controlling technique, aimed at regulating the energy consumption in the distribution network. In the demand response technique, the load demand is controlled across controllable appliances and is incentivised to limit electricity usage at times of high retail price or during the congestion in the network. Under DR, the consumption pattern is modified to accommodate time based load demand. A significant work is carried out in the domain of demand response, which is limited to analysing the scope of DR without considering the potential of dynamic ratings. This thesis thereby contributes in bridging the gap between demand response and dynamic thermal ratings in the distribution network. The work is carried out to obtain maximum utilization across the distribution transformer without investing into battery energy storage system as analysed in the previous chapter.

In result of increased congestion, particularly during peak hours, [19] has investigated peak load shaving through vehicle to house energy transfer to avoid overloading in the distribution network. A similar work is carried out in [20], where, demand side management is implemented through distributed energy storage system technique. Furthermore, to reduce loading impact and avoid loss of life across distribution transformers, the application of demand response is carried out in [21]-[24]. In [25], a similar approach is carried out with the help of particle swam optimization technique to reduce EV charging impact. Dynamic unit pricing or time of use (ToU) based pricing techniques when implemented with demand response can minimize the electricity cost for residential, commercial and industrial consumers. The work is moreover implemented in [26]-[28].

A growing trend towards battery electric vehicles (BEVs) usage imposes an additional loading on distribution transformers that need to be addressed through smart load reduction techniques, like demand response. To this end, the studies carried out in [29]-[31] have implemented BEV load management techniques to reduce loading stress across distribution transformers in the low voltage distribution network.

1.2 Thesis Outline

This PhD thesis is about obtaining the maximum capacity utilization across transmission line and maximum capacity utilization across distribution transformer under dynamic weather. The weather influence can be categorized into two types (detailed explanation is provided in ‘Manuscript-1’): 1) weather influencing the electrical and thermal characteristics of the assets, and 2) weather influencing the power flow in the network before and after the contingencies. The work reported in this thesis is based on asset handling under component and system modelling, where it is considered that the ambient impact on transmission line and distribution transformer can delay the costly upgrading and asset replacement needs.

Maximum utilization of overhead lines is based on thermal loadability that further relies on weather conditions and the span topography; the issues addressed in ‘Manuscript-1’ and ‘Manuscript-2.’ In ‘Manuscript-1,’ it is found that favourable weather conditions improve the power transfer capability of overhead lines based on the technique, widely known as the dynamic thermal rating (DTR). An excess electricity transfer based on DTR technique mainly relies on weather conditions, physical dimensions of the conductor, and on coordination between electrical and thermal loading states, thereby resulting in minimized congestion in the overhead transmission network under favorable weather conditions.

Contrary to overhead lines rated under dynamic weather conditions, the overhead lines rated under static weather conditions have limited power transfer capacity to avoid congestion and line overloading. Rating and operating them under actual weather and loading conditions with electro-thermally coupled parameters can significantly increase line loadability. The lack of coordination between electrical and thermal parameters is also proved to reduce power transfer limit of overhead lines due to a fixed line resistance

calculated under maximum line temperature, in contrast to temperature dependent line resistance calculated under dynamically varying actual line temperatures.

‘Manuscript-1’ further shows that favourable weather conditions can increase thermal loadability limit of an overhead line (OHL) through reduced line resistance that in turn increases the power transfer limit under electro-thermally coordinated (ETC) line rating technique. Contrary to that, due to lack of coordination between electrical and thermal loading parameters, for instance in the DTR technique, an efficient and optimal line loading is not obtained or in other words, it lacks in benefiting from the favourable weather conditions. In this manuscript, ETC line rating technique is applied across an OHL passing through an extensive geographical area with exposure to multiple weather conditions. In addition, the results from the presented technique are compared to those obtained under conventional line rating techniques under static and dynamic weather conditions.

Due to multiple weather conditions across an entire route of the test OHL, each line span faces these different weather conditions. Hence, spans with worst ambient conditions (lowest wind speed, highest ambient temperature and highest solar radiation) have the lowest thermal and current loadabilities in terms of electricity transmission and are moreover named as critical spans or hot-spots. Spans of overhead lines passing through multiple geographical regions and over varying terrains mainly face diverse weather conditions and thus need to be monitored to obtain reliable estimates of line loadability. Amongst such spans, the line spans facing the worst weather and being the longest in length possess lower thermal loadability than the rest of the line spans and thus restrict the line flow and are therefore known as critical spans or the bottlenecks. Identifying critical spans is important in allowing utility providers to monitor their overhead transmission network spanning over large geographical regions. The technique to identify spans exhibiting the minimum thermal loadability, further known as “critical span identification technique,” is presented in ‘Manuscript-2.’

‘Manuscript-2’ focuses on identifying the critical spans through a developed critical spans identification technique. The technique helps towards identifying these bottlenecks in the overhead transmission network to obtain an optimal power transfer by utilizing the maximum capacity utilization under sag limits. The technique further determines the optimal number and placement of sensors across the entire test OHL, dividing the line into non-uniform segments, each carrying multiple length spans passing through flat and non-flat terrains. The resulting critical spans determine the line loadability that can

effectively relieve congestion from the transmission network, based on allowable vertical clearance from the ground.

In ‘Manuscript-2,’ line temperature and sag across critical spans identified under the proposed technique are validated with conventional technique, that further proves the computational efficiency of the proposed technique versus the conventional technique. The active power flow, AC resistance, bus voltage magnitude and line temperature are calculated across identified critical spans with the help of the newly developed weather-integrated power flow tool from ‘Manuscript-1.’ Based on the obtained results, the line flow under real weather conditions has shown an improved line capacity capable of mitigating the line congestion and avoiding the load shed while maintaining the line temperature, sag across the most critical span within the maximum allowable temperature (MAT), and sag limits.

Like overhead lines, thermal capacity of distribution transformer changes under ambient conditions. Ambient temperature is considered an important weather element towards affecting the thermal loadability, winding and oil temperatures in the distribution transformer. These issues are moreover addressed in ‘Manuscript-3’ that considers thermal and electrical loadings across a 200-kVA distribution transformer (DT) referred as a test distribution transformer. The test DT is loaded under a combined residential and battery electric vehicle (BEV) load. To counteract DT loading beyond the nominal rating, the test DT is connected to the battery energy storage system (BESS). The objective is to obtain maximum capacity utilization of the test DT under multiple BEV charging scenarios and to find the loading impact on the voltage profile across each consumer service point and across DT insulation. The technique is proposed under weather optimized battery storage integration and is thus termed as dynamic rating operated DT (DRoDT) integration with BESS. The proposed technique is based on providing the benefits, like active power support to flatten the load spikes, reactive power support to boost voltage, maximum efficiency and reduced ageing across the test DT.

In ‘Manuscript-4,’ an alternate technique is introduced to avoid capital and operational costs associated with BESS with obtaining the same benefits. The proposed technique involves the application of demand response and smart BEV charging techniques to achieve objectives identical to that obtained under DRoDT-BESS integration in ‘Manuscript-3.’ The manuscript deals with controlling the residential and BEV loading to provide flexibility to the distribution system operators (DSOs) in terms of effective DT

loading. Both techniques are moreover found with providing an optimal DT loading and the regulated voltage across each end-user.

In this thesis, the main goal of asset management in the HV transmission network is to enable and operate the overhead line at maximum capacity utilization to benefit transmission system operator (TSO). The overhead transmission line operating under 132 kV is investigated as the subject asset in the overhead transmission network. The subject transmission asset is further referred as the test OHL. The test OHL is considered passing through a large geographical area with diverse weather conditions. Each span of the test OHL is considered to face different time and space-based conditions. The time dependent conditions are weather based, whereas the space dependent conditions are span topography based. The influence of both conditions can be seen in impacting the electrical and thermal states across each span of the OHL. This extensive variation in electrical and thermal states between each line span has the potential of impacting system's reliability based on line loading and may subsequently result in line outage. To avoid the line outage, electrical and thermal loading states across selective spans are considered to represent the reliable loading states for the entire test OHL. The selective spans are referred as critical spans and are also known as 'hot-spots' or the 'bottlenecks.' The entire 'Manuscript-2' is dedicated to finding the location, number, sag and corresponding electrical and thermal loading states across each identified critical span. The span-based electrical and thermal loading states are then used to determine the span sagging levels for the entire loading duration across the test OHL. The critical spans are the line spans with minimum thermal loadability and contribute to limiting the power flow passing through an OHL. Finding the critical spans is important when determining the optimal and reliable power flow with no violation in sag and temperature limits. The knowledge of critical spans is of utmost importance before loading the OHL. The OHL loaded before the identified critical spans can face two issues, 1) sag limit violation across the span with minimum thermal loadability, and 2) voltage limit violations across the span with the highest resistance.

The test OHL is loaded to reach the maximum thermal capacity close to the thermal equilibrium, a state in which the line temperature stops changing over the loading interval. Thermal equilibrium of any OHL depends upon the surrounding weather conditions and the difference between heat gained and heat lost in the OHL. A term known as heat balance equation (HBE) is used to represent the equilibrium state across any OHL. Depending upon the cross-sectional area, a variation can be found in a line reaching its thermal equilibrium state within a certain amount of time or not. Thermal inertia of any

OHL determines the time an OHL can take to reach the thermal equilibrium state. The entire ‘Manuscript-1’ is dedicated to determining the resistance, voltage, line flow, electrical and thermal loading states across the test OHL before and after the contingencies under the presence of identified critical spans from ‘Manuscript-2.’

The test OHL is loaded under static and dynamic weather conditions to find the static and dynamic thermal limit or thermal line ratings, represented as static thermal limit or static thermal line rating (STLR) and dynamic thermal limit or dynamic thermal line rating (DTLR). The test OHL is investigated under non-steady system state. Under the non-steady system state, both weather and line loading conditions are considered as time-variant. Due to volatility associated with weather and loading conditions, the temperature dependent AC resistance across the critical spans along thermal inertia is used in finding the line flow and the per-unit voltage. These parameters further decide the test OHL’s electrical and thermal loadabilities for reliable electricity transfer during each loading interval. During their absence, the calculated line flow will be lower than the actual line capacity, hence unable to address the line congestion and load shedding.

The main goal of asset management in the LV distribution network as carried out in this thesis was to enable and operate the distribution transformer (DT) under maximum capacity utilization to benefit both distribution network operators (DNOs) and the consumers. To achieve this, the test DT was connected to a stationary centralized battery energy storage system (BESS) and was operated under dynamic electrical and thermal loading states. DT loading was divided into electrical and thermal loadings. Electrical loading was observed under residential and BEV charging loads, besides in case when DT was connected to BESS, charging of BESS was considered as separate loading across test DT. Thermal loading was observed in result of electrical loading combined with effect of ambient temperature. The maximum capacity utilization enabled test DT to supply an uninterrupted electricity while operating at maximum efficiency and exposed to minimum loss of life (LoL). The care was taken to decide the appropriate size selection of the BESS, suitable for the test system in order to achieve the required loading goals while operating under optimal charging/discharging range.

The proposed framework was based on combination of dynamic rating operated distribution transformer (DRoDT) with BESS. The test bed was built in Simulink and involved single-phase loads across a neighbourhood of 40 households that were connected to a 200-kVA DT. The secondary of the test DT was connected to BESS and the load points through RL-type XLPE service cable. Each household was considered

with residential and BEV loadings, where the segregated residential and BEV charging loads were connected to the secondary of the test DT. Results were analysed under multiple weather-dependent loading scenarios before and after BESS to examine DT operation related to maximum capacity and optimal loading. The entire ‘Manuscript-3’ is dedicated to efficient asset management of the distribution transformer. The presence of BESS was seen in terms of providing the reactive power support to maintain voltage at each load point to the nominal level.

‘Manuscript-4’ was based on applying the demand response and smart BEV charging techniques on a test system as presented in ‘Maunscript-3.’ The goal was to investigate the potential of demand response and smart BEV charging against BESS implementation towards maximum capacity across the test DT. The methodology involved classification of residential load in shiftable and non-shiftable. Residential and BEV charging load were operated under time of use (ToU) and non-time of use pricing models. Under non-ToU pricing model, the unit price was considered constant for the entire day, where electrical loading across test DT after shifting the load of shiftable appliances was observed as reduced load peaks during the entire loading duration. Under ToU pricing model, unit price was based on loading trend, i.e., low unit price during off-peak hours and high unit price during peak-hours. The ToU pricing model resulted in shifting of residential and BEV charging loads in accordance to the unit pricing. Under this scenario, the load shifting across shiftable appliances in the entire neighbourhood was carried out during peak-hours due to involvement of the high unit pricing.

Similarly, under ToU pricing model, charging across all BEVs was allowed during off-peak hours, an approach similar to the coordinated BEV charging, which is discussed in ‘Manuscript-3.’ The work presented in ‘Manuscript-4’ can be considered an extension to ‘Manuscript-3’, where an algorithm was designed to bring voltage across each household within limits by applying the demand response technique in contrary to BESS. The same electric vehicle charging scenarios were analysed in the identical test network with exception of controlling the base load through a machine learning based approach. The base load controlling was carried out in the form of categorising them as shiftable and non-shiftable loads

1.3 Thesis Contribution

The work presented in this thesis contributes towards obtaining the maximum asset utilization in high and low voltage electricity networks. Underutilization and overutilization of assets are common issues causing congestion, ageing and overloading. To contribute scientifically, the work presented in this thesis comprises the techniques in improving the asset utilization to obtain maximum capacity, minimum congestion and the increased hosting capacity. The entire thesis work is divided in the form of Manuscripts, where the work presented in each Manuscript has unique contribution towards obtaining the optimal maximum asset utilization in the electricity network.

‘Manuscript-1’ and ‘Manuscript-2’ contribute in the aspects of improving the power handling capacity of the overhead lines under optimal power transfer. The techniques are developed such that the resulting line loading minimizes line congestion, avoids ground clearance across thermally limited spans, combines line’s electrical and thermal characteristics for optimal and reliable power transfer through availing the real weather conditions.

‘Manuscript -3’ and ‘Manuscript-4’ are dedicated towards addressing the capacity limit of a distribution transformer when loaded under an excessive BEV charging load. In Manuscript-3, dynamic thermal rating is implemented with BESS, whereas in Manuscript-4, the application of demand response technique is carried out with dynamic thermal rating. The following benefits are furthermore obtained in result of hybrid techniques:

- increased hosting capacity in the LV network
- regulated voltage across each household
- maximum efficiency based electrical loading
- minimum ageing based thermal loading
- optimal asset utilization in the LV network

In addition, ‘Manuscript-3’ is based on obtaining the maximum capacity utilization under the proposed technique, which embeds a centralized battery energy storage system with dynamic thermal ratings to obtain an effective load sharing strategy. The proposed technique in addition to providing the maximum capacity utilization also offer benefits like regulated voltage, effective congestion management, minimal loss of life and an improved insulation strength of the distribution transformer.

In comparison to the approach presented in ‘Maunscript-3’, the hybrid technique in ‘Manuscript-4’ is aimed at obtaining the identical benefits but without the battery energy storage system. Besides, ‘Maunscript-4’ investigates the potential of utilizing the demand response with smart BEV charging technique towards obtaining the benefits like peak shaving, reduced thermal and electrical stress across the distribution transformer, regulated voltage and efficient transformer loading. The obtained results indicate benefits for both distribution system operator and the consumers.

1.3 Manuscripts in One Thesis

This thesis is based on the work presented in the form of Manuscripts. The entire objective of this thesis is divided into multiple tasks, where each Manuscript is dedicated to address each task. Manuscripts are prepared in order to address the individual problem laying under the main theme of the entire PhD project. When combined, the individual work as addressed in each Manuscript is considered to represent the entire PhD project.

References

- [1] H. Banakar, N. Alguacil and F. D. Galiana, "Electrothermal coordination part I: theory and implementation schemes," in *IEEE Transactions on Power Systems*, vol. 20, no. 2, pp. 798-805, May 2005. doi: 10.1109/TPWRS.2005.846196.
- [2] N. Alguacil, M. H. Banakar and F. D. Galiana, "Electrothermal coordination part II: case studies," in *IEEE Transactions on Power Systems*, vol. 20, no. 4, pp. 1738-1745, Nov. 2005. doi: 10.1109/TPWRS.2005.857836.
- [3] M. Wang and X. Han, "Study on electro-thermal coupling optimal power flow model and its simplification," *IEEE PES General Meeting*, Providence, RI, 2010, pp. 1-6. doi: 10.1109/PES.2010.5589644.
- [4] A. Kubis and C. Rehtanz, "Application of a combined electro-thermal overhead line model in power flow and time-domain power system simulations," in *IET Generation, Transmission & Distribution*, vol. 11, no. 8, pp. 2041-2049, 1 6 2017. doi: 10.1049/iet-gtd.2016.1626.
- [5] J. Shu, R. Guan and L. Wu, "Optimal power flow in distribution network considering spatial electro-thermal coupling effect," in *IET Generation, Transmission & Distribution*, vol. 11, no. 5, pp. 1162-1169, 30 3 2017. doi: 10.1049/iet-gtd.2016.0909.

-
- [6] X. Dong et al., "Calculation of Power Transfer Limit Considering Electro-Thermal Coupling of Overhead Transmission Line," in *IEEE Transactions on Power Systems*, vol. 29, no. 4, pp. 1503-1511, July 2014. doi: 10.1109/TPWRS.2013.2296553.
- [7] X. Dong, C. Kang, Y. Ding and C. Wang, "Estimating the Wind Power Integration Threshold Considering Electro-thermal Coupling of Overhead Transmission Lines," in *IEEE Transactions on Power Systems*. doi: 10.1109/TPWRS.2019.2906291.
- [8] "Oncor's pioneering transmission dynamic line rating (DLR) demonstration lays foundation for follow-on deployments," U.S. Dept. Energy, MD, USA, 2014. Final Report of Oncor-DOE Smart Grid Development Project fully documenting the DOE supported DLR project: https://www.smartgrid.gov/files/FTR_Final_Oncor_DE-OE0000320.pdf.
- [9] J. Teh and I. Cotton, "Critical span identification model for dynamic thermal rating system placement," in *IET Generation, Transmission & Distribution*, vol. 9, no. 16, pp. 2644-2652, 3 12 2015. doi: 10.1049/iet-gtd.2015.0601.
- [10] M. Matus *et al.*, "Identification of Critical Spans for Monitoring Systems in Dynamic Thermal Rating," in *IEEE Transactions on Power Delivery*, vol. 27, no. 2, pp. 1002-1009, April 2012. doi: 10.1109/TPWRD.2012.2185254.
- [11] J. W. Jerrell, W. Z. Black and T. J. Parker, "Critical span analysis of overhead conductors," in *IEEE Transactions on Power Delivery*, vol. 3, no. 4, pp. 1942-1950, Oct. 1988. doi: 10.1109/61.194004.
- [12] J. Wan *et al.*, "Determination of critical span in real time using proper orthogonal decomposition," *2013 Seventh International Conference on Sensing Technology (ICST)*, Wellington, 2013, pp. 816-821. doi: 10.1109/ICSensT.2013.6727765.
- [13] A. Hatibovics, "Determination of the lowest point of the conductor in inclined spans based on a known maximal sag of the parabola," *22nd International Conference and Exhibition on Electricity Distribution (CIRED 2013)*, Stockholm, 2013, pp. 1-4. doi: 10.1049/cp.2013.0583.
- [15] Z. Qiao and J. Yang, "Comparison of centralised and distributed battery energy storage systems in LV distribution networks on operational optimisation and financial benefits," in *The Journal of Engineering*, vol. 2017, no. 13, pp. 1671-1675, 2017, doi: 10.1049/joe.2017.0616.
- [16] M. Z. Degefa, H. Sæle, J. A. Foosnaes and E. Thorshaug, "Seasonally variant deployment of electric battery storage systems in active distribution networks," in *CIRED - Open Access Proceedings Journal*, vol. 2017, no. 1, pp. 1975-1979, 10 2017, doi: 10.1049/oap-cired.2017.0757.
- [17] S. Nykamp, T. Rott, N. Dettke and S. Kueppers, "The project "ElChe" Wettringen: storage as an alternative to grid reinforcements - experiences, benefits and challenges from a DSO point of," *International ETG Congress 2015; Die Energiewende - Blueprints for the new energy age*, Bonn, Germany, 2015, pp. 1-6.

-
- [18] J. L. Lorente, X. A. Liu, R. Best and D. J. Morrow, "Energy storage allocation in power networks – A state-of-the-art review," 2018 53rd International Universities Power Engineering Conference (UPEC), Glasgow, 2018, pp. 1-6, doi: 10.1109/UPEC.2018.8542106.
- [19] L. Zhao and V. Aravinthan, "Strategies of residential peak shaving with integration of demand response and V2H," 2013 IEEE PES Asia-Pacific Power and Energy Engineering Conference (APPEEC), Kowloon, 2013, pp. 1-5.
- [20] Barzkar, Arash, and Seyed Mohammad Hassan Hosseini. "A novel peak load shaving algorithm via real-time battery scheduling for residential distributed energy storage systems." *International Journal of Energy Research* 42.7 (2018): 2400-2416.
- [21] N. G. Paterakis, I. N. Pappi, O. Erdinç, R. Godina, E. M. G. Rodrigues and J. P. S. Catalão, "Consideration of the Impacts of a Smart Neighborhood Load on Transformer Aging," in *IEEE Transactions on Smart Grid*, vol. 7, no. 6, pp. 2793-2802, Nov. 2016.
- [22] S. N. G. Gouriseti, H. Kirkham and D. Sivaraman, "A review of transformer aging and control strategies," 2017 North American Power Symposium (NAPS), Morgantown, WV, 2017, pp. 1-6.
- [23] Y. Yao and W. Gao, "Relieving the pressure of electric vehicle battery charging on distribution transformer via particle swarm optimization method," 2014 North American Power Symposium (NAPS), Pullman, WA, 2014, pp. 1-5.
- [24] A. N. M. M. Haque, M. T. Rahman, P. H. Nguyen and F. W. Bliet, "Smart curtailment for congestion management in LV distribution network," 2016 IEEE Power and Energy Society General Meeting (PESGM), Boston, MA, 2016, pp. 1-5.
- [25] Haque, A. N. M. M., et al. "Demand response for real-time congestion management incorporating dynamic thermal overloading cost." *Sustainable Energy, Grids and Networks* 10 (2017): 65-74.
- [26] M. Muratori and G. Rizzoni, "Residential Demand Response: Dynamic Energy Management and Time-Varying Electricity Pricing," in *IEEE Transactions on Power Systems*, vol. 31, no. 2, pp. 1108-1117, March 2016.
- [27] Yan, Xing, et al. "A review on price-driven residential demand response." *Renewable and Sustainable Energy Reviews* 96 (2018): 411-419.
- [28] Ma, Kai, et al. "Residential power scheduling for demand response in smart grid." *International Journal of Electrical Power & Energy Systems* 78 (2016): 320-325.
- [29] López, M. A., et al. "Demand-side management in smart grid operation considering electric vehicles load shifting and vehicle-to-grid support." *International Journal of Electrical Power & Energy Systems* 64 (2015): 689-698.

- [30] A. Soares, Á. Gomes, C. H. Antunes and C. Oliveira, "A Customized Evolutionary Algorithm for Multiobjective Management of Residential Energy Resources," in *IEEE Transactions on Industrial Informatics*, vol. 13, no. 2, pp. 492-501, April 2017.
- [31] Ghazvini, Mohammad Ali Fotouhi, et al. "Demand response implementation in smart households." *Energy and buildings* 143 (2017): 129-148.

Chapter 2

2.1 Introduction to Manuscript 1

This Manuscript deals with proposing a technique to increase the power transfer capacity of an overhead line by considering the thermally limited line spans. The technique takes into account the parameters which are not considered in the conventional IEEE-based methods. In the proposed technique, a combined electro-thermal line model under weather dependent conditions is presented, resulting in a reliable and efficient power transfer, useful to mitigate congestion and avoid any emergency load-shedding. The Manuscript also presents the sensitivity analysis to find the correlation between weather parameters and the line temperature by examining the impact of each weather parameter on degree of changes in the line temperature. The realistic case scenarios are presented to find the potential of the overhead line in terms of congestion and load shed management under the presence of critical spans.

The Manuscript is published in the journal of ‘Electric Power Systems Research’ under title: “Non-steady state electro-thermally coupled weather-dependent power flow technique for a geographically-traversed overhead-line capacity improvement.” *Electric Power Systems Research* 177 (2019): 106017.

2.2 Manuscript 1

Non-Steady State Electro-Thermally Coupled Weather-Dependent Power Flow Technique for a Geographically-traversed Overhead-line Capacity Improvement

Saifal Talpur*, T. T. Lie, R. Zamora

School of Engineering, Computer and Mathematical Sciences, Auckland University of Technology, New Zealand

*Corresponding author email: saifal.talpur@aut.ac.nz

Abstract

Overhead lines rated under conventional line rating techniques have limited power transfer capacity to avoid congestion and line overloading. Rating and operating them under actual weather and loading conditions with electro-thermally coupled parameters can significantly increase line loadability. As a result, line congestion and overloading

can be minimized, thus avoiding load shedding. This paper presents an electro-thermally coupled (ETC) line rating technique for an overhead line passing through a large geographical area and exposed to multiple weather conditions. The presented technique, using a dynamic weather scenario, was found to enable efficient and reliable transfer of excess electricity to avoid load shedding. Because the line passed through a large geographical area, regions exposed to the worst weather exhibited the lowest thermal and current loadability with regard to electricity transmission. This paper therefore focuses on these spans to find the line temperature, temperature-dependent line AC resistance, branch active power flow and bus voltage magnitude based on time- and space-dependent weather conditions in comparison to time- and space-independent weather conditions, using the newly developed weather-integrated power flow tool. The paper also addresses the sensitivity between weather-dependent line temperature and associated weather across critical spans, where weather affecting critical spans is used to determine the line temperature.

Keywords: *Electro-thermal line rating, line overloading and load-shed management, weather-dependent power flow and sensitivity analysis*

ABBREVIATIONS

ACSR	Aluminium Conductor Steel Reinforced
DLR	Dynamic Line Rating technique
ETC	Electro-Thermally Coupled line rating technique
ETC-DWLR	Electro-Thermally Coupled Dynamic Weather Line Rating technique
ETC-SWLR	Electro- Thermally Coupled Static Weather Line Rating technique
HBE	Heat Balance Equation
MAT	Maximum Allowable Temperature limit of the overhead line
NIWA	National Institute of Water and Atmospheric Research
OHL	Overhead Line
PTL	Power Transfer Limit of the overhead line
TL	Thermal Limit of the overhead line
TSO	Transmission System Operator

NOTATIONS

$I(t)$	Time- and loading-dependent flow of current	$P_{losses}(t)$	Ohmic losses
$T_c(t)$	Time- and space-dependent line temperature speed)	X	Independent variables (temp. & wind
A_s	Solar absorptivity	Y	Dependent variable (line temperature)
k_f	Thermal conductivity	σ_1	Standard deviation of X
D	Diameter	σ_2	Standard deviation of Y
H	Altitude from sea level	$V_{corr,1}$	Correlated partial variance between wind speed and line temperature
R_e	Reynolds number	$V_{corr,2}$	Correlated partial variance between ambient and line temperatures
M_{air}	Air density	ρ_1	Partial derivative of X
R_e	Reynolds number	ρ_2	Partial derivative of Y
Nu	Nusselt number	n	Length of input variables
ε	Emissivity	V_{corr}	Covariance between X and Y variables
σ	Stephan Boltzmann constant	V_{Total}	Total correlated partial variance
k_{ac}	AC/DC resistance ratio	S_{index}	Sensitivity index between the weather elements and the line temperature
$C_h^{max}(t)$	Time- and space-dependent line heating state	$T_{max,i}^\varphi$	Max. Ref. Temperature at critical span
$C_c^{min}(t)$	Time- and space-dependent cooling state	$T_{c,i}^\varphi$	Conductor Temperature at critical span
$\Delta_{h,l}$	Heating time constant	m	Conductor mass
$\Delta_{c,l}$	Cooling time constant	C	Specific heat capacity
T_c^{max}	Maximum allowable temperature	$T_{ETC,h,i}^\varphi$	Cond. Temp. at critical span in heating
T_a^φ	Ambient Temp. at φ section	$T_{ETC,c,i}^\varphi$	Cond. Temp. at critical span in cooling
V_s^φ	Wind speed at φ section	$Sag_{ETC,i}^\varphi$	Sag at critical span
Q_{solar}^φ	Solar rad. at φ section	V_i^φ	Voltage at critical span
P_j^φ	Joule heat gain	$T_{updated_ref,i}^\varphi$	Updated Ref. Temp. at critical span
P_s^φ	Solar heat gain	$T_{updated_ref,i}^\varphi$	Updated Ref. Temp. at critical span
Q_r^φ	Radiative heat loss	$R_{updated_ref,i}^\varphi$	Updated Ref. Resist. at critical span
Q_c^φ	Convective heat loss		
T_{ref}^φ	Ref. Temp. at φ section		
$T_{ini_ref,i}^\varphi$	Initial Ref. Temp. at critical span		

1. Introduction

The rising demand for electricity requires added power transfer through overhead lines, which results in thermal problems in transmission lines and may affect their annealing characteristics [1]. Therefore, using the electro-thermally coupled (ETC) line rating technique for additional power transfer will be useful when considering the overhead line (OHL) thermal inertia during line loading. ETC provides flexibility for transmission operators when it comes to effectively loading the lines, by considering thermal inertia, temperature-dependent line resistance and real-time weather and loading conditions.

Overhead lines are important utilities assets because of their role in transferring power from generation sources to load centres. The power transfer limit of overhead lines is usually determined by their critical line temperature (associated with critical spans), which determines their thermal limit in transferring electricity. Hence, the power transfer limit of any overhead line is correlated with its thermal limit. Transformation of a line's thermal limit into its power limit or vice versa can be done using the heat balance equation (HBE), which is influenced by the line loading and local weather conditions [2].

Worst-case weather assumptions, coupled with fixed line resistances, ignoring critical spans, reduce the power transfer limit of overhead lines, become the main cause of line congestion, and reduced power transfer in electricity networks. In contrast, actual weather conditions coupled with load-dependent line resistance across critical spans increase the power transfer capacity of overhead lines. The increased power transfer limit helps to minimize line congestion and avoid load shedding in the network. The added power transfer margin in overhead lines can help in dispatching extra energy from fast-responding and/or cost-effective generators, as well as reducing outages associated with time-dependent reserves.

The dynamic line rating (DLR) technique was initially proposed in [1, 3] and has been investigated extensively due to its potential to increase line capacity by avoiding thermal overloading [1]. In [4]-[5], weather-dependent line ratings are calculated without considering the conductive heating and cooling impact on line resistance, line flows and bus voltage magnitude. In [5], the thermal rating of lines is calculated under generic weather conditions rather the independently assessed span-based weather conditions proposed in this paper. DLR based on thermal and voltage limit considerations is investigated in [6], where the authors use fixed terrain and fixed weather conditions throughout the line length. From a line operational perspective, the computed line ratings

can therefore cause inaccurate sag levels. Additionally, the authors in [6] recommend multiple environmental data sets with terrain variability and weather station-based locational requirements to achieve the accuracy in line ratings that are investigated in the current study.

An extensive research is carried out in previous years to address congestion in overhead lines through utilizing the potential of mutual coupling between electrical and thermal elements of an overhead line. The concept of an electro-thermally coupled (ETC) line rating technique was first proposed in [7, 8] and the idea was to exploit the benefit of the line thermal inertia and thermal time delay in transferring additional electricity through the overhead lines to avoid congestion and load-shedding in the electricity network. However, these papers did not consider geospatial weather conditions over the line length. In the ETC technique, the line temperature and its current carrying capability are coupled to create electro-thermal coordination. As a result, the line temperature limit is converted into the maximum current carrying limit to obtain the power transfer capability of the transmission component [8].

Some important formulations regarding the ETC technique are also investigated in [9]–[11]. For example, the ETC approach as presented in [9] is investigated from a power flow perspective by assuming that the weather parameters are time-invariant throughout the operation of the line. The simplified model presented, if implemented using actual weather scenarios, will affect the line temperature accuracy and line sagging levels. The work presented in [10] considers the ETC technique without investigating the complete thermal dynamics of the overhead line. This means that the authors in [10] disaggregated power flow and time domain simulations; i.e., real weather elements were not incorporated in determining the active power flow through the overhead lines, as is done in the current study using the weather-based power flow tool. Similarly, [10] investigated time- and space-independent weather scenarios with no consideration of critical line spans. As overhead lines consist of non-uniform spans and traverse large geographical areas with multiple weather conditions, the disaggregation of spatial- and temporal-dependent weather from the line's electrical and thermal behaviors will yield non-reliable sagging across critical and noncritical line spans.

In contrast to [10], the current study presents an ETC technique with sensitivity analysis, where the sensitivity analysis is carried out to analyze the most and least sensitive weather parameters from the set of weather elements across monitored critical spans. The results obtained confirm higher sensitivity between wind speed and thermal line ratings than

between ambient temperature and thermal line rating. This paper therefore fills a research gap. Critical spans based on spatial- and temporal-dependent weather with minimum thermal loadability are considered in order to provide the input weather elements in determining the line temperature, line AC resistance and branch active power flow.

The ETC technique in [11] is considered in steady-state in the absence of thermal inertia. Thus, it reduces the scope of line rating implementation in the presence of actual weather conditions. To estimate the ETC line rating technique for an overhead line passing through a large geographical area, it is necessary to monitor the weather conditions across every span of the line. Due to varying weather, terrain and span-length variability, it is important to select the spans operating at the highest temperatures, known as critical spans [12]. A critical span is not a fixed span; rather it varies with ambient conditions [13]-[14] and span topography and can therefore be found in multiple locations at different times in an overhead line passing through multiple geographical regions with varying ambient data sets. To address the spatial variability in ambient conditions, the entire overhead line studied in this paper was monitored to give a reliable estimate of weather-dependent critical spans.

Papers [15]-[17] further explored the ETC line rating technique, where [15, 16] validated the electro-thermal line modelling concept experimentally. According to [15], conductor heating takes place when current flows through an overhead line and conductor cooling takes place when input power as the product of dissipated current and voltage drop provides a linear relationship between power and temperature. Findings in [16] proved that to get a reliable estimate of the line temperature, system modelling must consider the coupling effect between electrical and thermal models of an overhead line. When any overhead line is loaded to dispatch excess electricity, reliability becomes of utmost importance for the transmission system operators (TSOs). Further, the change in line flows and voltage stability due to line's thermal inertia and the loading temperature raises the reliability concerns for TSOs. Hence, to overcome these issues, authors in [17] have proposed a methodology to find reliable supply of electricity under ETC based cable emergency rating. Reference [18] has shown that the potential of ETC based line rating technique to enhance the reliable line flow besides line physical characteristics is also influenced by the time synchronization between weather data and the network load demand. However, the work has involved statically varying thermal and voltage constraints under steady state operation of an OHL in place of non-steady state based dynamically varying constraints. Hence, the applicability of the presented approach

cannot be considered feasible under incidents like sudden load changes and temporary line outages.

Due to additional dependence on line series resistance and thermal inertia, weather based line rating techniques particularly the ETC technique cannot be optimally utilized until the network load conditions are integrated with thermal behaviour of the OHL. Reference [19] has addressed this problem on underground cables. However, the work has not addressed the impact of load changes on cable charging current that eventually will affect the voltage profile. Thermal loading affects power flows that in result causes voltage drop. Charging current based voltage variations when added with ETC based cable loading will result in voltage stresses which can ultimately affect the voltage stability. To address this issue, this paper has presented the integration of network load conditions with thermal behaviour of the OHL. The resulting line flow is then used to provide the voltage profile across load bus under ETC and non-ETC based thermal line ratings.

In conjunction with validating the proof of concept from [19], this paper has studied the applicability of thermal rating techniques on overhead lines instead of underground cables. The techniques are implemented based on network and component modelling perspectives, where weather and load dependent line temperature is integrated with load flow simulations to find the optimum line flows in relieving the line congestion. As voltage stability is not considered in this paper, subject line's power transfer limit (PTL) is therefore determined by thermal limit instead of voltage, where the line's thermal limit is decided by spans with minimum thermal loadability (hot spots).

The dynamically varying hot spots with time and space make it hard to consider one thermal rating for the entire line operation. Therefore, this paper considers multiple line spans with minimum thermal loadability to determine line rating of the entire line. The resulting thermal loadability of the line hot spots is then used to find the PTL of the subject line at each loading step that further determines voltage sag across the load bus. In this paper, OHL's PTL is increased by enhancing the receiving end load demand at constant sending end generation until the subject line attains the maximum allowable temperature (MAT) limit.

The authors in [20] have considered OHL's PTL based on ETC formulation, where the work has involved analysing the difference in PTL with and without considering the temperature dependent changes on the line series resistance and the line flows. The resulting PTL is referred as based on line's thermal limit. Similarly, the authors have demonstrated that when operating under thermal limits, the overhead line experiences

comparatively lower power transfer margin than when operating under voltage stability limits. Additionally, the ETC based thermal line ratings are studied under fixed weather and steady-state loading, a gap that is moreover addressed in this paper.

In [21], thermal line monitoring scheme is introduced to measure the temperature across line spans under thermal transients. The work has involved non-steady thermal states under variable weather, where the line is loaded under assumed loading conditions and without realizing the impact on the load voltage. The work suggests the importance of electro-thermal coupling in overhead lines, but the proof of concept is not validated either mathematically or analytically. To address the gap from [21], this paper investigates and proves the importance of electrothermal line modelling under realistic loading scenarios across a transmission line containing multiple critical spans. Additionally, this paper presents results from both the proposed and the conventional line rating techniques for validation.

The work in [22] has addressed improving the OHL's power transfer limit based on techniques as discussed in [20] introducing the electricity flow from wind generators under ETC technique. The paper considered applying the ETC technique under weather obtained from two different locations. This paper evaluates the potential of ETC technique with sensitivity analysis of the ambient elements from critical locations across the entire line. The resulting power transfer capability of the overhead line is found effectively mitigating the line congestion.

2. Motivation

Significant work on DLR and ETC technique was conducted in [3]-[11], and the remaining unaddressed issues are investigated in this paper, which implemented the ETC technique, so it was applicable under both static and dynamic weather conditions when influenced by line thermal inertia and the line's AC resistance. This study fills the gap identified in previous research [3]-[11] by presenting a weather-integrated ETC line rating technique that incorporates time- and space-dependent weather elements across thermally limited line spans, in addition to temperature-dependent line resistance and thermal inertia of lines under realistic loading scenarios.

The power flow tool was developed to capture time- and space-variable weather conditions with time- loading scenarios to dynamically couple the subject line's electrical and thermal parameters to determine the active power flow through the subject line and

the load bus voltage magnitude. Line temperature, power flow and voltage magnitudes from weather-integrated ETC-based line rating techniques are compared to non-ETC-based line rating techniques to determine the impact of coupling on a line's thermal loadability in a non-steady system state.

The presented ETC-based line rating technique can be useful to avoid short-term overloading and congestion across thermally limited overhead lines, mainly when a nearby overhead line or a cost-effective generator is required to be out of service for maintenance purposes. In the conventional non-ETC-based DLR technique, the absence of electrothermal coupling eliminates a line's thermal inertia, causing the line to operate at its maximum thermal limit at every step change in load current regardless of variation in weather elements. This approach results in reduced power flow that makes conventional non-ETC-based line rating techniques unsuitable for congestion minimization in an interconnected electricity network.

The sensitivity analysis carried out in this paper provides sensitivity to time- and space-varying weather conditions in loading variant heat transfer through the subject overhead line. Since the line's thermal rating is limited by the presence of critical spans that are critical because they are experiencing the worst weather under the longest span, sensitivity analysis helps in determining the least and most sensitive weather elements in critical span temperature measurement.

The rest of the paper is organized as follows. Section 3 presents mathematical modelling and sensitivity analysis of the proposed weather influenced electro-thermal line rating technique. Section 4 deals with practical aspects of the proposed line rating technique. Section 5 presents the developed power-flow tool. Section 6 summarizes the findings of the paper and Section 7 concludes the paper.

3. Line rating and weather data sensitivity analysis

This paper investigates electro-thermally coupled (ETC) and non-electro-thermally coupled (conventional) line rating techniques under both static and dynamic weather conditions. Under actual weather conditions, this is termed the electro-thermally coupled dynamic weather line rating (ETC-DWLR) technique and when considering assumed weather conditions, it is termed the electro-thermally coupled static weather line rating (ETC-SWLR) technique. In both actual and fixed weather based ETC techniques, the subject line is investigated under mutually coupled thermal and electrical modeling states.

The thermal model of the subject overhead line is based on the line temperature at its maximum current carrying capability under certain weather conditions without violating the ground clearance infringement. The resulting line temperature is thereafter used to find the line AC resistance, which is then used to determine the active power flow through the subject line. Similarly, the line's electrical model is based on line ampacity and temperature-dependent AC resistance. With regard to the significance of both models in determining the line loadability, their coupling effect is therefore considered in the presented line rating technique to find the line temperature, line flow, weather and loading-dependent line AC resistance and the load bus voltage magnitude.

The relationship between electrical and thermal parameters in an overhead line provides a window of time for transmission operators to effectively monitor and load the lines. In the conventional line rating techniques, because there is no coupling involved between the line's electrical and thermal characteristics, the obtained line loadability does not consider the change in the line's electrical model due to changes in its thermal model and vice versa, resulting in lower and less reliable line loadability.

In this paper, the main objective of the presented line rating technique was to address the correlation between the electrical and thermal dynamics of overhead lines during static and dynamic weather conditions such that a line's heating and cooling states are fully incorporated in the algorithm to help mitigate line congestion and load shedding conditions. The thermal rating of the line was computed by considering the presence of critical spans in the subject overhead line. Comprehensive analysis to identify the critical spans and the associated factors was beyond the scope of this study and therefore not considered.

3.1 Line rating techniques

3.1.1 Electro-thermal line rating technique

The ETC technique used in this paper includes electrical and thermal models of the subject overhead line. The electrical model considers the sending-end power and voltage as the model inputs and provides the receiving end power and voltage as its outputs. Similarly, the thermal model considers line current, line AC resistance, line dimensions, wind speed, ambient temperature and solar radiation as the model inputs and produces the line temperature as an output. To obtain the line's thermal limit, both the electrical and thermal models for the subject line were operated in conjunction to avoid any ground-clearance infringement.

Mathematically, the coupled electro-thermal model of any overhead line can be formulated based on non-steady state HBE as shown in (1). Equation (1) [2] describes the solar and joule effects as heating factors, with convection and radiation as the cooling factors when exposed to ambient weather,

$$m * C \frac{dT_c(t)}{dt} = k_{ac} * R_{dc} * I^2(t) * T_c(t) + P_s(t) - (Q_c(t) + Q_r(t)) \quad (1)$$

where m is the conductor mass, C is the conductor's specific heat capacity measured as the ratio between conductor heat capacity and its mass in J/kg·°K, $I(t)$ is the time- and loading-dependent flow of current, and $T_c(t)$ is the time- and space-dependent line temperature.

Similarly, in (2) $P_s(t)$ represents time- and space-dependent solar heat gain, which is a function of the line's solar absorptivity A_s , its diameter D , and time- and space-dependent global solar radiation $Q_{solar}(t)$, causing line heating due to solar radiation.

$$P_s(t) = D * Q_{solar}(t) * A_s \quad (2)$$

Line cooling mainly depends upon convection and radiation. The time- and space-dependent convective cooling $Q_c(t)$ depends on the difference between the ambient and line temperatures as well as the time- and space-dependent wind speed $V_s(t)$ as shown in (3) and (5) respectively,

$$Q_c(t) = k_f * Nu * \pi [T_c(t) - T_a(t)] \quad (3)$$

where k_f is thermal conductivity in Wm⁻¹°K⁻¹ as shown in (4) [23].

$$k_f = 2.42 * 10^{-2} + 7.2 * 10^{-1} * \left(\frac{T_c(t) + T_a(t)}{2} \right) \quad (4)$$

Conductor altitude from sea level H with wind direction normal to the subject overhead line results in the Reynolds number R_e as shown in (5) [23],

$$R_e = \frac{M_{air} * V_s(t) * D}{\left[(1.32 * 10^{-5}) + \left\{ (9.5 * 10^{-8}) * \left(\frac{T_c(t) + T_a(t)}{2} \right) \right\} \right]} * \left[1 - (H) * \frac{(6.5 * 10^{-3})}{288.16} \right]^{-5.256} \quad (5)$$

where M_{air} is the air density in kg/m³, Nu is Nusselt number dependent on Reynolds number as shown in (6) [23].

$$Nu = (0.64 * R_e^{0.2}) + (0.2 * R_e^{0.61}) \quad (6)$$

Similarly, as a result of the time- and space-dependent ambient temperature $T_a(t)$, the radiative cooling $Q_r(t)$ as shown in (7) varies with time and space and is dependent upon the ability of the conductor to emit the heat energy (emissivity) ϵ , difference between

ambient and conductor temperatures, conductor diameter, and the constant σ , known as the Stephan Boltzmann constant and equal to $5.67 \cdot 10^{-8}$.

$$Q_r(t) = \sigma * \varepsilon * \pi * D * [(T_c(t) + 273)^4 - (T_a(t) + 273)^4] \quad (7)$$

In a non-steady system state, HBE as shown in (1) is used to couple the line temperature and line AC resistance; i.e., a change in line temperature will affect the line AC resistance and vice versa due to their linear relationship as shown in (8). The presented ETC technique is therefore useful when the system is in a non-steady state. Also, as shown in (8), the line AC resistance depends upon the DC resistance, line reference temperature T_{ref}^0 , the temperature coefficient of resistance for aluminium in an aluminium conductor steel reinforced (ACSR) conductor α and the constant k_{ac} [23],

$$R_{ac}(t) = k_{ac} * R_{dc} * \sum_{T_c^0}^{T_c^{max}} * [1 + \alpha(T_c(t) - T_{ref}^0)] \quad (8)$$

where the line AC/DC resistance ratio k_{ac} in (9) is calculated after considering the line current density. The current density, moreover, is based on current redistribution and the magnetic core losses inside the overhead line [23]-[24].

$$k_{ac} = \frac{R_{ac}}{R_{dc}} \quad (9)$$

Based on (8), the higher the line temperature, the higher the line AC series resistance will be. Similarly, any decrease in the line temperature will reduce the line AC resistance. A time-dependent step increase in the load current from $I_1(t)$ to $I_2(t)$ will cause heating of the ACSR conductor. This step change in the line current, when coupled with solar heat gain, will increase the line temperature to its maximum value $T_c^{max}(t)$ in time t during the time- and space-dependent conductor heating state $C_h^{max}(t)$ as shown in (10) [23].

$$C_h^{max}(t) = \frac{(I_2^2(t) * R_{ac}(t)) + (P_s(t))}{\pi * D * (T_c^{max}(t) - T_a(t))} \quad (10)$$

The line temperature, based on the line loading and actual weather conditions, determines the dynamic line ampacity. The ETC-based coordination between the line temperature and its ampacity during conductor heating in the dynamic state is calculated using (11).

$$T_{ETC,t} = \frac{\left(\begin{array}{l} R_{ac}(t) * I_2^2(t) * (1 - \alpha * T_{ref}^0) \\ + (D * (P_s(t) + \pi * C_h^{max}(t) * T_a(t))) \end{array} \right)}{(\pi * D * C_h^{max}(t)) - (\alpha * k_{ac} * R_{dc} * I_2^2(t))} \quad (11)$$

As shown in (11), the line temperature in a combined ETC technique further helps in determining the after-contingency rise in the line temperature and its associated overload current during time $\Delta t(t_i - t_{i-1})$ as shown in (12),

$$T_{ETC,h} = T_{ETC,t} - \left[(T_{ETC,t} - T_{ETC,t-1}) e^{\left(-\frac{\Delta t}{\Delta_{h,l}} \right)} \right] \quad (12)$$

where the heating time constant $\Delta_{h,l}$ as shown in (13) is considered responsible for determining the duration of line temperature rise in the dynamic heating state.

$$\Delta_{h,l} = \frac{m * C}{(\pi * D * C_h^{max}(t)) - (\alpha * k_{ac} * R_{dc} * I_2^2(t))} \quad (13)$$

In the ETC-based line rating technique, contingency-influenced rise in the line temperature varies over time and depends on the conductor's specific heat capacity, conductor mass, line loading and ambient weather. As shown in (11), time- and loading-dependent overload current $I_2(t)$ causes conductor heating during step time Δt . In the ETC-based line rating techniques, during the line heating state, the initial temperature from the pre-load state $T_{ETC,t-1}$ is used to calculate the line temperature in time t_i as shown in (12), where the heating time constant $\Delta_{h,l}$ as shown in (13) is considered responsible for determining the duration of the line temperature rise in the dynamic heating state.

After attaining the maximum safe temperature limit during contingency, the overhead line returns to the post-disturbance or cooling state, where the temperature across it starts falling from its peak limit to the pre-load steady state. Equation (14) represents the fall in the line temperature from its maximum to minimum value during its time- and space-dependent cooling state $C_c^{min}(t)$ [23].

$$C_c^{min}(t) = \frac{(I_1^2(t) * R_{ac}(t)) + (P_s(t))}{\pi * D * (T_c^{min}(t) - T_a(t))} \quad (14)$$

During the cooling state, the overhead line follows the same pattern of linear variation that it experiences during the heating state but in the reverse direction, i.e., the line experiences a linear drop in temperature. This linear drop in overhead line temperature can be determined using (15).

$$T_{ETC,t+1} = \frac{\left(R_{ac}(t) * I_1^2(t) * (1 - \alpha * T_{ref}^0) \right) + \left(D * (P_s(t) + \pi * C_c^{min}(t) * T_a(t)) \right)}{(\pi * D * C_c^{min}(t)) - (\alpha * k_{ac} * R_{dc} * I_1^2(t))} \quad (15)$$

As shown in (15), the post-overload current $I_1(\mathbf{t})$ causes line cooling during step time $\Delta t(\mathbf{t}_i - \mathbf{t}_{i-1})$. Line cooling takes the initial temperature from the previous loading state $T_{ETC,t}$ and calculates the line temperature during time \mathbf{t}_{i+1} in the conductor's cooling state as shown in (16),

$$T_{ETC,c} = \left| T_{ETC,t+1} - \left[(T_{ETC,t+1} - T_{ETC,t}) e^{\left(\frac{-\Delta t}{\Delta_{c,l}} \right)} \right] \right| \quad (16)$$

where the cooling time constant $\Delta_{c,l}$ as shown in (17) is responsible for determining the duration of the line temperature drop in the dynamic cooling state.

$$\Delta_{c,l} = \frac{m * C}{(\pi * D * C_c^{min}(t)) - (\alpha * k_{ac} * R_{dc} * I_1^2(t))} \quad (17)$$

The line temperature from the coupled electro-thermal model gives the time- and space-dependent ohmic losses $P_{losses}(\mathbf{t})$ as shown in (18).

$$P_{losses,l}(t) = I^2 * R_{ac}(T_c(t)) \quad (18)$$

The line reactance X_l is not directly affected by temperature variations and therefore the effect of line temperature on conductance G_{ij} as shown in (19) will be higher than on the line susceptance B_{ij} as represented in (20).

$$G_{ij}(T_c(t)) = \frac{R_{ac}(T_c(t))}{R_{ac}^2(T_c(t)) + X_l^2} \quad (19)$$

$$B_{ij}(T_c(t)) = \frac{-X_l}{R_{ac}^2(T_c(t)) + X_l^2} \quad (20)$$

3.1.2 ETC versus conventional line rating technique

The electro-thermally coupled line rating technique under both static and dynamic weather conditions incorporates the line temperature change effect on the line's AC resistance. The impact of temperature-dependent line AC resistance is thereafter investigated with regard to line flow and the bus voltage magnitude. The conventional non-ETC-based line rating technique works under non-steady-state HBE, where the line resistance remains constant irrespective of changes in line temperature, making them mutually uncoupled in every step-change in line current. It is therefore, in the non-ETC-based technique, the line's temperature limit is transferred into the MAT thermal limit, leading to reduced electricity transfer.

In the presented ETC-based line rating technique, the subject overhead line is operated under its temperature limit until it reaches thermal equilibrium, taking advantage of a cool line to achieve higher active power flow in comparison to the non-ETC-based technique.

Due to the non-transfer of the subject line's temperature limit into the thermal limit, the thermal inertia of the overhead line helps in coupling the line's electrical and thermal behaviours, causing higher active power flow than the conventional non-ETC-based line rating technique. In this study, the AC resistance of the subject overhead line was kept constant at $0.2592 \Omega/\text{km}$ by keeping $T_c^{max} = 80^\circ\text{C}$ and $T_{ref}^0 = 20^\circ\text{C}$ under all loading and environmental conditions. The conventional line rating technique was calculated through (2)-(17) under real-time weather based non-steady-state HBE.

3.2 Sensitivity analysis

Sensitivity analysis is carried out to determine the impact of time-varying weather inputs on time-dependent heat transfer through the overhead line. It is performed to show the effectiveness of the proposed line rating technique in relation to actual loading and the weather data. In this study, sensitivity analysis is carried out for the presented ETC-DWLR technique; 1) to determine a correlation between weather elements across critical spans versus weather elements at all line spans and 2) to evaluate a correlation between wind speed and line temperature and between ambient and line temperatures.

3.2.1 Variance of ambient variables

To predict the variance in ambient weather between critical and all line spans, a variance analysis is considered, providing the percentage variation in the ambient weather at critical spans versus the ambient weather at line spans of the subject overhead line. The results obtained from the variance analysis are further shown in Table 1-7.

Table 1 Critical span versus all line spans at $t=0^+$ min.

Critical spans	Wind speed (%)	Ambient temperature (%)	Solar radiation (%)
Span-1	4.8	2.6	3.0
Span-2	5.1	2.5	8.3
Span-3	4.2	3.8	17.9

Table 2 Critical span versus all line spans at $t=5^+$ min.

Critical spans	Wind speed (%)	Ambient temperature (%)	Solar radiation (%)
Span-1	2.1	4.3	6.6
Span-2	6.3	3.5	2.0
Span-3	6.5	3.1	17.7

Table 3 Critical span versus all line spans at $t=10^+$ min.

Critical spans	Wind speed (%)	Ambient temperature (%)	Solar radiation (%)
Span-1	6.8	3.7	1.6
Span-2	12.2	2.4	6.5
Span-3	11.9	2.8	23.1

Table 5 Critical span versus all line spans at $t=20^+$ min.

Critical spans	Wind speed (%)	Ambient temperature (%)	Solar radiation (%)
Span-1	7.7	3.1	6.2
Span-2	17.2	2.9	11.1
Span-3	17.3	4.0	31.4

Table 4 Critical span versus all line spans at $t=15^+$ min.

Critical spans	Wind speed (%)	Ambient temperature (%)	Solar radiation (%)
Span-1	5.8	1.4	12.9
Span-2	13.4	3.5	0.3
Span-3	13.3	6.1	37.4

Table 6 Critical span versus all line spans at $t=25^+$ min.

Critical spans	Wind speed (%)	Ambient temperature (%)	Solar radiation (%)
Span-1	9.8	4.7	1.9
Span-2	21.1	2.2	22.0
Span-3	21.5	1.8	29.4

Table 7 Critical span versus all line spans at $t=30^+$ min.

Critical spans	Wind speed (%)	Ambient temperature (%)	Solar radiation (%)
Span-1	1.1	6.9	5.2
Span-2	0.1	3.3	0.3
Span-3	0.4	0.0	1.4

3.2.2 Sensitivity of line ratings to ambient variables

A global sensitivity index between 1) wind speed and line temperature and 2) ambient and line temperature was created with the help of the variance-based sensitivity analysis method as presented in [25]-[27]. According to this method, the variance-based sensitivity index between the correlated input parameters is required to provide the degree of sensitivity of the line temperature to the weather elements further shown in equations (21)-(26).

The correlation of wind speed and ambient temperature with line temperature is achieved using Pearson's correlation coefficient r to provide a correlation estimate between independent and dependent variables. In equation (21), the numerator shows the product of two variables subtracted from their respective means and the denominator adjusts the

variable scaling to give identical units [28]. The value of the correlation coefficient from equation (21) [28] is used in (22)-(23) [25] to find the covariance between independent variables (ambient temperature and wind speed) \mathbf{X} and the dependent variable \mathbf{Y} (line temperature). The resulting covariances are then used in (24)-(25) to produce the sensitivity index as shown in (26).

$$r_{(1,2)} = \frac{\sum_{i=1}^n (X_i - \bar{X}_i)(Y_i - \bar{Y}_i)}{\{\sum_{i=1}^n (X_i - \bar{X}_i)^2 \sum_{i=1}^n (Y_i - \bar{Y}_i)^2\}^{1/2}} \quad (21)$$

As shown in (21), n is the length of input variables. The value r_1 of input variable \mathbf{X} and value of r_2 of input variable \mathbf{Y} are averaged across all the critical spans from $t=0^+$ min to $t=30^+$ min to get the correlated partial variance $V_{corr,1}$ between wind speed and line temperature and the correlated partial variance $V_{corr,2}$ between ambient and line temperatures as shown in (22) and (23), respectively.

$$V_{corr,1} = 2r_1 \sigma_1 \sigma_2 \rho_1 \rho_2 + r_1^2 \rho_1^2 \sigma_1^2 + r_1^2 \rho_2^2 \sigma_2^2 \quad (22)$$

$$V_{corr,2} = 2r_2 \sigma_2 \sigma_1 \rho_2 \rho_1 + r_2^2 \rho_1^2 \sigma_1^2 + r_2^2 \rho_2^2 \sigma_2^2 \quad (23)$$

As shown in (22)-(23), the standard deviations σ_1 of \mathbf{X} and σ_2 of \mathbf{Y} with their respective partial derivatives ρ_1 and ρ_2 give the covariance between independent and dependent variables as the correlated partial variance matrix as shown in (24). The resulting correlation from (21) is used to find the covariance between \mathbf{X} and \mathbf{Y} as shown in (22)-(24).

$$V_{corr} = [V_{cor,1} \quad V_{cor,2}]^T \quad (24)$$

$$V_{Total} = \sum_{i=1}^n \rho_{i,1}^2 \sigma_{i,1}^2 + \sum_{i=1}^n \rho_{i,2}^2 \sigma_{i,2}^2 + 2 \rho_{(a,b)} \sigma_1 \sigma_2 \rho_1 \rho_2 + 2 \rho_{(a,b)} \sigma_1 \sigma_2 \rho_1 \rho_2 \quad (25)$$

The total correlated partial variance (25) is used to determine the sensitivity index between the weather elements and the line temperature as shown in (26) [25]-[27].

$$S_{index} = \frac{V_{corr}}{V_{Total}} \quad (26)$$

It is important to analyse the influence of weather elements on line temperature when determining the thermal loadability of the overhead lines. The obtained results are moreover shown in section 4.4.

4. Case study

To analyze and validate the effectiveness of the presented ETC-DWLR technique in comparison to the ETC-SWLR and DLR techniques, temperature and line-flow through the subject overhead line were calculated using the MATPOWER embedded developed

power-flow tool as mentioned in section 5. Network modeling and power-flow analysis under two loading scenarios were carried out on following test system facing multiple weather conditions.

4.1 Test System

The system modeling was performed on an IEEE-39 bus system as shown in Fig. 1 using DigSILENT PowerFactory. The base IEEE-39 bus model in [29] was modified by adding two overhead lines between bus-37 and bus-30 in Area-1 of the test system to analyze the validity of the ETC-DWLR in comparison to ETC-SWLR and DLR. For this purpose, a 100 km-long Line-1 in Area-1 with an operating voltage of 132 kV was considered as the subject overhead line. The line was loaded based on two realistic loading scenarios where the line's thermal capacity was checked during a non-steady state of the modelled power system. The line current from the test system was fed into the line thermal capacity algorithm to find the maximum thermal capacity of the subject line under the constraints of minimum allowable ground clearance of the line spans and the MAT limit of the line. The modeled system in Fig. 1 is referred as the test system throughout this paper.

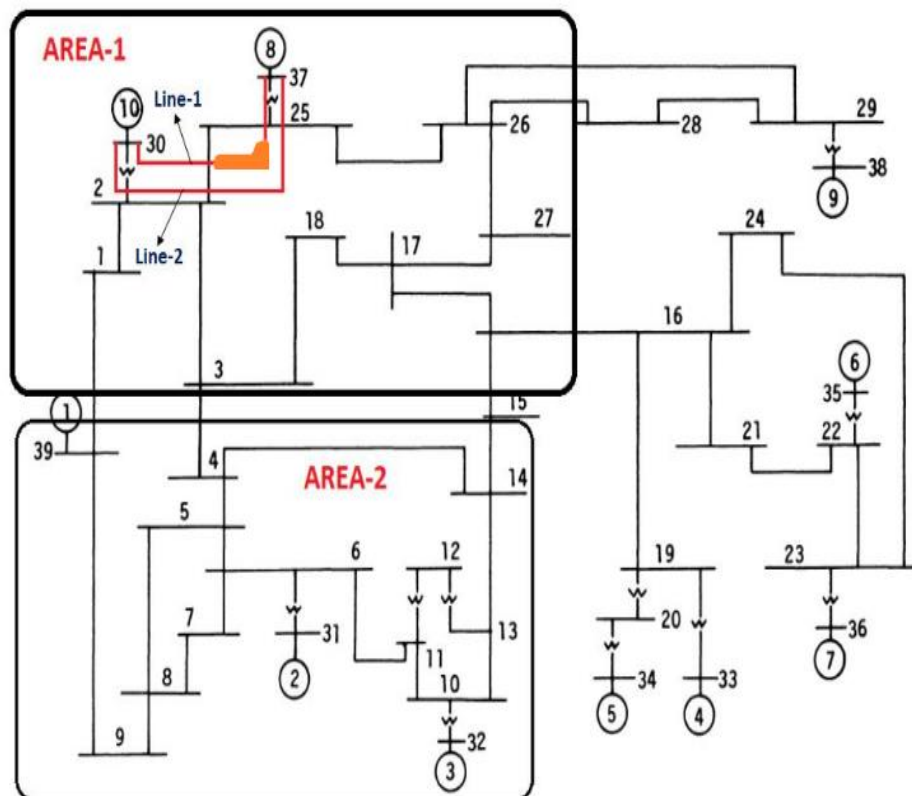


Fig. 1 Modified IEEE 39 bus system with overhead lines added in Area-1

4.2 Weather data

The subject overhead line (Line-1) in Fig. 1 passed through a large geographical region spanning varying terrains and was exposed to complex weather conditions. In addition, the subject overhead line had multiple segments and each segment had n non-equidistant spans, based on their geographical locations in accordance with the IEEE-39 bus structure. The test system was established in New Zealand and therefore the 1-hour weather data (ambient temperature, wind speed and solar radiation) from 12:30 pm to 13:30 pm on 1 January-2018 were obtained from NIWA [30] and applied to a 100 km-long overhead line passing three weather stations situated in the North Island of New Zealand. The subject line was considered to be a semi-urban type with 12% ultimate tensile strength (UTS) [31]. The physical dimensions of overhead lines as added in area-1 of the test system are shown in Table 8.

Table 8 The studied overhead lines physical dimensions

Overhead Lines	Diameter (mm)	Conductor Mass (kg/m)	Coefficient of linear expansion $\times 10^{-6}/^{\circ}\text{C}$
Line-1	17.5	0.677	19.4
Line-2	31.5	1.96	20.6

4.3 Loading scenarios

4.3.1 Temporary line outage

In the test scenario, Line-2 in the test system is disconnected for some time to carry out maintenance work. During this period, Line-1, as the subject overhead line, carries excess power and is therefore checked for thermal capacity in terms of thermal delay. Based on the line thermal inertia, the overhead conductor could be loaded reliably without violating the ground clearance requirements. The objective of the presented ETC technique is to load the subject line to find its maximum power transfer capacity when operating under the MAT limit as set at 80°C .

The line flow results in Table 9 are based on weather- and loading-dependent line resistance, where Line-1 is checked during heating and cooling states after the disconnection and restoration of Line-2, respectively. The weather data used to obtain the results as shown in Table 9 are based on critical-span 3, assumed to be the most critical span during the line transient loading. From $t=10^{+}$ min to $t=20^{+}$ min, Line-2 is disconnected, causing Line-1 to enter the heating state. Later, at $t=20^{+}$ min, Line-2 is restored, reducing the load-flow on Line-1, placing it in the cooling state. During the

dynamic system state from $t=10^+$ min to $t=20^+$ min, Line-2 experiences contingency and the resulting temperature across Line-1 plays an important role in the line sagging level. When Line-2 is disconnected at $t=10^+$ min, the transmission operator has two options; either to import electricity from Gen-10 in the test system, which has a low up-ramping capability (hence responding slowly to peak-loads) or to load Line-1 based on the presented line rating technique. The former option is not feasible for the transmission operator if Gen-08 has enough capacity to dispatch the required excess electricity through Line-1 when needed without any violation of Line-1 ground-clearance infringements. The time-varying line current from DIgSILENT PowerFactory was used to find line temperature through ETC-DWLR, ETC-SWLR and DLR techniques under critical span-1 and critical span-2 as shown in Table 10.

As evident from Table 9, after the Line-2 outage, the proposed ETC-DWLR approach helps in maximizing the power transfer potential from Line-1, in contrast to conventional DLR and the static weather-based ETC-SWLR techniques. As evident from Table 9, when Line-2 is restored at $t=20^+$ min, temperature across Line-1 starts dropping from the peak value until it reaches the pre-fault steady state. The ETC-DWLR technique as shown in Table 9 allows 6.18% additional power transfer compared to the ETC-SWLR technique and 7.75% higher than the DLR technique during Line-1 operation. In terms of finding the highest line temperature amongst all spans of the subject overhead line, the critical span with the highest sag from $t=10^+$ min to $t=20^+$ min was used to determine the thermal rating of the subject overhead line during this time. By facing the worst weather and having the longest length with a route passing through a varying terrain, it remained the span with the highest sag until weather conditions changed.

Table 9 Temporary line-2 outage management in case of critical span-3 under scenario-A

Time (Min.)	Temperature (°C)			Line Flows (MW)		
	ETC-DWLR	ETC-SWLR	DLR	ETC-DWLR	ETC-SWLR	DLR
	Line-1	Line-1	Line-1	Line-1	Line-1	Line-1
0	40.42	61.927	40.42	61.03	58.01	55.66
5	41.26	61.927	41.26	60.87	58.01	55.66
10	54.84	84.48	54.84	72.16	67.42	68.08
15	54.71	84.48	54.71	72.16	67.42	68.08
20	54.37	84.48	54.37	72.16	67.42	68.08
25	43.26	70.56	43.26	60.55	56.93	55.66
30	40.29	61.93	40.29	61.03	58.01	55.66

Table 10 Line-1 temperature in case of critical span-1 and critical span-2 under scenario-A

Time (Min.)	Temperature (°C) —Critical Span-1			Temperature (°C) —Critical Span-2		
	ETC-DWLR	ETC-SWLR	DLR	ETC-DWLR	ETC-SWLR	DLR
0	40.34	61.93	40.34	40.38	61.93	40.38
5	40.97	61.93	40.97	41.34	61.93	41.34
10	54.26	84.48	54.26	54.98	84.48	54.98
15	53.34	84.48	53.34	54.35	84.48	54.35
20	53.80	84.48	53.80	53.66	84.48	53.66
25	43.53	70.56	43.53	43.48	70.56	43.48
30	41.13	61.93	41.13	41.18	61.93	41.18

4.3.2 Line overloading and load-shedding management

The ETC and conventional line rating techniques were investigated under this scenario to check the effectiveness of the line rating techniques in avoiding line loading and effectively managing load shedding situations. Under this scenario, Line-2 is required to be out of service (e.g. because of maintenance) from $t=5^+$ min to $t=25^+$ min. Similarly, Gen-08 at Bus-37 in the test system dispatches 640 MW of active power during a continuous increment in load demand, as mentioned in Table 11. In this scenario, the main objectives of a transmission operator are to fulfil the load requirement in addition to avoiding the subject line from crossing the MAT limit.

As shown in Table 11, for critical span-3, the static worst weather elements in the ETC-SWLR technique result in line temperature above the MAT limit even at the base load of 50 MW in all case states, causing 24% higher congestion in the subject line than ETC-DWLR and 21.3% more congestion than the DLR technique. It means subject line under ETC-SWLR technique is more congested in comparison to ETC-DWLR than the DLR technique. The line current due to step change in load demand was obtained from DigSILENT PowerFactory and was used to find the line temperature through ETC-DWLR, ETC-SWLR and DLR techniques as shown in Table 12 for critical span-1 and critical span-2. The resulting line temperature determines the line AC resistance, which together with ambient and line physical data is provided to the MATPOWER-integrated tool described in section 5 to provide the line active power flow in presence of critical span-3 as shown in Table 13.

Due to reaching the MAT limit at the baseload, line operating under ETC-SWLR technique is not further loaded, hence a total of 102 MWh of electricity is not dispatched

under this technique through Line-1 to the load connected at bus-30 of the test system from $t=5^+$ min to $t=25^+$ min. From $t=25^+$ min to $t=30^+$ min, when 25% load is reduced from the previous step under both lines connected makes Line-1 attain temperature below the MAT limit hence causes an additional energy dispatch of 5.1% from the previous value. As shown in Table 11, the higher voltage drop using the DLR technique results from ignoring the line coupling between electrical and thermal behaviours, in contrast to the ETC-DWLR technique, where a cool line provides lower AC resistance and lower voltage drop, resulting in no line overload or load shedding. As shown in Table 14 and 15, at $t=20^+$ min when temperature across both overhead lines converge to near steady-state MAT value, the AC resistance of both lines becomes equivalent thus causing the identical line flow through the subject overhead line.

Table 11 Line-1 temperature in case of critical span-3 under scenario-B

Time (Min.)	Case-State(s) Type(s)	Line-1 Temperature (°C)		
		ETC-DWLR	ETC-SWLR	DLR
0	Baseload with Line-2 Disconnected	50.54	84.48	50.54
5	30% Increment in Baseload at Line-2 Disconnected	57.57	84.48	57.57
10	50% Increment in Baseload at Line-2 Disconnected	66.10	84.48	66.10
15	80% Increment in Baseload at Line-2 Disconnected	73.59	84.48	73.59
20	100% Increment in Baseload at Line-2 Disconnected	79.94	84.48	79.94
25	Line-2 is Restored at twice the Baseload	58.50	84.48	58.50
30	25% Load Decrease with Line-2 Connected	46.92	70.53	46.92

Table 12 Line temperature in case of critical span-1 and critical span-2 under scenario-B

Time (Min.)	Temperature (°C)—Critical Span-1			Temperature (°C)—Critical Span-2		
	ETC-DWLR	ETC-SWLR	DLR	ETC-DWLR	ETC-SWLR	DLR
0	50.52	84.48	50.52	50.55	84.48	50.55
5	57.31	84.48	57.31	57.68	84.48	57.68
10	65.49	84.48	65.49	66.24	84.48	66.24
15	72.45	84.48	72.45	73.40	84.48	73.40
20	79.57	84.48	79.57	79.44	84.48	79.44
25	58.77	84.48	58.77	58.72	84.48	58.72
30	47.77	70.53	47.77	47.81	70.53	47.81

Table 13 Line flows and load shed in case of critical span-3 under scenario-B

Time (Min.)	Line-1 Flows (MW)			Load Shed (MW) at Bus-30		
	ETC-DWLR	ETC-SWLR	DLR	ETC-DWLR	ETC-SWLR	DLR
0	72.72	67.42	68.08	0	0	0
5	82.56	67.42	78.67	0	145	0
10	89.12	67.42	86.60	0	235	0
15	101.64	67.42	100.38	0	362	0
20	111.60	67.42	111.60	0	440	0
25	92.50	67.42	88.69	0	42	0
30	75.29	70.85	70.19	0	0	0
Total energy shed (MWh)				0	102	0

4.4 Weather impact on line thermal loading

4.4.1 Sensitivity index between wind speed and line temperature

Fig. 2 shows the sensitivity index between wind speed and line temperature across three critical spans in scenario-A and scenario-B, where the correlation coefficient from (21) is averaged for line temperature from both scenarios from $t=0^+$ min to $t=30^+$ min. Based on Fig. 2, the computed real-time thermal line ratings in both scenarios were observed to be highly sensitive to wind speed, reaching as high as 0.621 or 62.1% at $t=20^+$ min across critical span-1 and as low as 0.404 or 40.4% at $t=30^+$ min across the same line span.

4.4.2 Sensitivity index between ambient and line temperature

The sensitivity index between ambient and line temperatures across critical span-1 under scenario-A and scenario-B is shown in Fig. 3 (a), whereas the same relationship across critical span-2 and critical span-3 under both scenarios is shown in Fig. 3 (b) and Fig. 3 (c) respectively, where the results obtained indicate that the line thermal rating is less sensitive to the ambient temperature in comparison to the wind speed and hence makes a less significant contribution to both conductor cooling and line loadability.

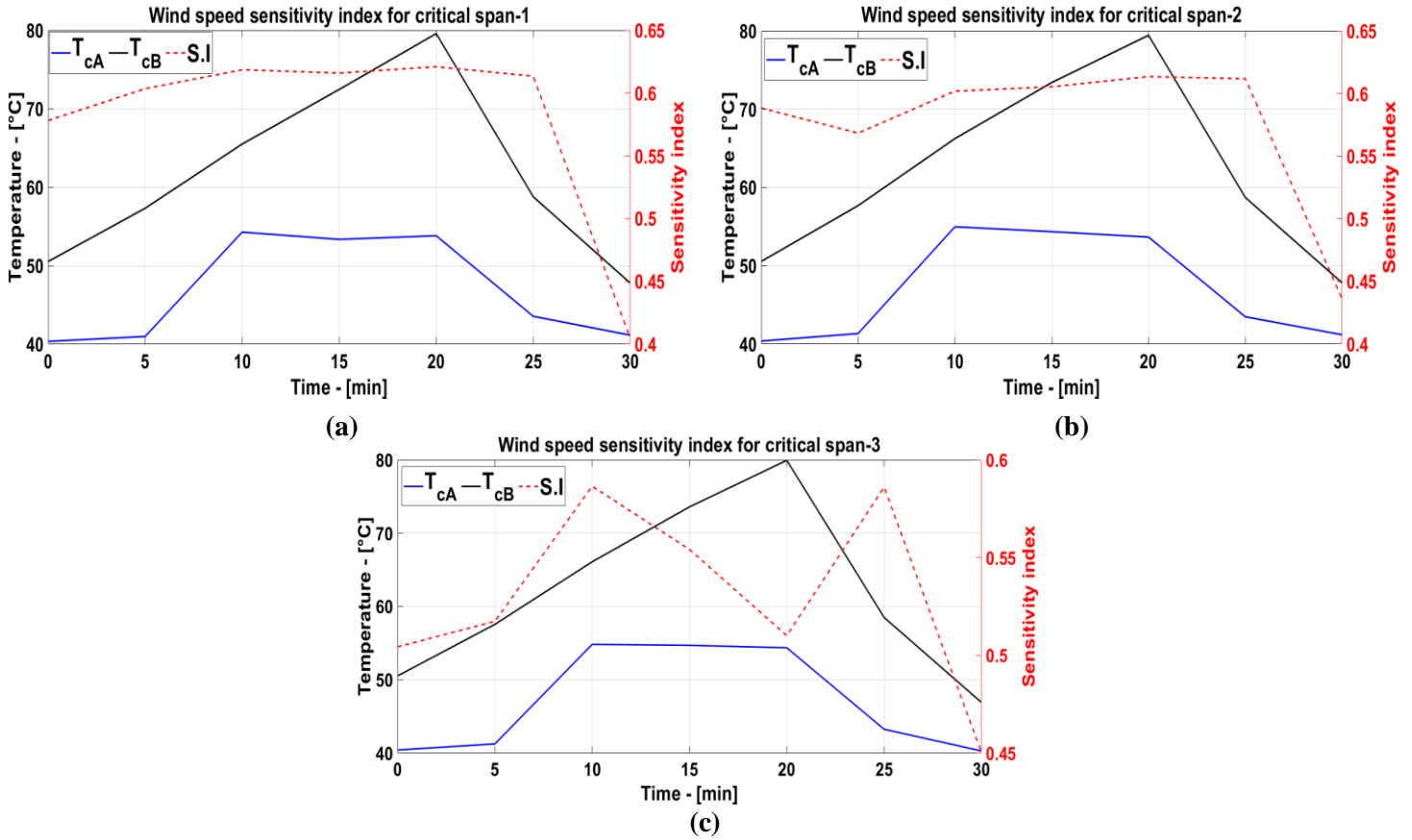


Fig. 2 Wind speed-line temperature sensitivity index across critical spans: a) # 1 b) # 2 c) # 3

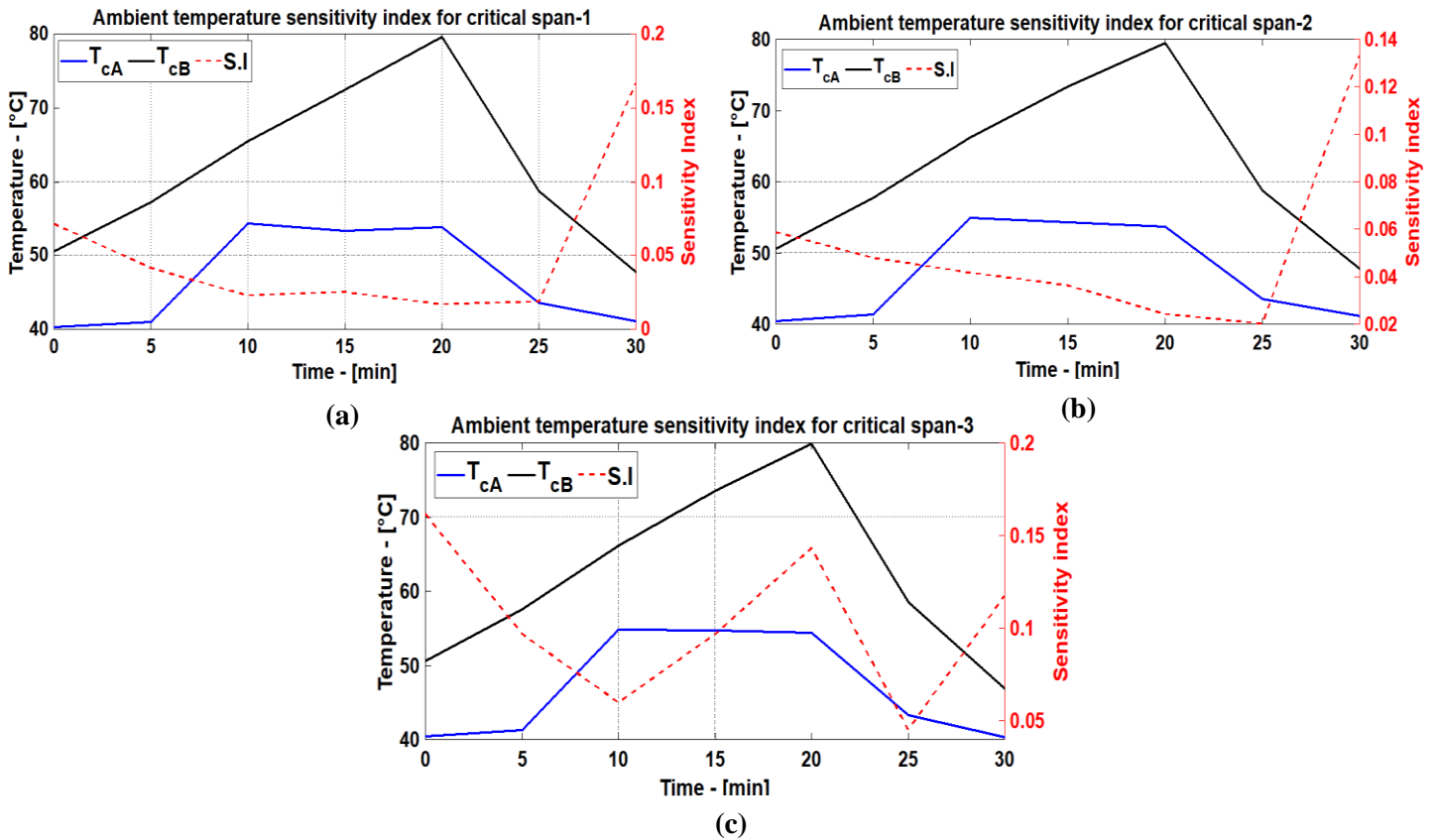


Fig. 3 Ambient & line temperature sensitivity index across critical spans: a) # 1 b) # 2 c) # 3

5. Weather-Dependent Power Flow Tool

Due to the influence of weather on thermal line loading, the ambient data must be incorporated with line loading to obtain the weather-influenced active power and the voltage magnitude. For this purpose, a MATPOWER [32] embedded power flow tool as shown in Fig. 4 is used to provide electro-thermally coupled parameters. The designed tool for power flow analysis includes weather and line temperature data across critical spans, physical data from overhead lines, generators, loads and buses in the IEEE-39 bus system from [29], [32] in addition to physical data from the added Line-1 and Line-2 in the presence of critical spans across Line-1. The flow chart as shown in Fig. 5 describes the calculation of line temperature under the investigated line rating techniques used as an input to the designed power flow tool, enabling determination of the bus voltage magnitude and sag across the critical spans through HBE and the updated line resistance. The line resistance used in the presented ETC technique is based on reference temperatures that are dependent on previous reference and line temperatures influenced by step-changes in line current and weather conditions.

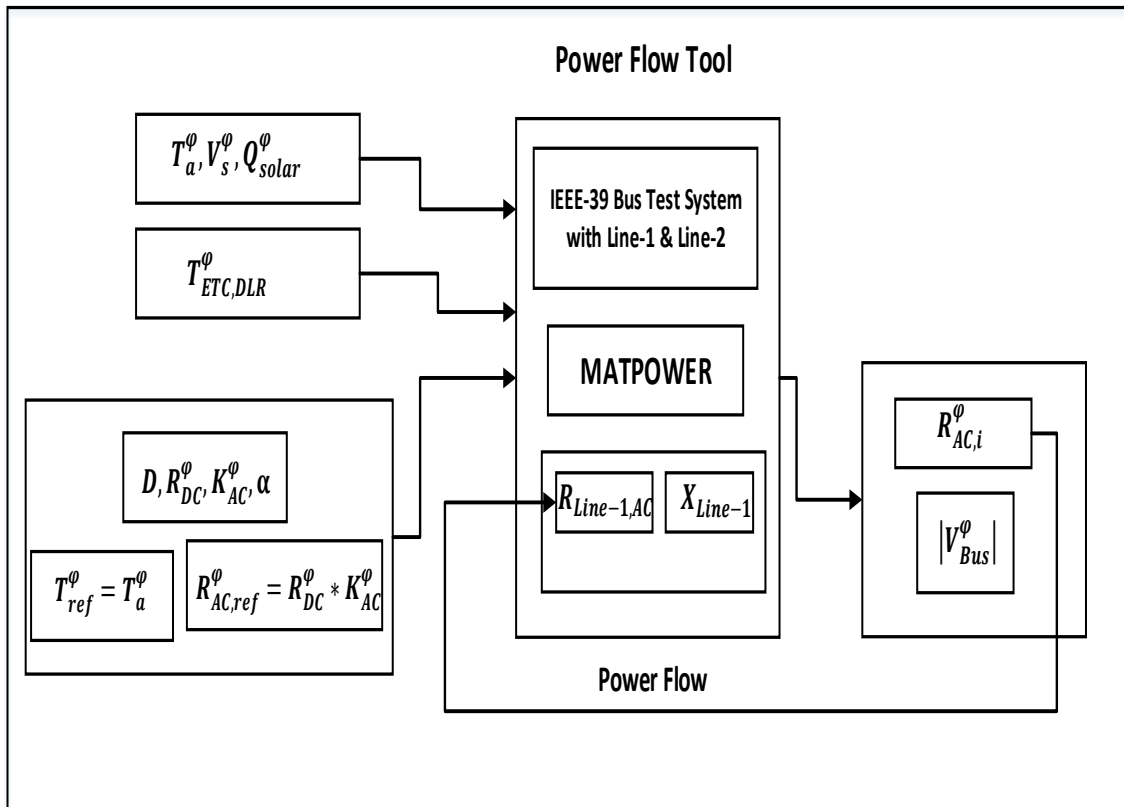


Fig. 4 ETC and weather-integrated line power flow-tool

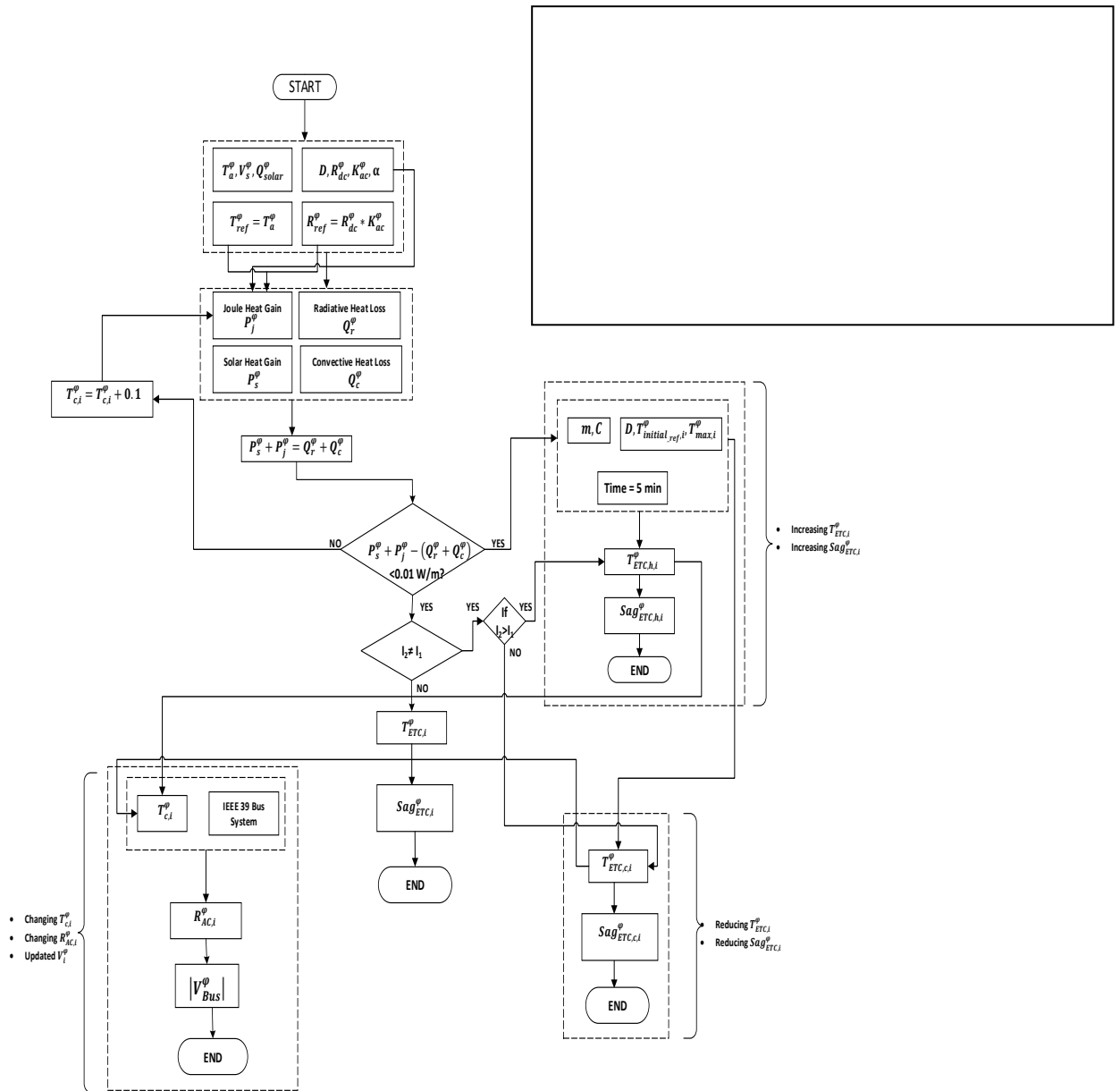


Fig. 5 Flow chart of the presented ETC line rating technique algorithm

5.1 Results and discussion

The weather and loading-dependent line resistance and bus voltage were investigated under scenario-A representing the line-disconnection and scenario-B representing the increased line congestion. Both scenarios were considered in the presence of critical spans to find their impact on the line resistance and bus voltage magnitude, shown in Table 14 and Table 15. The results obtain show that line loading, span-topography and weather conditions directly affect line resistance, which in turn changes the system voltage. By considering the critical line spans and the presented line rating techniques, the resulting voltage through the developed power-flow tool can be effective in both system planning

and operation.

Tables 14 and 15 show that the bus voltage decreased with increases in the line's AC resistance, and the line resistance under the ETC-SWLR technique was higher than under the ETC-DWLR technique due to the higher line temperature. Based on identical maximum span lengths with slight differences in weather conditions across all critical spans, the change in line resistance from the ETC-SWLR to ETC-DWLR technique was reduced on average by 8.5% under all critical line spans in scenario-B.

Table 14 Span resistance versus bus voltage under scenario—A

Time (min)	Critical Span-1 (ETC-DWLR)		Critical Span-1 (ETC-SWLR)		Critical Span-2 (ETC-DWLR)		Critical Span-2 (ETC-SWLR)		Critical Span-3 (ETC-DWLR)		Critical Span-3 (ETC-SWLR)	
	R (Ω /km)	V (pu)										
0	0.233	0.966	0.252	0.965	0.233	0.966	0.252	0.965	0.233	0.966	0.252	0.965
5	0.234	0.966	0.252	0.965	0.234	0.966	0.252	0.965	0.234	0.966	0.252	0.965
10	0.245	0.957	0.271	0.956	0.246	0.957	0.271	0.956	0.245	0.957	0.271	0.956
15	0.244	0.957	0.271	0.956	0.245	0.957	0.271	0.956	0.245	0.957	0.271	0.956
20	0.245	0.957	0.271	0.956	0.245	0.957	0.271	0.956	0.245	0.957	0.271	0.956
25	0.236	0.966	0.259	0.965	0.236	0.966	0.259	0.965	0.236	0.966	0.259	0.965
30	0.234	0.966	0.252	0.965	0.234	0.966	0.252	0.965	0.233	0.966	0.252	0.965

Table 15 Span resistance versus bus voltage under scenario—B

Time (min)	Critical Span-1 (ETC-DWLR)		Critical Span-1 (ETC-SWLR)		Critical Span-2 (ETC-DWLR)		Critical Span-2 (ETC-SWLR)		Critical Span-3 (ETC-DWLR)		Critical Span-3 (ETC-SWLR)	
	R (Ω /km)	V (pu)										
0	0.242	0.957	0.271	0.956	0.242	0.957	0.271	0.956	0.242	0.957	0.271	0.956
5	0.248	0.939	0.271	0.956	0.248	0.939	0.271	0.956	0.248	0.939	0.271	0.956
10	0.255	0.923	0.271	0.956	0.255	0.923	0.271	0.956	0.255	0.923	0.271	0.956
15	0.261	0.892	0.271	0.956	0.262	0.892	0.271	0.956	0.262	0.892	0.271	0.956
20	0.267	0.864	0.271	0.956	0.267	0.864	0.271	0.956	0.267	0.864	0.271	0.956
25	0.249	0.896	0.271	0.956	0.249	0.896	0.271	0.956	0.249	0.896	0.271	0.956
30	0.239	0.94	0.259	0.939	0.239	0.94	0.259	0.939	0.239	0.94	0.259	0.939

6. Discussion

This paper presents the concept of a coupling effect between electrical and thermal models of an overhead line passing through a large geographical area under multiple weather conditions. The electro-thermal coupling effect of an overhead line was investigated under both static and dynamic weather conditions. Additionally, HBE was investigated in non-steady state system modeling, where besides the impact of line resistance and the environmental conditions on thermal loading of an overhead line, the line's thermal inertia was also considered in determining the capacity of the thermally limited overhead line.

In this paper, mutual coupling between OHL's thermal and power transfer limits resulted in improved line loading efficiency in comparison to the conventional line rating technique involving the decoupled power transfer and thermal limits. Optimal line loading and the line congestion minimization in addition to depending on number and thermal limit of critical spans were also found with dependence on time synchronization between weather and load changes besides electrical and thermal characteristics of the overhead line. To consider these factors, the ETC-based weather integrated power flow tool was developed to find the load and weather dependent dynamic changes in heating and cooling of the overhead line. After incorporating these changes, the tool provided the updated temperature-dependent line series resistance which was later used to find the line flows and the corresponding voltage across the load bus under both the proposed and conventional line rating techniques. The summary of technical and economic benefits identified by using the weather incorporated ETC based proposed line rating technique is provided below.

- i. The proposed line rating technique due to involving the line thermal inertia and temperature-dependent line resistance provides enough loading time for electricity dispatch from slower but less expensive generation reserves. A possible economic benefit can be attained in case of electricity dispatch from wind power plants due to wind speed correlation between line cooling and the wind generation.
- ii. It involves thermal inertia in the non-steady or dynamic loading state causing the overhead line to obtain thermal equilibrium gradually. Due to this time delay from the loading time, transmission operators have flexibility in making optimum decisions regarding line flows based on both power transfer and

thermal limits. The obtained loading flexibility not only helps in reliable power transfer but also in avoiding or rescheduling the electricity dispatch from costly generation sources.

- iii. Due to loading flexibility, transmission operators have enough time in shifting the load flow from critical line paths to non-critical ones before critical lines attain the thermal equilibrium. By doing so, an anticipated congestion in the network can be minimized by increasing the line flow towards less congested high thermal-inertia lines and decreasing the line flow from highly congested low thermal-inertia lines. This optimum power transfer in the entire transmission network can result in economic and technical benefits; economic benefit in terms of delaying the line upgrading, while technical benefit in terms of relived congestion.
- iv. The proposed technique provides actual temperature-dependent line resistance that can benefit by reducing I^2R losses, causing higher power flow at minimum voltage dips in comparison to the conventional line rating techniques at the same line temperature and weather conditions.

The results obtained by using the real weather integrated ETC based line rating technique were validated with the conventional line rating technique, which ignores the temperature-dependent line resistance when determining the line flows. Based on these results, line resistance and thermal inertia were found to improve the line's thermal capacity by 7.75% when handling a line outage and 3.51% when handling line overloading (to avoid load shedding) under actual geospatial weather conditions.

When the subject overhead line was loaded to handle excess power due to line-disconnection, the presented ETC technique under dynamic weather conditions was found to have 6.17% more thermal capacity than the same technique applied under non-geospatial static worst-weather conditions. Similarly, when the same overhead line operating under geospatial weather conditions was used to avoid load-shedding, it was found to have 31.57% more thermal capacity than when operating under non-geospatial weather assumptions during the same loading scenario.

Variance and sensitivity analysis between weather and line temperature were presented to provide the ratings sensitivity, especially in the wind speed region of 10-14 kph (due to its high sensitivity). The results from the sensitivity analysis indicate that the thermal line ratings were highly sensitive to wind speed in comparison to ambient temperature.

Future work will be related to validating the presented line rating algorithm with field measurements to find the maximum thermal rating of thermally limited overhead lines. The work will also focus on numerical weather predictions to predict the geo-spatial weather conditions across electrically and thermally limited overhead lines in a multi-area power system, operating in dynamic and transient system states.

7. Conclusion

This study has presented a methodology for loading overhead lines based on electro-thermally coupled, dynamic weather-dependent line rating techniques. The ETC line rating technique as presented in this paper was used for dynamic-state system analysis applications, where short-term overloading of the overhead line was investigated under dynamic weather conditions. The ETC-DWLR technique, when compared with ETC-SWLR and conventional DLR techniques, was found to be efficient in minimizing line congestion and avoiding load-shedding situations. The calculated power flow through the subject overhead line showed that the proposed technique can mitigate congestion of the electricity network by excess risk-free power transfer. To analyze the sensitivity of the resulting line temperature to the ambient conditions, the sensitivity analysis undertaken showed a wider sensitivity range across wind speed than ambient temperature.

This study also analyzed the weather and loading impact in the presence of critical spans on the line AC resistance and the bus voltage magnitude through the designed line-modeling tool. The proposed approach investigated the environmental impact on the line AC resistance and voltage magnitude under critical line spans passing through flat and non-flat terrain. The results obtained showed that the line resistance calculated under the actual geospatial weather and dynamic loading states was more efficient in determining a reliable voltage magnitude than that found under the non-geospatial static weather states.

References

- [1] M. W. Davis, "A new thermal rating approach: The real time thermal rating system for strategic overhead conductor transmission lines -- Part I: General description and justification of the real time thermal rating system," in *IEEE Transactions on Power Apparatus and Systems*, vol. 96, no. 3, pp. 803-809, May 1977. doi: 10.1109/T-PAS.1977.32393.

-
- [2] IEEE Standard for Calculating the Current-Temperature Relationship of Bare Overhead Conductors," in *IEEE Std 738-2012 (Revision of IEEE Std 738-2006 - Incorporates IEEE Std 738-2012 Cor 1-2013)*, vol., no., pp.1-72, 23 Dec. 2013. doi: 10.1109/IEEESTD.2013.6692858.
- [3] M. W. Davis, "A new thermal rating approach: The real time thermal rating system for strategic overhead conductor transmission lines -- Part II: Steady state thermal rating program," in *IEEE Transactions on Power Apparatus and Systems*, vol. 96, no. 3, pp. 810-825, May 1977. doi: 10.1109/T-PAS.1977.32394.
- [4] Poli, Davide, et al. "The possible impact of weather uncertainty on the Dynamic Thermal Rating of transmission power lines: A Monte Carlo error-based approach." *Electric Power Systems Research* 170 (2019): 338-347.
- [5] Viafora, Nicola, et al. "Day-ahead dispatch optimization with dynamic thermal rating of transformers and overhead lines." *Electric Power Systems Research* 171 (2019): 194-208.
- [6] L. Dawson and A. M. Knight, "Applicability of Dynamic Thermal Line Rating for Long Lines," in *IEEE Transactions on Power Delivery*, vol. 33, no. 2, pp. 719-727, April 2018. doi: 10.1109/TPWRD.2017.2691671.
- [7] H. Banakar, N. Alguacil and F. D. Galiana, "Electrothermal coordination part I: theory and implementation schemes," in *IEEE Transactions on Power Systems*, vol. 20, no. 2, pp. 798-805, May 2005. doi: 10.1109/TPWRS.2005.846196.
- [8] N. Alguacil, M. H. Banakar and F. D. Galiana, "Electrothermal coordination part II: case studies," in *IEEE Transactions on Power Systems*, vol. 20, no. 4, pp. 1738-1745, Nov. 2005. doi: 10.1109/TPWRS.2005.857836.
- [9] M. Wang and X. Han, "Study on electro-thermal coupling optimal power flow model and its simplification," *IEEE PES General Meeting*, Providence, RI, 2010, pp. 1-6. doi: 10.1109/PES.2010.5589644.
- [10] A. Kubis and C. Rehtanz, "Application of a combined electro-thermal overhead line model in power flow and time-domain power system simulations," in *IET Generation, Transmission & Distribution*, vol. 11, no. 8, pp. 2041-2049, 16 2017. doi: 10.1049/iet-gtd.2016.1626.
- [11] J. Shu, R. Guan and L. Wu, "Optimal power flow in distribution network considering spatial electro-thermal coupling effect," in *IET Generation, Transmission & Distribution*, vol. 11, no. 5, pp. 1162-1169, 30 3 2017. doi: 10.1049/iet-gtd.2016.0909.

-
- [12] J. W. Jerrell, W. Z. Black and T. J. Parker, "Critical span analysis of overhead conductors," in *IEEE Transactions on Power Delivery*, vol. 3, no. 4, pp. 1942-1950, Oct. 1988. doi: 10.1109/61.194004.
- [13] Muñoz, F., et al. "Case study of the increase in capacity of transmission lines in the Chilean system through probabilistic calculation model based on dynamic thermal rating." *Electric Power Systems Research* 170 (2019): 35-47.
- [14] "Oncor's pioneering transmission dynamic line rating (DLR) demonstration lays foundation for follow-on deployments," U.S. Dept. Energy, MD, USA, 2014.
- [15] Chatzipanagiotou, P., and V. Chatziathanasiou. "Dynamic thermal analysis of a power line by simplified RC model networks: Theoretical and experimental analysis." *International Journal of Electrical Power & Energy Systems* 106 (2019): 288-293.
- [16] Theodosoglou, Ioanna, et al. "Electrothermal analysis and temperature fluctuations' prediction of overhead power lines." *International Journal of Electrical Power & Energy Systems* 87 (2017): 198-210.
- [17] Shuran Liu and K. Kopsidas, "Reliability evaluation of distribution networks incorporating cable electro-thermal properties," 2016 Power Systems Computation Conference (PSCC), Genoa, 2016, pp. 1-7. doi: 10.1109/PSCC.2016.7541003.
- [18] K. Kopsidas, C. Tumelo-Chakonta and C. Cruzat, "Power Network Reliability Evaluation Framework Considering OHL Electro-Thermal Design," in *IEEE Transactions on Power Systems*, vol. 31, no. 3, pp. 2463-2471, May 2016. doi: 10.1109/TPWRS.2015.2443499.
- [19] R. Olsen, J. Holboell and U. S. Gudmundsdóttir, "Electrothermal Coordination in Cable Based Transmission Grids," in *IEEE Transactions on Power Systems*, vol. 28, no. 4, pp. 4867-4874, Nov. 2013. doi: 10.1109/TPWRS.2013.2278040.
- [20] X. Dong et al., "Calculation of Power Transfer Limit Considering Electro-Thermal Coupling of Overhead Transmission Line," in *IEEE Transactions on Power Systems*, vol. 29, no. 4, pp. 1503-1511, July 2014. doi: 10.1109/TPWRS.2013.2296553.
- [21] A. Kubis and C. Rehtanz, "Synchrophasor based thermal overhead line monitoring considering line spans and thermal transients," in *IET Generation, Transmission & Distribution*, vol. 10, no. 5, pp. 1232-1239, 7 4 2016. doi: 10.1049/iet-gtd.2015.0852.

-
- [22] X. Dong, C. Kang, Y. Ding and C. Wang, "Estimating the Wind Power Integration Threshold Considering Electro-thermal Coupling of Overhead Transmission Lines," in *IEEE Transactions on Power Systems*. doi: 10.1109/TPWRS.2019.2906291.
- [23] Deb, Anjan K. *Powerline ampacity system: theory, modeling and applications*. CRC Press, 2017.
- [24] Morgan, Vincent T. "The thermal behaviour of electrical conductors." (1997).
- [25] Groen, Evelyne A., et al. "Methods for global sensitivity analysis in life cycle assessment." *The International Journal of Life Cycle Assessment* 22.7 (2017): 1125-1137.
- [26] Xu, Chonggang, and George Zdzislaw Gertner. "Uncertainty and sensitivity analysis for models with correlated parameters." *Reliability Engineering & System Safety* 93.10 (2008): 1563-1573.
- [27] Saltelli, Andrea, et al. "Variance based sensitivity analysis of model output. Design and estimator for the total sensitivity index." *Computer Physics Communications* 181.2 (2010): 259-270.
- [28] Lee Rodgers, Joseph, and W. Alan Nicewander. "Thirteen ways to look at the correlation coefficient." *The American Statistician* 42.1 (1988): 59-66.
- [29] T. Athay, R. Podmore and S. Virmani, "A Practical Method for the Direct Analysis of Transient Stability," in *IEEE Transactions on Power Apparatus and Systems*, vol. PAS-98, no. 2, pp. 573-584, March 1979. doi: 10.1109/TPAS.1979.319407.
- [30] National Institute of Water and Atmospheric Research (NIWA). [Online]. Available: <https://cliflo.niwa.co.nz/>. Accessed on 31st May 2019.
- [31] Ausgrid (2015) Network standard NS220. "Overhead design manual, NW000-S0092." Ausgrid.
- [32] R. D. Zimmerman, C. E. Murillo-Sanchez, and D. Gan, *MATPOWER 4.0*. Ithaca, NY: Cornell Univ., 2011. [Online]. Available: <http://www.pserc.cornell.edu/matpower/>. Accessed on 31st May 2019.

Chapter 3

3.1 Introduction to Manuscript 2

This Manuscript addresses the issue of critical span identification across an overhead line. The Manuscript presents a technique that is developed to identify space and time dependent critical spans at the least computational cost. Due to varying nature of critical spans across any overhead line facing multiple weather conditions; this Manuscript is therefore designed to capture the dynamically varying critical spans during each loading step. The identified critical spans are not considered fixed, rather they vary with time and space. The proposed technique identifies the dynamically varying critical spans after considering the weather and span topography at each line span.

The Manuscript is published in the journal of ‘Electrical Power Systems Research’ under the title: “Application of dynamic thermal rating: Overhead line critical spans identification under weather dependent optimized sensor placement.” *Electric Power Systems Research* 180 (2020): 106125.

3.2 Manuscript 2

Application of dynamic thermal rating: Overhead line critical spans identification under weather dependent optimized sensor placement

Saifal Talpur*, T. T. Lie, R. Zamora

School of Engineering, Computer and Mathematical Sciences, Auckland University of Technology, New Zealand

*Corresponding author email: saifal.talpur@aut.ac.nz

Abstract

Dynamic thermal rating (DTR) for an overhead transmission line is a viable and cost-effective technique based on real weather conditions to mitigate congestion and avoid load shedding for reliable transfer of the required electricity. Spans of overhead lines passing through multiple geographical regions face diverse weather conditions and varying terrain, and thus need to be monitored to obtain reliable estimates of line loadability. Spans facing the worst weather and with the longest length determine the absolute minimum line loadability and are therefore known as critical spans. Identifying critical spans is important in allowing utility providers to monitor their overhead transmission networks spanning large geographical regions. This paper focuses on identifying critical spans using the proposed technique to find the bottleneck to the overhead transmission network for optimum power transfer. It determines the optimal

number and placement of sensors across the entire test line, dividing the line into non-uniform segments, each carrying multiple length spans passing through flat and non-flat terrains. The resulting critical spans determine the line loadability that can effectively relieve transmission line congestion, based on the allowable vertical clearance to the ground. The outcome of the proposed technique is validated against the conventional technique for critical span identification.

Keywords: *Dynamic thermal rating, critical line spans, optimal sensor placement, non-uniform line segmentation, weather conditions and span topography, congestion and load shed management*

1. Introduction

To meet the growing demand for electricity, overhead transmission lines are required to transfer additional electricity with no ground clearance infringements. The capacity of overhead transmission lines is determined by their physical dimensions, surrounding weather conditions, maximum allowable temperature and the allowable distance from the ground. An overhead line passes through multiple geographical regions, where each span faces considerably different weather conditions.

As each span of an overhead line differs in length, weather conditions and route, the span elongation across each line span varies depending on space and time, even under the same loading and operational conditions. Therefore, the dynamic thermal rating (DTR) for the entire line cannot be calculated by ignoring the individual span lengths and their surrounding weather conditions as these may cause adverse sagging across spans facing the worst weather conditions during the loading period. The spans with minimum clearance to the ground at specific loading condition are called critical spans.

Critical spans operate at the highest temperature with the lowest current-carrying capability in a tensioning section between two towers. The span topography and ambient conditions across a line span are critical in its ability to transfer the required electricity. Because of the time- and space-dependent weather conditions affecting an overhead line, critical spans do not remain fixed or static; they rather vary over the entire length. Critical spans with the longest length passing across valleys, river-crossings, highways and varying terrains, face comparatively the worst real-time weather. The critical spans in an overhead line cause hot-spot temperature, which is a primary variable for determining the line loadability. Thermal line ratings based on hot-spot temperatures provide reliable

thermal-limit estimates in comparison to computing the thermal line rating based on an overall estimate of weather elements across an overhead line with no consideration of critical spans.

A critical line span is a span exposed to the worst weather elements, of the longest length, passing over varying terrains. Critical spans play an important role in solving the optimal power flow problem in terms of considering the thermal constraints across the entire line-length. The location and corresponding line temperatures across critical spans are very important for system operators in dynamically assessing the line hot-spot temperatures and thus finding reliable line loadabilities, as investigated in this paper. Critical span identification will help utilities to decide when and how much load an overhead transmission line can safely carry. Critical spans experience comparatively higher hot-spot temperatures at the same thermal loadability to non-critical line spans. Therefore, this paper focuses on identifying these spans to determine a reliable line-loadability within allowable sag limits.

The proposed technique validates the concepts as presented in [1]-[2], that the critical span is not a fixed span; rather it varies with space and time. The proposed technique thus suggests an optimum number and placement of sensors across the entire line. Instead of placing sensors across some assumed or non-validated critical spans, the proposed technique will find the optimum sensor placements for monitoring of time- and space-dependent weather across each line span. To address the spatial variability in ambient conditions, the entire test line in this paper was monitored to give a reliable estimate of weather-dependent critical spans. The line was therefore divided into multiple segments from the sending to the receiving ends.

Due to involving the optimized segment locations, this segmentation approach will have less computational burden compared to the segmentation technique in [3] and [4], where each line span is considered as a segment. This study broadened the segmentation approach used in [3]-[4], which segmented a large overhead line based on ambient temperature differences but ignored the span length effect and weather influences on span sagging levels. The segmented approach in this paper addresses both system-level studies and detailed component modeling, advancing the line-segmentation approach in [3]-[4], which focuses on system-level studies rather than detailed component modeling.

Critical span identification in a DTR-operated overhead line was carried out in [5] to determine the line sagging limits in comparison to the approach presented in [6]. The critical span identification technique in [5] focuses on identifying the critical spans based

on correlation benchmarks between minimum line ratings derived from initially assumed line critical spans, giving the global minimum of the line thermal capacity, and the line thermal capacity derived from all line spans. A higher correlation benchmark between both ratings is the decisive factor in considering the span as critical. The technique has a limited scope as it requires knowledge of one critical span in order to identify the other critical spans. The critical span identification technique presented in [5] is similar to the identification technique in [6].

Because the technique ignores the span-topography and terrain levels in critical span identification, the derived sagging levels in [5] may be different to those determined by considering span topography and terrain variability. The sag across critical spans will therefore result in unreliable estimations of distance from the ground. The algorithm also does not consider the critical span sagging during static weather conditions and considers line loading above the maximum allowable temperature (MAT) limit, which may result in excessive sag, reduced tensile strength and increased conductor aging. Additionally, in [6] the distance between segments is chosen without consideration of optimal sensor placements. The drawback of this random selection can be in terms of weather estimation data across each segment and hence across each line span between segments, resulting in unreliable line thermal ratings. The critical span identification technique as presented in [6] requires a set of monitoring stations to achieve the required confidence level. It means, in case of non-availability of the required set of weather stations, monitoring of a selected set of spans, rather than every line span across the entire line, can be done. Also, to find the correlation-based confidence level between thermal capacity across each span and thermal capacity across the whole line, the algorithm will impose a huge computational cost for critical span identification. Additionally, as the algorithm does not consider the effect of dynamic thermal ratings on span sagging levels, the estimated thermal rating for the whole line may result in excessive sagging levels, particularly across the identified critical spans. Multiple critical spans exist across a single overhead line. Hence, identifying the factors that influence the location and number of critical spans is crucial for utility providers [7]. This paper refines the methods proposed in [5]-[7] to identify critical line spans based on varying terrain levels not addressed in [5] and sag modelling not considered in [6] and [7]. Location of critical spans across any overhead line requires knowledge about weather elements and the span topography, the factors that were ignored in [8] and [9] while determining the critical spans. The installation of weather monitoring

sensors across every span of an overhead line passing through a vast geographical region would require a huge capital investment.

In order to achieve the required accuracy across each line span at a reduced cost, this paper introduces a novel method to provide weather data across every span of an overhead line passing through a large geographical region while facing multiple weather patterns across varying terrains. The proposed technique enhances transmission planning and sensor installment by determining the optimal number and location of sensors across each segment in the test overhead line to locate critical spans during the entire operation of the test line. The proposed technique in this paper fills the gap identified in [1]-[9] by considering the weather and span topography individually across each span in all line segments of the test overhead line, giving a reliable estimation of critical spans or the bottlenecks. The proposed technique provides optimal number and location for sensor installation to identify critical spans across the test overhead line. Thermal line ratings based on the identified critical spans result in line flow with no ground clearance infringements. In addition to critical sag monitoring during dynamic weather conditions, the presented approach also considers span sagging levels during static weather conditions. The research gap summary over literature [1]-[9] along with contribution of this study is shown in Table 1. To fill the research gap illustrated in [1]-[9], this paper presents a unique methodology:

- i. To determine the optimal number and placement of sensors using a supervised sensor placement approach.
- ii. To identify the critical line spans using weather and span length considerations to produce no ground clearance infringements in any line span.
- iii. To determine the temperature and sagging level across all line spans and across the identified critical spans to find the minimum line thermal rating capacity during both static and dynamic weather conditions.

Table 1 Literature, research gap and contributions summary

Research gap from the literature	Contributions of the study
<p>The study in [1]-[2] considered identification of spans with highest temperature or minimum loadability without taking into account the span topography information along with weather elements across each line span.</p>	<p>An optimization algorithm is developed to find the minimum optimum number and sensor placements for considering the ambient conditions across the entire test line including short distances and remote locations to find temperature and sag across each line span based on span topography and ambient data available from a few weather stations.</p>
<p>In [3]-[4], a non-uniform line segmentation approach was carried out with following unaddressed issues:</p> <ul style="list-style-type: none"> • Number and placement of segments was determined through variation in ambient temperature from the threshold. • Ambient temperature was the only weather parameter considered in terms of determining the line temperature between and across the segments. 	<p>In the developed algorithm, line segmentation is carried out under system and component level modelling to further assist in the identification of weather and topography based critical spans with following contributions over [3] and [4].</p> <ul style="list-style-type: none"> • An optimized sensor numbering, and placement based on location of reference weather stations between the line sending end to the line receiving end was obtained. • The resulting line segments were used to determine the weather across and between each line segment in the entire line length.
<p>The approach presented in [5]-[6] for critical span identification have left following gaps:</p> <ul style="list-style-type: none"> • Critical spans are identified without considering the span topography and the type of terrains. • The process to identify critical spans requires knowledge about the span with smallest ground clearance or minimum thermal loadability in advance. • The techniques are presented under steady-state thermal line modelling that mainly identify time and space independent critical spans under thermal equilibrium state due to considering the constant weather and loading conditions. 	<p>The proposed design algorithm fills the gap from [5]-[6] with following contributions:</p> <ul style="list-style-type: none"> • Critical span identification technique considers span topography and the rugged terrains (mainly the case in New Zealand) besides span weather conditions to accurately determine the number and placement of time and space dependent critical spans during each loading time interval. • The proposed technique does not require in advance the knowledge of span with minimum thermal loadability. • Non-steady state modelling under realistic loading scenarios is considered to validate accuracy and computational efficiency of the proposed algorithm under time-space dependent ambient, time dependent loading and space dependent terrain conditions.
<p>The gaps and contributions from [7]-[9] are:</p> <ul style="list-style-type: none"> • The testing was carried out on a single test span under steady-state heat-balance [7]. • In [8], an optimized sensor placement technique was designed without considering the span sag-temperature relationship. The study presented in [9] examined sagging across inclined spans and provided the detailed mathematical modelling. 	<p>A detailed mathematical modelling approach is employed in this paper under non-steady state heat balance after addressing the following gaps from [7]-[9]:</p> <ul style="list-style-type: none"> • The designed algorithm has considered weather, span topography and type of terrains across all line spans before deciding the hot spots. • The presented study provided the proof of concept validation with conventional critical span technique and is found reliable. • The study has addressed sagging across both levelled and inclined spans while passing through flat and non-flat terrains respectively.

By considering both geo-spatial weather and temporal loading conditions towards affecting the sag across each span of the test line, the proposed critical span identification technique provides a true representation of the maximum thermal capacity limit of the line. The proposed technique provides an effective solution for computing thermal line ratings using real-weather conditions, where utility companies, due to non-availability or difficulty in measuring or estimating the real weather conditions across every span of an overhead line, are currently obliged to use static thermal line ratings based on conservative assumptions that ignore fluctuating time- and space-dependent weather conditions. The proposed technique besides involving less computational burden is a viable solution for utility companies for determining the thermal capacity of their overhead assets effectively and reliably under no ground clearance violations during the excess electricity transfer. Critical spans identified under both the conventional and the proposed technique are compared to examine the reliability and computational efficiency of the proposed technique.

The rest of the paper is structured as follows: Section 2 highlights thermal line rating and discusses the test system and weather modelling. Section 3 presents the design methodology of the proposed and conventional critical span identification techniques. Section 4 presents the case study. Section 5 provides the obtained results. Section 6 summarizes the findings of the paper.

2. Line Model

2.1. Non-steady state electro-thermal line modelling

Overhead lines are rated statically and dynamically. In both conditions, the conductor rating is calculated using the heat balance between heat gain and heat loss via the heat balance equation (HBE) under steady and non-steady state conditions. In this paper, HBE was considered under non-steady system state, where, electro-thermally coupled (ETC) line modeling [10] was examined. The purpose of utilizing the ETC technique was to increase the line utilization and in result remove line congestion and possible load-shedding, further demonstrated in [10]. The HBE under dynamic or non-steady state conditions as shown in (1) consists of heat absorption and heat emission [11]. Heat absorption takes place due to load-dependent flow of current in the core and the surface of the conductor ($I_s^2(t)$) and due to the ability of the conductor to absorb time varying solar radiations $P_s^s(t)$. Heat emission is the phenomenon that takes place due to heat

convection ($Q_s^c(t)$) and heat radiation ($Q_s^r(t)$) from the overhead conductor [12]-[13] as shown in (1).

$$m * C \frac{dT_s(t)}{dt} = \left((k_{ac} * R_{dc} * I_s^2(t) * T_s(t)) + (P_s^s(t)) - (Q_s^c(t)) + (Q_s^r(t)) \right) \quad (1)$$

where m is the conductor mass, C is the conductor's specific heat capacity measured as the ratio between the conductor's heat capacity and its mass in J/kg·°K, $P_s(t)$ represents solar heat gain, $Q_c(t)$ and $Q_r(t)$ represent convective and radiative cooling, respectively. $I_s(t)$ is the time and line loading-dependent flow of current through span s , and $T_s(t)$ is the space- and time-dependent span temperature.

The HBE under steady and non-steady system states acts differently, i.e., under steady or constant system states, the sum of heat absorption and heat conduction is always identical causing the overhead line under thermal equilibrium state. Contrary to that, under changing ambient and loading conditions, the difference between heat absorption and heat conduction becomes greater than zero leading to thermal inequilibrium state as studied in [10]. This additional energy due to involving thermal inertia causes thermal instability in the overhead line, further dependent on conductor's mass and specific heat capacity. In this paper, HBE under non-steady thermal state is considered due to a linear relationship between span length, conductor mass and thermal inertia that is further needed when identifying the line spans with minimum thermal loadability and critical sagging. Additionally, the line thermal rating technique under non-steady state can be used to accurately determine the maximum optimal capacity of the overhead line and the time it can stay overloaded and thereby allowed optimum power flow under safe allowable conductor temperature limit.

In this paper, the test line is loaded from a lower $I_1(t)$ loading current to a higher loading current $I_2(t)$ current causing conductor in heating state $C_h^{max}(t)$ as described in (2) [10] and from a higher $I_2(t)$ to a lower $I_1(t)$ loading current making conductor under the cooling state $C_c^{min}(t)$ as described in (3) [10]. The cycle is continued until the test overhead line reaches its MAT limit $T_c^{max}(t)$.

$$C_h^{max}(t) = \frac{(I_2^2(t) * R_{ac}(t)) + (P_s(t))}{\pi * D * (T_c^{max}(t) - T_a(t))} \quad (2)$$

From (3), it is evident that higher conductor diameter D and lower ambient temperature $T_a(t)$ reduce conductor heating and allows more current to flow at lower series AC resistance $R_{ac}(t)$.

$$C_c^{min}(t) = \frac{(I_1^2(t) * R_{ac}(t)) + (P_s(t))}{\pi * D * (T_c^{min}(t) - T_a(t))} \quad (3)$$

2.2. Test system modelling

To testify and validate the proposed algorithm on realistic case scenarios, a realistic test system resembling the New Zealand's north island transmission network (as shown in Fig. 1) was modeled in DIgSILENT®. The modelled power system involved two parallel overhead lines connected between Huntly power station and the Penrose substation, situated in New Zealand's north island transmission network as shown in Fig. 2. Physical dimensions of both overhead lines as taken from [14] are provided in Table 2, where Line-1, referred to as the test overhead line throughout this paper, is a Grape aluminium conductor steel reinforced (ACSR), 86 km in length with an operating voltage of 132 kV. The modeled system in Fig. 2 is referred as the test system throughout this paper.

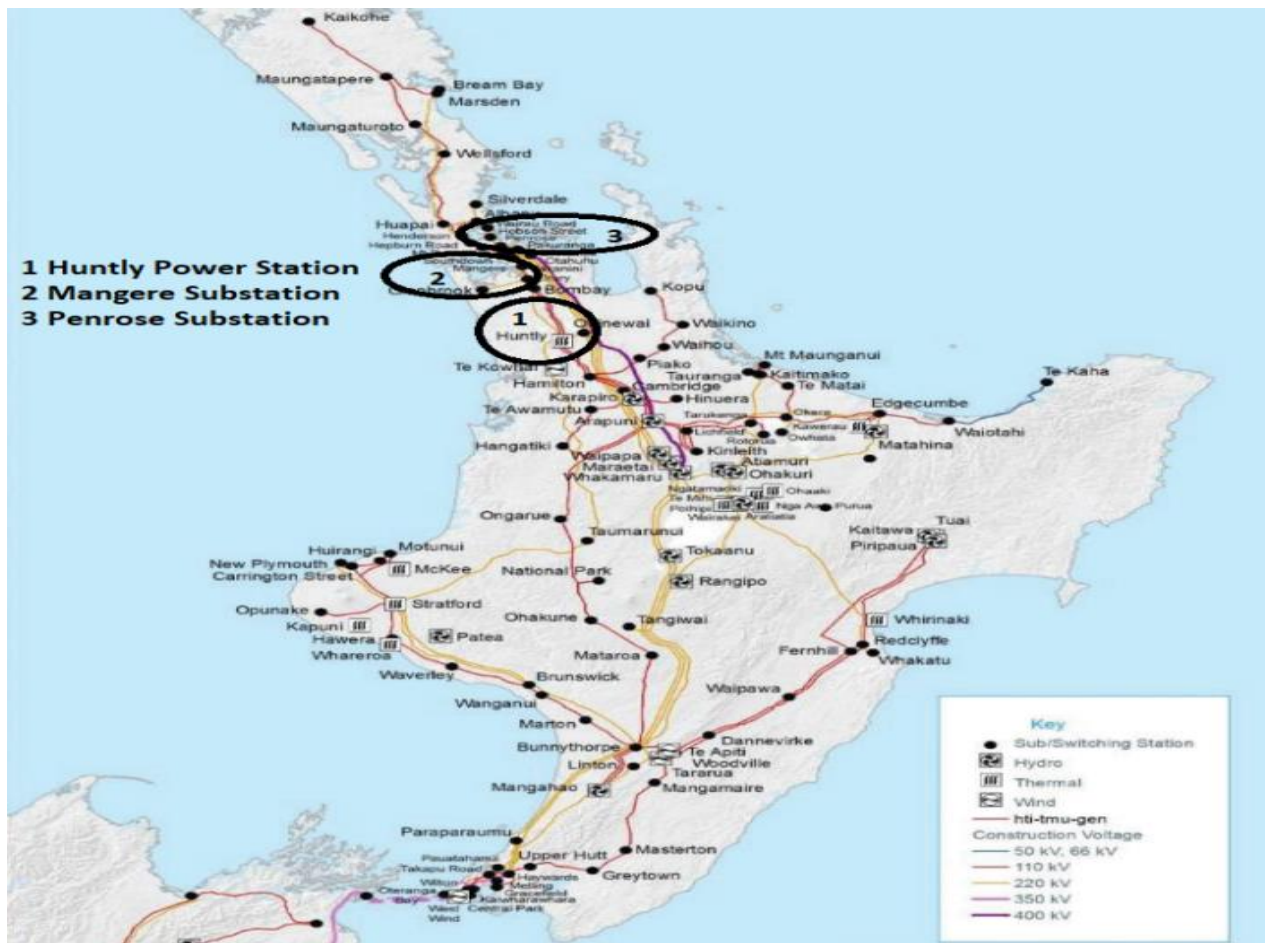


Fig. 1 Transpower's north island transmission network in New Zealand

The test overhead line was assumed to have multiple segments and each segment had a number of non-equidistant spans. The 10-min interval-based ambient data consisting of ambient temperature, wind speed and solar radiation on a hottest day in January-2019 was collected from [15] and filtered to 5-min intervals from reference weather stations across the route of the subject overhead line as shown in Table 3.

Table 2 Line physical dimensions

Overhead Lines	Diameter (mm)	Conductor Mass (kg/m)	Coefficient of linear expansion $\times 10^{-6}/^{\circ}\text{C}$
Line-1	17.5	0.677	19.4
Line-2	31.5	1.96	20.6

Table 3 Line segmentation

Segment	Reference weather stations	Total Number of spans	Spans near weather stations
Huntly-Mangere	Pukekohe & Mangere	457	2
Mangere-Penrose	Owairaka	60	1

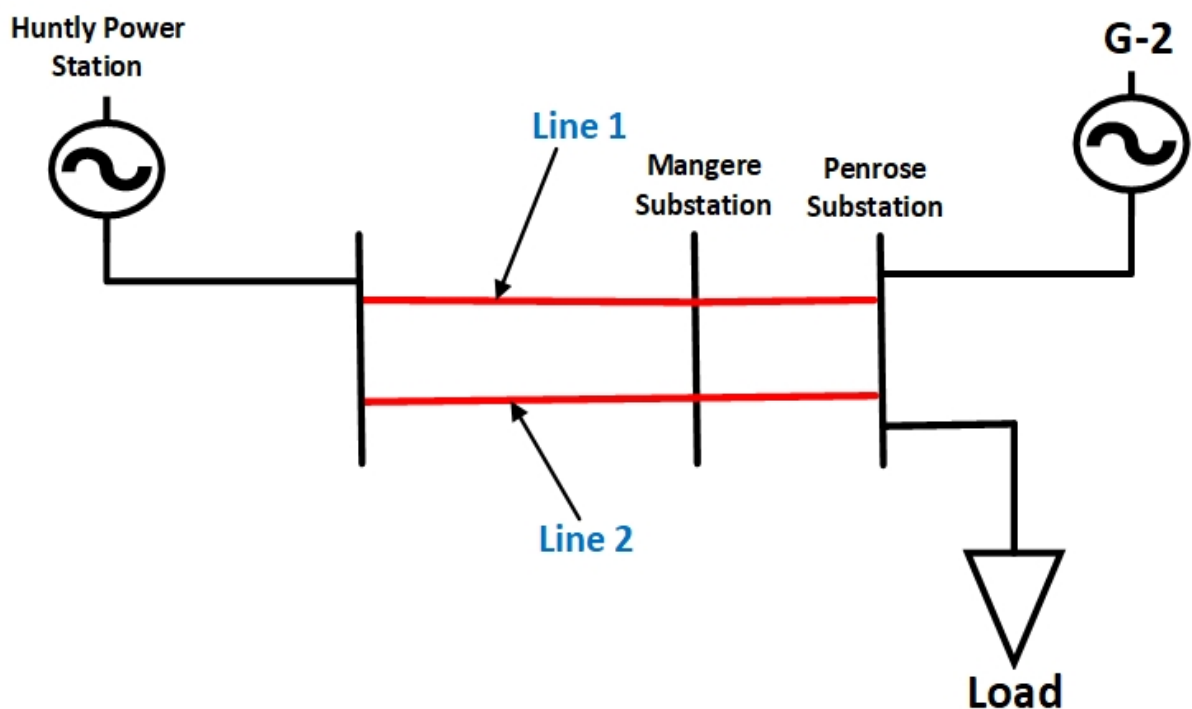


Fig. 2 Single line diagram of modelled test system

For the sag modeling, the test overhead line was considered to be a semi-urban type with 12% ultimate tensile strength (UTS) [14]. Further shown in Fig. 2 and Table 3, the test overhead line sending-end at Huntly power station has a nearby weather station at Pukekohe. Similarly, the receiving-end of the test line at Penrose substation has a nearby weather station at Owairaka. The test overhead line was assumed to run between Huntly power station and the Penrose substation with reference weather stations at Pukekohe, Mangere and Owairaka with total number of spans as shown in Table 3.

The line was divided into multiple segments from the line sending-end to the line receiving-end, with each segment containing multiple spans with real weather data obtained from 3 weather stations [15]. The length of these spans varied between 80 m and 240 m and were taken from [14], where the longest line spans were assumed to pass through varying terrain. The test overhead line spanning over three weather stations with each weather station representing a single line span (the line between two towers).

In the test system, the cost-effective and fast-responsive based re-dispatchable electricity generation at Huntly power station was transferred to the load through test line and Line-2. At the time when Line-2 was disconnected for temporary maintenance, the most feasible option to avoid load shedding was to pass excess electricity through the test line under the DTR technique in place of costlier and slow-responsive generation dispatch from G-2. To mitigate possible congestion (due to N-1 state), the test line was operated under the DTR technique. The test overhead line was loaded based on two practical case scenarios where the line's thermal capacity was checked during the dynamic state of the modelled power system. The line current from the test system was fed into the line thermal capacity algorithm to find the maximum thermal capacity of the test line under the constraints of minimum allowable ground clearance of the critical spans and the line's MAT limit (set at 80°C).

2.3. Weather modelling

Due to the limited weather stations near the test overhead line, the weather data across spans distant from the weather stations were derived from the weather data across spans near to the reference weather stations, as shown in Table 3, using a piece-wise linear regression technique [16]. The purpose of using this technique is twofold: 1) it needs few inputs to give the desired outputs and 2) the resulting outputs meet the set threshold criteria and therefore the estimated unknown parameters fall within the specified data range.

The derived weather data across spans at each segment-start and segment-end (represented as optimal sensor locations, further described in section 3.1) were then used to find the unknown weather data for each span in the test line. In (4), parameters related to the known weather data are given as the inputs, while the estimated value of weather elements across every span in each segment of the test overhead line is the output.

$$E(Y|X) = (\alpha * (Y_{min}, X_{min})) + (\sum_{s=2}^N (X_s * \beta_s) * |(Y_{max}, X_{max}) - (Y_{min}, X_{min})|) \quad (4)$$

where $E(Y|X)$ is the estimated value of dynamic weather elements ($T_N^a(t)$, $V_N^s(t)$, $Q_N^s(t)$) across all the line spans in one segment of the test line, from the segment-start to the segment-end with respect to span lengths in the whole segment. α is the intercept coefficient. Y_{min} is the minimum value of weather elements in a segment. X_{min} is the minimum segment distance from the line sending-end. X_s is the distance from the first reference weather check-point of the segment to the next consecutive span of the segment. β_s is the slope parameter of spans ($2 \leq s \leq N$) in every segment of the test line. Y_{max} is the maximum value of weather elements in a segment. X_{max} is the maximum segment distance from the line sending-end and N is the total number of spans in the entire segment. The same procedure is then used for all segments in the test line.

3. Critical span identification algorithms

3.1. Proposed algorithm design overview

To identify critical spans in the test overhead line, it is considered that any long overhead line passing through several geographical regions will face multiple weather conditions due to changes in altitude, wind pressure and terrain topography [3]. The flow-chart in Fig. 3 presents the proposed methodology to identify multiple critical spans across the entire line, operating under both static and dynamic line rating techniques. Fig. 3 further illustrates segmenting the test line to identify the critical spans through mathematical modelling, described in Step 1 through Step 3 and in Algorithm 1 through Algorithms 2(a) and 2(b). After critical span identification, sag-modelling was carried out in Step 4.

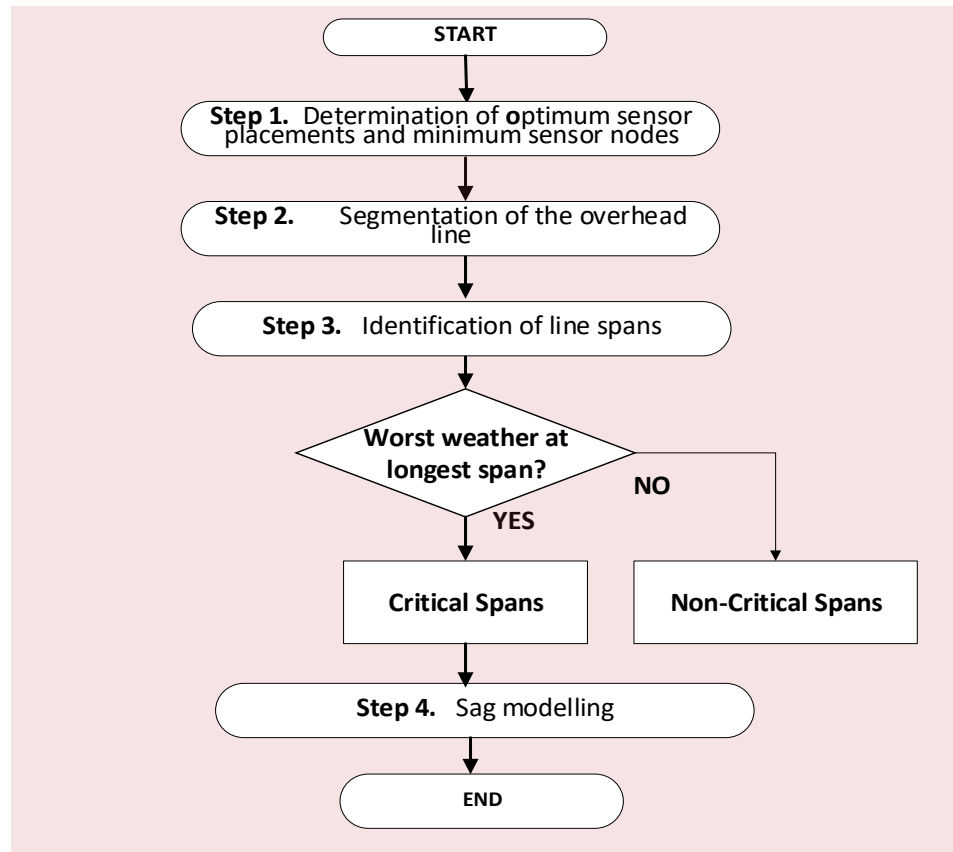


Fig. 3 Simplified flow-chart for proposed critical span identification

Step 1) Optimal Sensor Placement

The optimal number and placement of sensor nodes across the test overhead line was determined from the line sending-end to the line receiving-end. The sensor placement was carried out in such a way that weather data across every line segment was required to estimate the weather conditions in every line span. In the calculation, i represents sensor node placement, where 1 represents optimal sensor placement and 0 represents non-optimal sensor placement. \mathbf{l} is the length of the test line, 86km in this case. To determine the minimum number and optimal placement of the sensor nodes, the sparse-aware sensor selection (SparSenSe) technique [17]-[18] was used, as discussed in (5)-(8).

$$w_i \in \{0, 1\}, i \in \|\mathbf{l}\| \quad (5)$$

When the i^{th} variable of the selection vector \mathbf{w} is 1, the sensor placement is optimal, and its corresponding measurement is used over \mathbf{l} . As shown in (6), the first variable of the selection vector represents the sending-end of the line while the last variable represents the receiving-end of the test overhead line.

$$\mathbf{w} = [w_{BEG,1}, \dots, w_{END,M}]^T \quad (6)$$

Similarly, the size of the vector \mathbf{u} , representing the line segments as shown in (7), is greater than the size of the selection vector \mathbf{w} in (6). This means the calculated sensor measurement nodes M will be lower than the total number of segments n due to the lack of sensor placement across segment-ends near the weather stations over the line length l . This condition is further discussed in Step 2.

$$\mathbf{u} = [u_1, \dots, u_n]^T, \quad M < n \quad (7)$$

The minimum optimization problem in (8) is solved by keeping the mean square error (MSE) below the threshold γ of 1%.

$$\begin{aligned} (\hat{w}, \hat{u}) &:= \arg \min \{ \|w\|_1 \} \\ w &\in [0,1]^M, u \\ \text{s.t. } &\{(w, u) \in (0 \leq \gamma \ll 1)\} \end{aligned} \quad (8)$$

Equations (5)-(8) represent a linear inequalities problem and are therefore solved using a MATLAB-based convex optimization (CVX) toolbox [19]. Steps to find the optimal sensor numbers and placements, as shown in Algorithm 1, use the total line length and reference node locations from the nearby weather stations as the reference distances to initialize the optimum sensor placement technique.

Algorithm-1: minimum sensor number & optimal placements

Input: Set $w_i^* > \gamma$, where $0 \leq \gamma \ll 1$, to get $w_i^* \neq 0$

Step-1: Determine the optimum sensor placements

```

for  $w_i^* \neq 0$ 
     $w_i^* > \gamma$ 
    optimum sensor placement = SparSenSe  $[(\hat{u}, \gamma)]$ 
end

```

Step-2: Determine the required minimum sensor nodes

```

for optimum sensor number =  $(w_{BEG,1} : 1 : w_{END,M})$ 
    MSE = optimum sensor placement  $\{(1:n), \hat{u}\}$ 
end

```

Output: $w_i^* = [(\hat{u}, \text{MSE})]$

Step 2) Line Segmentation

The purpose of line segmentation is to find the individual weather conditions across each span of the test overhead line. Due to the limited number of available weather stations from the line-sending end to the line-receiving end, weather elements across spans near the weather stations were taken as reference values for estimating the unknown weather elements across the rest of the segment-ends, as mentioned in Step 2.3. The estimated weather data across each segment-end were used to find the unknown weather data at every span between two consecutive segments for the entire length of the test line. The proposed line segmentation approach is described in detail in Steps 2.1-2.3.

Step 2.1) Based on the Algorithm 1 output, optimum sensor-placement was carried out over the entire test line. The resulting sensor placement was found to divide the line into 50 non-equidistant segments, where each segment carried one tensioning section ϕ . The minimum distance between two consecutive tensioning sections from the SparSenSe technique was found to be 1 km at 18 locations, and the maximum distance obtained was 7 km at one location. As shown in (9), each segment along a line of length x consists of a tensioning section ϕ with s spans ranging between 80 m to 240 m in length. The resulting non-equidistant spans were arranged by shuffling the array of span elements in MATLAB®.

$$x_{seg}^{\phi_1, \dots, \phi_n} \equiv [x_s^{\phi_1}, x_s^{\phi_2}, \dots, x_s^{\phi_n}]^T, s = 1, 2, \dots, N \quad (9)$$

The division of $x_{seg}^{\phi_1, 2, \dots, n}$ segments as shown in (9) was based on an optimal number of sensor placements; i.e., a segment was proposed between two sensor nodes, where each end of the segment is considered as a weather check-point. Thereafter, each individual segment was observed to carry N number of spans ranging between 80 m and 240 m in length. The model followed in creating the line segments is further explained in Step 2.2. Step 2.2) As shown in (10), the known weather elements across spans near the reference weather stations in Table 3 were used to find the unknown weather elements at the segments across weather check-points using the linear piece-wise regression technique [16, 20] as shown in (4).

$$\begin{aligned} x_k^R &: [T^a(x_k), V^s(x_k), Q^s(x_k)]^T \\ x_{k+1}^R &: [T^a(x_{k+1}), V^s(x_{k+1}), Q^s(x_{k+1})]^T \\ x_{k+2}^R &: [T^a(x_{k+2}), V^s(x_{k+2}), Q^s(x_{k+2})]^T \end{aligned} \quad (10)$$

In (10), \mathbf{x}_k^R represents the set of weather elements at span k belonging to the first reference weather-station; similarly \mathbf{x}_{k+1}^R represents the set of weather elements at span $k + 1$, belonging to a second reference weather-station and \mathbf{x}_{k+2}^R represents the set of weather elements at span $k + 2$, belonging to the third reference weather station.

Step 2.3) The known weather elements from Step 2.2 across each segment-end of the line were used to determine the unknown weather elements at every line span between each line segment, using the piece-wise regression technique [16, 20], where to maintain accuracy in the estimated weather elements, the threshold $\Delta_{Threshold}$ was kept at 0.1. To meet the $\Delta_{Threshold}$ limit, the proposed line-segmentation technique resulted in a non-uniformly distributed line model as shown in Fig. 4.

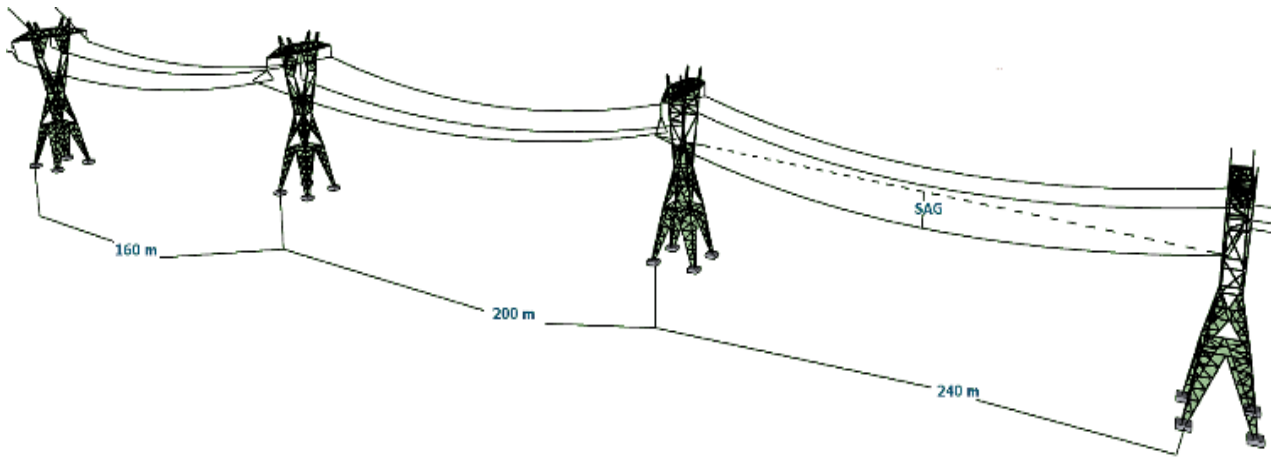


Fig. 4 Line sag modelling sketch in a tensioning section

Step 3) Critical Span Formulation

In this step, mathematical modelling of the proposed critical span identification technique was used to identify the set of critical line spans. The process of identifying the critical line spans in the test overhead line was carried out using the following sub-steps. This step was to identify the line spans passing through flat and non-flat terrains that had the longest length and faced the highest ambient temperature, lowest wind speed and highest solar radiation, using the ‘span length weather optimization problem’ (SLWOP).

The optimization problem starts with the segmented line carrying n number of segments, where each line segment carries N number of spans with a total set of line spans $R_s(\mathbf{x}_{seg}^{\varphi_1, \dots, \varphi_n})$ from the line sending-end to the receiving-end with a total set of multiple

critical $R_c(x_{seg}^{\varphi_1, \dots, \varphi_n})$ spans and a total set of multiple non-critical line spans $R_o(x_{seg}^{\varphi_1, \dots, \varphi_n})$ as shown in (11).

$$R_s(x_{seg}^{\varphi_1, \dots, \varphi_n}) = (R_c(x_{seg}^{\varphi_1, \dots, \varphi_n}) + R_o(x_{seg}^{\varphi_1, \dots, \varphi_n})) \quad (11)$$

SLWOP₁^φ as shown in (12) elaborates the modelling procedure in selecting the critical line spans that face the highest ambient temperature in a dynamic-weather Scenario. The procedure starts by searching for the maximum ambient temperature across all line spans lying across n segments of the test overhead line x_1, \dots, x_n from the line sending-end to the line receiving-end, to identify the critical spans during loading time t . The proposed formulation in (12) meets the condition that the obtained critical line span c_{AB} lying between towers **A** and **B** carries the longest length of all spans in the total set of line spans facing the maximum ambient temperature $T_{c_{AB}}^a(x_{seg}^{\varphi_1, \dots, \varphi_n})$.

$$\text{SLWOP}_1^\varphi: \quad \underbrace{\max}_{\forall c_{AB} \in R_c \in R_s(x_{seg}^{\varphi_1, \dots, \varphi_n})} \sum_{s=1}^{s_N} \{T_{c_{AB}}^a(x_{seg}^{\varphi_1, \dots, \varphi_n}) \in T_s^a(x_{seg}^{\varphi_1, \dots, \varphi_n})\} \quad (12)$$

$$\text{s.t. } \beta_{s_1, \dots, s_N}^{x_{seg}^{\varphi_1, \dots, \varphi_n}} > \alpha_{c_{AB}}^{x_{seg}^{\varphi_1, \dots, \varphi_n}} \geq \max(L_{c_{AB}}(x_{seg}^{\varphi_1, \dots, \varphi_n})) \forall R_c \in R_s \in$$

$$\max \{T_{c_{AB}}^a(x_{seg}^{\varphi_1, \dots, \varphi_n}) \wedge t, T_{c_{AB}}^a(x_{seg}^{\varphi_1, \dots, \varphi_n}) \vee t\}$$

Based on the mathematical formulation of **SLWOP₁^φ**, span c_{AB} is an identified critical line span lying between towers **A** and **B** in a segment that belongs to a set of multiple critical spans R_c that are a subset of the total line span set R_s . Further, **SLWOP₁^φ** is subject to the required sagging level, i.e., the calculated sag $\alpha_{c_{AB}}^{x_{seg}^{\varphi_1, \dots, \varphi_n}}$ across the identified critical span based on the DTR technique is less than the maximum allowable sag $\beta_{s_1, \dots, s_N}^{x_{seg}^{\varphi_1, \dots, \varphi_n}}$ (see Section 5). To find another critical line span at the next loading time $t + 1$, **SLWOP₁^φ** is updated and the procedure is continued until all critical spans are identified.

Similarly, **SLWOP₂^φ** as shown in (13) elaborates the procedure in selecting the critical line spans facing the lowest wind speed in a dynamic-weather scenario. The procedure starts searching for the lowest wind speed across all n segments (x_1, \dots, x_n) of the overhead line from the line sending-end to the line receiving-end to identify the critical spans during loading time t . The proposed formulation in (13) meets the condition that the obtained critical line span has the longest length.

$$\text{SLWOP}_2^\varphi: \quad \underbrace{\min}_{\forall c_{AB} \in R_c \in R_s(x_{seg}^{\varphi_1, \dots, \varphi_n})} \sum_{s=1}^{s_N} \{V_{c_{AB}}^s(x_{seg}^{\varphi_1, \dots, \varphi_n}) \in V_s^s(x_{seg}^{\varphi_1, \dots, \varphi_n})\} \quad (13)$$

$$\begin{aligned} \text{s.t. } & \beta_{s_1, \dots, s_N}^{x_{seg}^{\varphi_1, \dots, \varphi_n}} > \alpha_{c_{AB}}^{x_{seg}^{\varphi_1, \dots, \varphi_n}} \geq \max(L_{c_{AB}}(x_{seg}^{\varphi_1, \dots, \varphi_n})) \forall R_c \in R_s \in \\ & \min \{V_{c_{AB}}^s(x_{seg}^{\varphi_1, \dots, \varphi_n}) \wedge t, V_{c_{AB}}^s(x_{seg}^{\varphi_1, \dots, \varphi_n}) \vee t\} \end{aligned}$$

Considering the mathematical formulation of \mathbf{SLWOP}_2^φ , span c_{AB} from $R_s(x_{seg}^{\varphi_1, \dots, \varphi_n})$ is an identified critical line span lying between towers A and B belonging to the set of critical spans R_c that is a subset of the total line span set R_s . Further, \mathbf{SLWOP}_2^φ is subject to the required sagging level, i.e., the calculated sag $\alpha_{c_{AB}}^{x_{seg}^{\varphi_1, \dots, \varphi_n}}$ across the identified critical span based on the DTR technique is less than the maximum allowable sag $\beta_{s_1, \dots, s_N}^{x_{seg}^{\varphi_1, \dots, \varphi_n}}$ (see Section 5). To find another critical span at the next loading time $t + 1$, \mathbf{SLWOP}_2^φ is updated and the procedure is continued until all critical spans are identified.

To consider solar radiation effects in identifying the critical line spans, \mathbf{SLWOP}_3^φ , as shown in (14), was used to determine the critical line spans facing the highest solar radiation in the given weather conditions. The optimization problem starts by searching all line spans in (11), selecting those line spans that are the longest in length and face the highest solar radiation. The search is carried out across all n segments (x_1, \dots, x_n) of the test overhead line during loading time t . The proposed formulation in (14) meets the condition that the obtained critical line span c_{AB} lying between tower A and B carries the longest length amongst all spans in the total set of line spans $R_s(x_{seg}^{\varphi_1, \dots, \varphi_n})$ experiencing the maximum solar radiation $Q_{c_{AB}}^s(x_{seg}^{\varphi_1, \dots, \varphi_n})$.

$$\mathbf{SLWOP}_3^\varphi: \quad \max_{\forall c_{AB} \in R_c \in R_s(x_{seg}^{\varphi_1, \dots, \varphi_n})} \sum_{s_1}^{s_N} \{Q_{c_{AB}}^s(x_{seg}^{\varphi_1, \dots, \varphi_n}) \in Q_s^s(x_{seg}^{\varphi_1, \dots, \varphi_n})\} \quad (14)$$

$$\begin{aligned} \text{s.t. } & \beta_{s_1, \dots, s_N}^{x_{seg}^{\varphi_1, \dots, \varphi_n}} > \alpha_{c_{AB}}^{x_{seg}^{\varphi_1, \dots, \varphi_n}} \geq \max(L_{c_{AB}}(x_{seg}^{\varphi_1, \dots, \varphi_n})) \forall R_c \in R_s \in \\ & \max \{Q_{c_{AB}}^s(x_{seg}^{\varphi_1, \dots, \varphi_n}) \wedge t, Q_{c_{AB}}^s(x_{seg}^{\varphi_1, \dots, \varphi_n}) \vee t\} \end{aligned}$$

Based on the mathematical formulation of \mathbf{SLWOP}_3^φ , span c_{AB} from $R_s(x_{seg}^{\varphi_1, \dots, \varphi_n})$ is an identified critical line span lying between towers A and B which belongs to a set of multiple critical spans R_c that further are a subset of the total line span set R_s . Further, \mathbf{SLWOP}_3^φ is subject to the required sagging level, i.e., the calculated sag $\alpha_{c_{AB}}^{x_{seg}^{\varphi_1, \dots, \varphi_n}}$ across the identified critical span based on the DTR technique is less than the maximum

allowable sag $\beta_{s_1, \dots, s_N}^{x^{\varphi_1, \dots, \varphi_n, seg}}$ (see Section 5). To find another critical line span at the next loading time $t + 1$, \mathbf{SLWOP}_3^φ is updated and the procedure continues until all critical spans are identified.

To locate the critical line spans in the test overhead line, the optimization problems \mathbf{SLWOP}_1^φ , \mathbf{SLWOP}_2^φ and \mathbf{SLWOP}_3^φ need to be satisfied until all critical line spans are identified in the test line passing through multiple terrains under various weather conditions at an allowable distance from the lowest and/or mid-point of the catenary curve to the ground. The process is further demonstrated in Algorithms 2(a) and 2(b).

The proposed algorithm is based on selecting the minimum parameter value for wind speed and maximum parameter values for ambient temperature and the solar radiation in order to distinguish between critical and non-critical line spans. Similarly, in case of wind direction, the proposed algorithm requires to select either minimum or maximum value of the wind direction in order to identify the critical spans. It is important to mention that the direction of wind speed to conductor axis ranges between 0° and 90° , where 0° represents true parallel wind direction to the conductor axis while 90° represents true perpendicular wind direction to the conductor axis. Due to difficulty in obtaining the real weather data regarding the wind direction across every line span under each loading time interval, a fixed true perpendicular wind direction is therefore considered by the proposed algorithm and included in \mathbf{SLWOP} as shown in Algorithm 2(a). The reason to consider a fixed wind blow perpendicular to the span axis instead of a fixed wind blow parallel to the span axis was derived from [21], suggesting that at low wind speeds (that is mainly the case across critical spans), true parallel wind flow along overhead lines does not occur due to natural turbulence (associated with variable wind direction) occurring at low wind speeds.

Similarly, due to unavailability of field data regarding the orientation of 517 total line spans, it is almost impossible to program the algorithm such that it selects the wind direction that will provide the least cooling across individual line spans. As the span orientation data is important in finding the actual direction of wind speed with respect to span axis, their unavailability resulted in considering a fixed wind direction with respect to each span axis providing the least conductor cooling towards critical span identification. Similarly, as mentioned in [22] due to presence of rugged terrains (mainly in New Zealand), the line direction changes extensively. The said reasons result in the

selection of fixed wind direction to obtain an optimal solution of critical span identification during each loading interval.

Additionally, as mentioned in [7], wind flow along the conductor axis causes more variations in line temperature than the wind flow across the conductor axis. The crossflow wind will provide more stable location for the critical spans than the wind blowing down the axis of the conductor [7]. Therefore, another reason behind choosing a cross-flow wind direction over the concurrent wind flow was to find the stable location of critical spans during each loading time interval.

As in this paper, the primary purpose is to test the proposed algorithm on realistic simulated loading scenarios instead of validating it on actual overhead lines in the field, hence, the flow of wind direction was chosen such that it would cause least variations in line temperature and would result in stable location of critical spans across the entire subject overhead line at each loading time interval. Likewise, it is also advantageous for transmission system operators to receive less volatile thermal line ratings at each loading time towards making the better decisions regarding the line operation and the planning. Similarly, as the chosen overhead conductor is smaller than the conductor out for maintenance, hence being a smaller conductor and carrying huge loading, it experiences large temperature variations based on small changes in load current.

Algorithm 2(a): temperature across critical spans

$$\text{Input: } \left[\left[\underbrace{\{T_{CAB}^a, Q_{CAB}^s\}}_{\max_{\forall C_{AB} \in R_c \in R_s(x_{seg}^{\varphi_1, \dots, \varphi_n})}}, \underbrace{\{V_{CAB}^s\}}_{\min_{\forall C_{AB} \in R_c \in R_s(x_{seg}^{\varphi_1, \dots, \varphi_n})}} \right] \in \left[\underbrace{\{L_{CAB}(x_{seg}^{\varphi_1, \dots, \varphi_n})\}}_{\max_{\forall C_{AB} \in R_c \in R_s(x_{seg}^{\varphi_1, \dots, \varphi_n})}} \right] \in \left[\{SLWOP_1^\varphi, SLWOP_3^\varphi, SLWOP_2^\varphi\}_{C_{AB}}^s \right]$$

Step-1: With the help of the known weather stations data, optimal sensor placement at each segment-ends and the obtained number of spans in each line segment, the unknown weather data across each line span is used to estimate the set of weather elements across each critical span of the test line and is given as an input to this algorithm.

$$\text{for } \delta_{known}^{spans} = [x_k^R, x_{k+1}^R, x_{k+2}^R]^T$$

$$R_c(x_{seg}^{\varphi_1, \dots, \varphi_n}) = (R_s(x_{seg}^{\varphi_1, \dots, \varphi_n}) - R_o(x_{seg}^{\varphi_1, \dots, \varphi_n}))$$

$$\delta_{unknown}^{spans} = [T_{c_{AB}}^a, V_{c_{AB}}^s, Q_{c_{AB}}^s]^T$$

Step 2: Due to absence of field rating data, a perpendicular direction of wind speed θ_V to the axis of critical spans is considered (based on practice as followed in [13]). The \mathbf{SLWOP}_2^φ formulation is updated after wind direction consideration.

for ($\theta = 90^\circ$)

$$\left\{ \theta_{V,c_{AB}}^s \right\}_{90^\circ} \in \left[\underbrace{\{L_{c_{AB}}(x_{seg}^{\varphi_1, \dots, \varphi_n})\}}_{\max_{\forall c_{AB} \in R_c \in R_s(x_{seg}^{\varphi_1, \dots, \varphi_n})}} \right] \ni \left[\{\mathbf{SLWOP}_2^\varphi\}_{c_{AB}}^s \right]$$

Step 3: The resulting ambient-span length data from step 1, the critical span formulations from \mathbf{SLWOP}_1^φ , \mathbf{SLWOP}_2^φ and \mathbf{SLWOP}_3^φ , wind direction (normal to span axis)-span length data from step 2, and the line's physical dimensions were used as input to line rating techniques to find the line temperature across the identified critical spans in each segment of the test line and thus obtain the temperature across the most critical span of the line at time t and at subsequent timings, i.e., in case of DTR,

$$\mathbf{for} \ T_{DTR,c_{AB}}(x_{seg}^{\varphi_1, \dots, \varphi_n}) \leftarrow [(\max \sum_{\varphi=1}^n I_{max}^\varphi) \ni \text{Input}]$$

$$T_{DTR,c_{AB}}(x_{seg}^{\varphi_1, \dots, \varphi_n}) = \max [T_{DTR,c_{AB}}(x_{seg}^{\varphi_1}), \dots, T_{DTR,c_{AB}}(x_{seg}^{\varphi_n})]$$

where, the maximum line current I_{max} (based on Scenarios A & B) found at the MAT limit at loading time t and the subsequent loading times in the presence of real weather conditions were passed through each critical span in all line segments $x_{seg}^{\varphi_1, \dots, \varphi_n}$ to obtain the maximum critical span temperature using the DTR technique T_{DTR} . Similarly, in the case of STR, I_{max} found at MAT limit at loading time t and the subsequent loading times in presence of assumed-weather conditions were passed through each critical span in all line segments $x_{seg}^{\varphi_1, \dots, \varphi_n}$ to obtain the maximum critical span temperature under the STR technique T_{STR} , i.e.,

$$\mathbf{for} \ T_{STR,c_{AB}}(x_{seg}^{\varphi_1, \dots, \varphi_n}) \leftarrow [(\max \sum_{\varphi=1}^n I_{max}^\varphi) \ni \text{Input}]$$

$$T_{STR,c_{AB}}(x_{seg}^{\varphi_1, \dots, \varphi_n}) = \max [T_{STR,c_{AB}}(x_{seg}^{\varphi_1}), \dots, T_{STR,c_{AB}}(x_{seg}^{\varphi_n})]$$

where, T_{STR} was found after assuming the worst weather across each span of the test line. The resulting critical span-based temperature was thereafter used as the maximum temperature of the entire line during that time and line loading, and then for subsequent loading time intervals.

$$T_{DTR,cAB}(x_{seg}^{\varphi_1,\dots,\varphi_n}) \leq T_{MAT}(x_{seg}^{\varphi_1,\dots,\varphi_n}) \leq T_{STR,cAB}(x_{seg}^{\varphi_1,\dots,\varphi_n})$$

end

Output: $[T_{DTR,cAB}(x_{seg}^{\varphi_1,\dots,\varphi_n}), T_{STR,cAB}(x_{seg}^{\varphi_1,\dots,\varphi_n})]$

Algorithm 2(b): sag across critical spans

Input: $[T_{DTR,cAB}(x_{seg}^{\varphi_1,\dots,\varphi_n}), T_{STR,cAB}(x_{seg}^{\varphi_1,\dots,\varphi_n})]$

Step 1: The critical span-temperature from Algorithm-2(a) with span-topography and physical dimensions under both line rating techniques is used as an input to the line sag modelling to result in sagging across the critical spans. Due to dynamic weather conditions, the sag across critical line spans in presence of the actual weather (Sag_{DTR}) is lower than the sag under the worst weather (Sag_{STR}).

$$\begin{aligned} \text{for } Sag_{DTR,cAB}(x_{seg}^{\varphi_1,\dots,\varphi_n}) &\leftarrow T_{DTR,cAB}(x_{seg}^{\varphi_1,\dots,\varphi_n}) \\ Sag_{STR,cAB}(x_{seg}^{\varphi_1,\dots,\varphi_n}) &\leftarrow T_{STR,cAB}(x_{seg}^{\varphi_1,\dots,\varphi_n}) \\ \underbrace{Sag_{STR,cAB}}_{\substack{x_{seg}^{\varphi_1,\dots,\varphi_n} \\ \beta_{s_1,\dots,s_N} > \alpha_{cAB}}} &> \underbrace{Sag_{DTR,cAB}}_{\substack{x_{seg}^{\varphi_1,\dots,\varphi_n} \\ \beta_{s_1,\dots,s_N} > \alpha_{cAB}}} \end{aligned}$$

end

Output: $[Sag_{DTR,cAB}(x_{seg}^{\varphi_1,\dots,\varphi_n}), Sag_{STR,cAB}(x_{seg}^{\varphi_1,\dots,\varphi_n})]$

Step 4) Sag Modelling

The last step of the proposed technique is sag modelling of the identified critical line spans under static and dynamic weather conditions as shown in Algorithm 2(b). This study considered sagging across spans passing through both flat and non-flat terrains to better represent the change in movement of the lowest point(s) across the test overhead line. As obtained from the results (see Section 5), this movement in the lowest point (s) across the conductor changes from mid-span (in flat spans) to the lower suspension point (in non-flat spans). Span sagging was obtained by inputting the static and dynamic ampacity-based span temperature and the span lengths in (1)-(7) from [23] during both static and dynamic weather conditions under both scenarios. In addition to weather and loading conditions, span length is also an important factor in causing span sagging [23, 24] and is therefore considered in SLWOP.

Based on the obtained results, spans of smaller lengths facing the worst weather were found to exhibit minimum sagging even at loading temperatures above the MAT limit; hence such spans, despite facing conductor temperatures above the safe allowable limit, were still categorized as non-critical line spans because of the clearance margin available. Therefore, it can be concluded that span-length is an important factor in determining span sagging, in addition to weather conditions, and thus cannot be neglected when identifying critical line spans. This important factor is however ignored in the critical-span identification techniques proposed in [5]-[8].

3.2. Proposed versus conventional algorithm implementation overview

The conventional critical span identification technique as discussed in this paper starts by back-calculating the temperature across each line span through ampacity and weather conditions surrounding individual spans in the entire test overhead line. On the other hand, the proposed technique in this paper under SLWOP methodology searches each line span to identify the spans with longest length and worst ambient conditions, further represented as critical spans. After initial critical span identification, the proposed technique calculates their temperature and the sagging-levels by allowing the maximum allowable current (ampacity) through the test overhead line. The spans with minimum thermal loadability are identified as critical spans and validated using the conventional technique. The procedure to find the sagging across critical (proposed technique) and all line spans (conventional technique) is illustrated in the flow chart as shown in Fig. 5.

The convergence of proposed technique to identify critical spans from all line spans took at average ~10 times lower computational time than the conventional technique for the same overhead line when executed in Intel Core i7-8700 CPU@3.2 GHz, 32.0 GB RAM system under a single Scenario condition from $t= 20$ min to $t= 25$ min. The proposed technique can therefore be considered as reliable, fast, efficient and computationally

inexpensive in identifying critical spans in a large overhead line passing through multiple terrains traversing varied geographical regions.

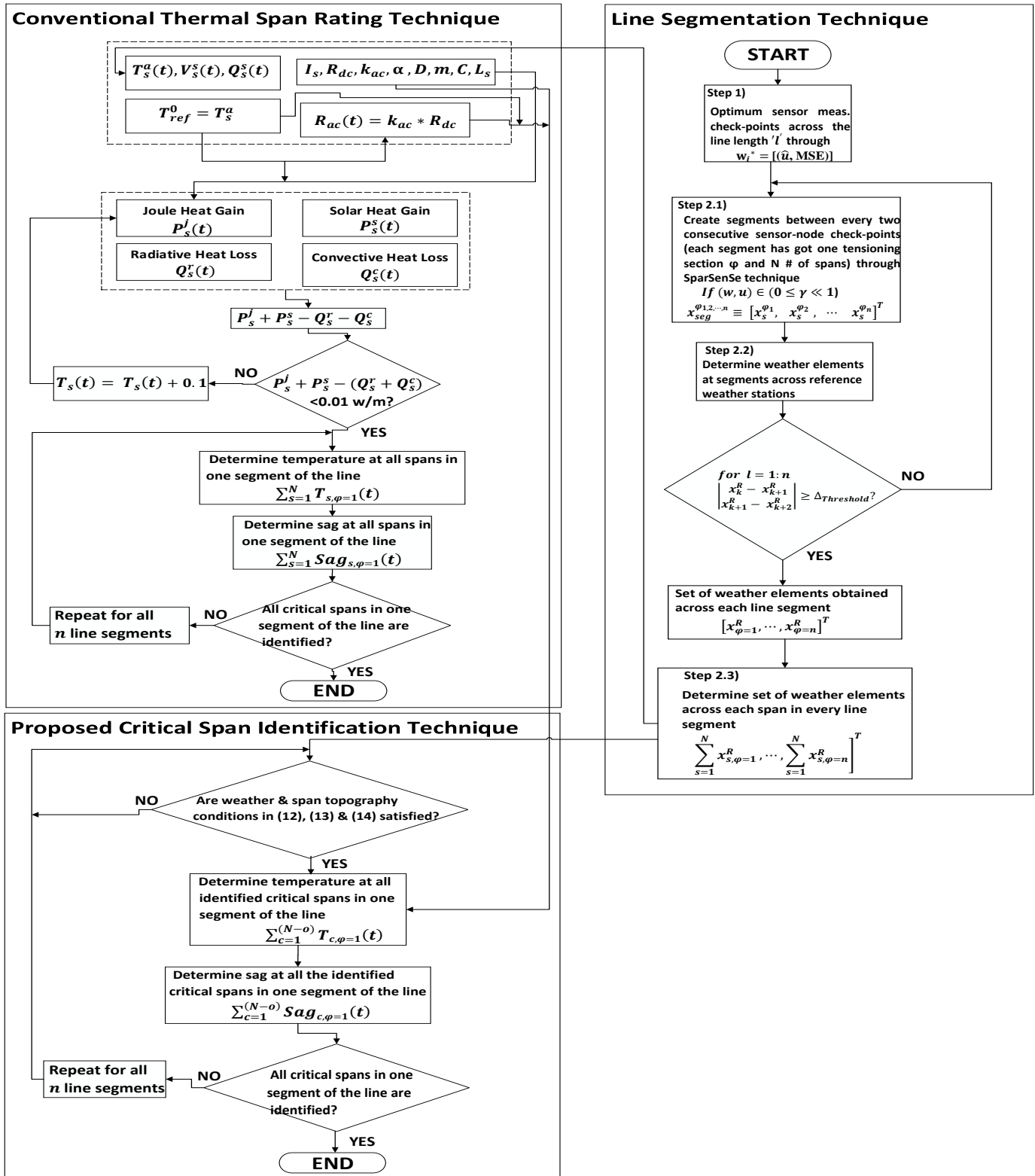


Fig. 5 Critical span identification through proposed and conventional algorithms

4. Case study

4.1. Background

To find the maximum thermal capacity, the test line was loaded under multiple time- and space-dependent weather conditions until it reached the maximum safe thermal limit. The applied loading conditions in the following Scenarios determined the line's ability to relieve congestion with no ground clearance infringement. The 10-min interval based ambient variables on a hottest day in January-2019 were taken from the weather stations as shown in Table 3 along the route of the test overhead line. The typical day selection was based on obtaining the less favourable weather conditions to find critical spans and their influence to limiting the line DTR.

Two case scenarios are carried out in this study to analyse the capacity of the test line to overcome possible congestion. The resulting congestion may jeopardise the system reliability if the test line is not provided with reliable ambient data across each span regardless of their orientation and location. The retrieval of weather data across each line span will enable the possibility of applying the DTR technique such that the line delivers optimum electricity at maximum potential and at no risk of thermal and voltage violations. This study helps in individual monitoring of span weather conditions to better estimate the ambient variable distribution across the entire route of the test line toward reliable line flow.

4.2. Scenario-A—Line outage

This scenario presents the N-1 contingency state in result of the Line-2 shutdown, making the test line to dispatch excess electricity. Following the N-1 contingency, the resulting line load may increase congestion across the test line mainly due to presence of line hot spots and due to their possible remote location from the weather stations toward receiving the reliable ambient data at each loading. The obtained results further indicate that the test line under DTR technique is capable to overcome the subsequent loading in comparison to the STR technique. Under this case scenario, the test line is investigated through static and dynamic weather conditions in the presence of a 55 MW base load from $t=0$ min to $t=30$ min. At $t=10$ min, the adjacent overhead line on the same tower was disconnected (simulating the need to carry out maintenance work) for 10 min and was thus restored at $t=20$ min. DTR-and static thermal rating (STR)-based conductor temperatures for critical spans in this Scenario are shown in Table 4.

Table 4 Critical spans temperature under Scenario—A

Time (min.)	Line-1 Current (A)	Critical Span-1 Temperature (°C)		Critical Span-2 Temperature (°C)		Critical Span-3 Temperature (°C)	
		DTR	STR	DTR	STR	DTR	STR
0	405	40.33	61.92	40.38	61.92	40.42	61.92
5	405	40.96	61.92	41.34	61.92	41.26	61.92
10	536	54.26	84.48	54.97	84.48	54.84	84.48
15	536	53.34	84.48	54.35	84.48	54.71	84.48
20	536	53.80	84.48	53.66	84.48	54.37	84.48
25	405	43.53	70.56	43.48	70.56	43.25	70.56
30	405	41.13	61.92	41.18	61.92	40.29	61.92

4.3. Scenario-B — Emergency overloading

The test overhead line in Scenario-B was examined under elevated time-domain load conditions. From $t=0$ min to $t=5$ min, line loading was investigated under static and dynamic weather conditions in the presence of critical spans under a 55 MW base load, resulting in critical span temperatures as shown in Table 5. At $t=5$ min, the base load was increased 1.3 p.u. At $t=10$ min, an additional increment to 1.5 p.u. was carried out, further continued to 1.8 p.u. at $t=15$ min and 2.0 p.u. at $t=20$ min. At $t=25$ min, the adjacent line on the same tower in the double AC circuit was restored while the test line was under twice the base load. At $t=30$ min, 0.2 p.u. load decrement was undertaken across the test overhead line.

The obtained results as shown in Table 5 indicate that, at $t=20$ min, when the test line experienced the worst loading combined with the worst weather, the DTR-based temperature across all critical spans was found slightly above the MAT limit of the test line, i.e., across critical span-1, it was found to 1.26% above, across critical span-2 and critical span-3 was found 1.08% and 1.67% respectively. The STR based temperature across all identified critical line spans was found above the MAT limit from $t=0$ min to $t=25$ min due to excess demand from the load side.

Table 5 Critical spans temperature under Scenario—B

Time (min.)	Line-1 Current (A)	Critical Span-1 Temperature (°C)		Critical Span-2 Temperature (°C)		Critical Span-3 Temperature (°C)	
		DTR	STR	DTR	STR	DTR	STR
0	536	50.52	84.48	50.55	84.48	50.54	84.48
5	596	57.31	84.48	57.68	84.48	57.57	84.48
10	636	65.49	84.48	66.24	84.48	66.10	84.48
15	696	72.45	84.48	73.40	84.48	73.59	84.48
20	737	81.01	84.48	80.87	84.48	81.34	84.48
25	553	58.77	84.48	58.72	84.48	58.50	84.48
30	479	47.77	70.53	47.81	70.53	46.92	70.53

5. Results

The conventional critical span identification technique starts by back-calculating the line temperature across each span through ampacity and surrounding weather conditions for each line span as shown in Fig. 5. The proposed technique under SLWOP methodology, as shown in Fig. 5 searches each line span to identify the spans with longest length and worst ambient conditions, further represented as critical line spans in the test line.

The design technique thereafter calculates the temperature and sagging across the identified critical spans by allowing the maximum allowable current (ampacity). The spans with the highest levels of sagging were then identified as critical spans and validated using the conventional technique. The line temperature across each span was used to find the individual span sagging.

5.1. Conventional technique based critical span sagging

When implemented from $t=20$ min to $t=25$ min under the worst loading conditions in Scenario-B, the conventional technique resulted in three critical span identifications at 42.92 km, 48.34 km and 55.64 km from the line sending-end, as shown in Fig. 6.

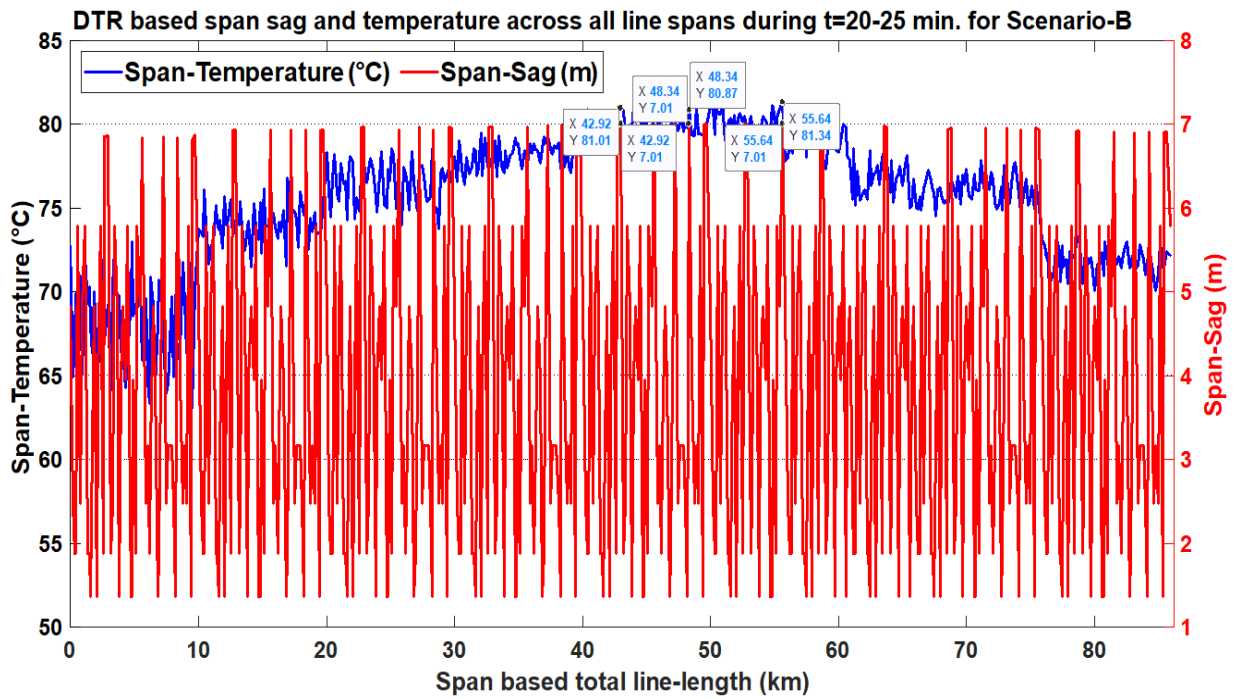


Fig. 6 Critical spans identification through conventional technique

5.2. Proposed technique based critical span sag-temperature validation

Based on results as shown in Fig. 7, the proof of concept of the proposed algorithm is validated. The results were obtained under worst loading conditions from t=20 min to t=25 min across the test line with all identified critical line spans passing through flat terrains. The results indicate that the proposed algorithm resulted in the same set of critical spans at the same locations as obtained under the conventional technique.

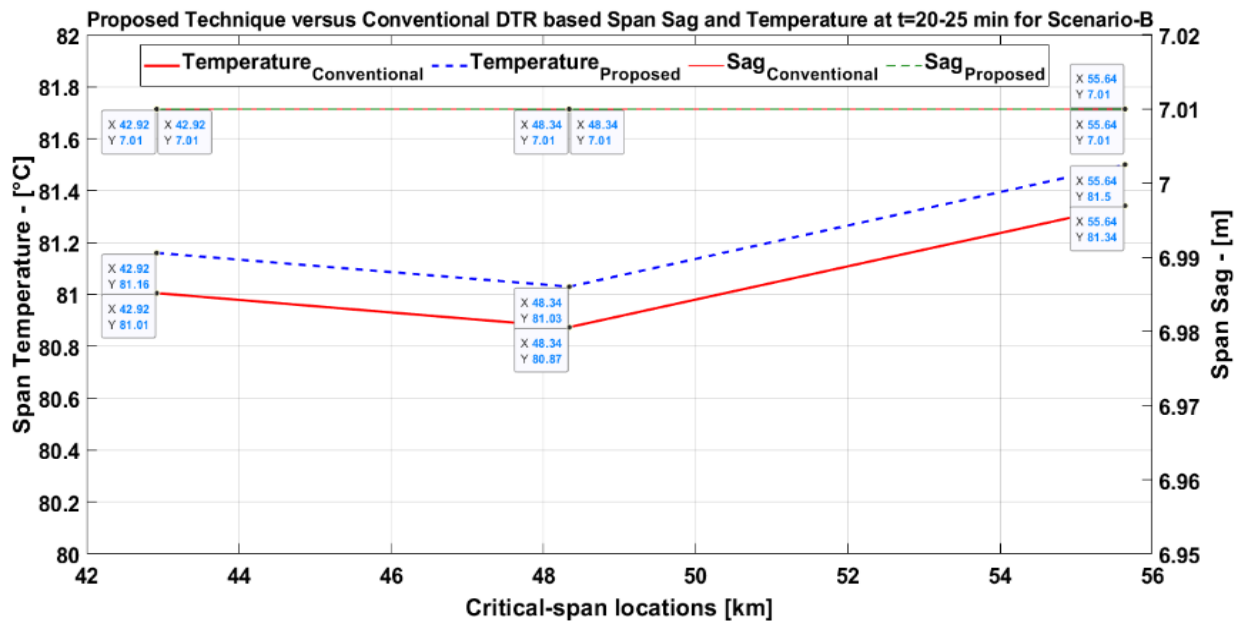


Fig. 7 Sag and temperature across all critical line spans passing through flat terrains based on conventional and proposed techniques under Scenario-B from t= 20 min to t= 25 min

To further validate the proposed technique, it was applied for all other temporal loadings, with and without space- and time-dependent weather conditions from $t=0$ min to $t=30$ min under both scenarios, resulting in critical span temperatures and their respective sagging levels as shown in Table 5 when passing through flat terrains and in Table 6 when passing through non-flat terrains. The results in Table 5 and Table 6 further indicate that critical span-1, when passing through non-flat terrain, experienced on average 2.88% more sag under the DTR technique than when passing through flat terrain subject to the same loading and weather.

Table 6 Sag across critical spans passing through flat terrains

Time (min)	Scenario-A						Scenario-B					
	Critical Span-1		Critical Span-2		Critical Span-3		Critical Span-1		Critical Span-2		Critical Span-3	
	DTR	STR	DTR	STR	DTR	STR	DT R	STR	DTR	STR	DTR	STR
	Sag (m)	Sag (m)										
0	6.56	6.79	6.56	6.79	6.56	6.79	6.67	7.05	6.67	7.05	6.67	7.05
5	6.56	6.79	6.57	6.79	6.57	6.79	6.76	7.05	6.76	7.05	6.76	7.05
10	6.71	7.05	6.72	7.05	6.71	7.05	6.85	7.05	6.85	7.05	6.85	7.05
15	6.70	7.05	6.71	7.05	6.71	7.05	6.93	7.05	6.95	7.05	6.95	7.05
20	6.70	7.05	6.70	7.05	6.71	7.05	7.01	7.05	7.01	7.05	7.01	7.05
25	6.59	6.89	6.59	6.89	6.59	6.89	6.76	7.05	6.76	7.05	6.75	7.05
30	6.57	6.79	6.57	6.79	6.56	6.79	6.64	6.89	6.64	6.89	6.63	6.89

Table 7 Sag across critical spans passing through non-flat terrains

Time (min)	Scenario-A						Scenario-B					
	Critical Span-1		Critical Span-2		Critical Span-3		Critical Span-1		Critical Span-2		Critical Span-3	
	DTR	STR										
	Sag (m)	Sag (m)										
0	6.75	6.99	6.75	6.99	6.75	6.99	6.86	7.25	6.86	7.25	6.86	7.25
5	6.75	6.99	6.76	6.99	6.76	6.99	6.95	7.25	6.96	7.25	6.96	7.25
10	6.90	7.25	6.91	7.25	6.91	7.25	7.05	7.25	7.05	7.25	7.05	7.25
15	6.89	7.25	6.90	7.25	6.91	7.25	7.14	7.25	7.15	7.25	7.15	7.25
20	6.90	7.25	6.90	7.25	6.90	7.25	7.21	7.25	7.21	7.25	7.22	7.25
25	6.78	7.09	6.78	7.09	6.78	7.09	6.95	7.25	6.95	7.25	6.95	7.25
30	6.76	6.99	6.76	6.99	6.75	6.99	6.83	7.09	6.83	7.09	6.82	7.09

Similarly, critical span-2, when passing through non-flat terrain, experienced on average 2.88% more sag under the DTR technique than when passing through flat terrain under the same weather and loading conditions. In case of critical span-3, when passing through non-flat terrain it experienced on average 2.91% more sag under the DTR technique than when passing through flat terrain under identical weather and loading conditions. Figs. 8-9 illustrate vertical sag across critical span-3 of the test line under DTR technique from $t=20$ min to $t=25$ min when passing through flat and non-flat terrains, respectively, under Scenario-B.

Besides sag, vertical distance of each line span to the ground is also important for transmission system operators to carry out reliable line loading. Due to unavailability of under span terrain topography data for each line span before and after the line loading, actual vertical clearance across critical spans was not found and is left as a future work subject to availability of the field data pertaining to span terrain topography. As a future work, the actual minimum vertical distance to ground will be considered across every line span while validating the proposed algorithm on real line loading.

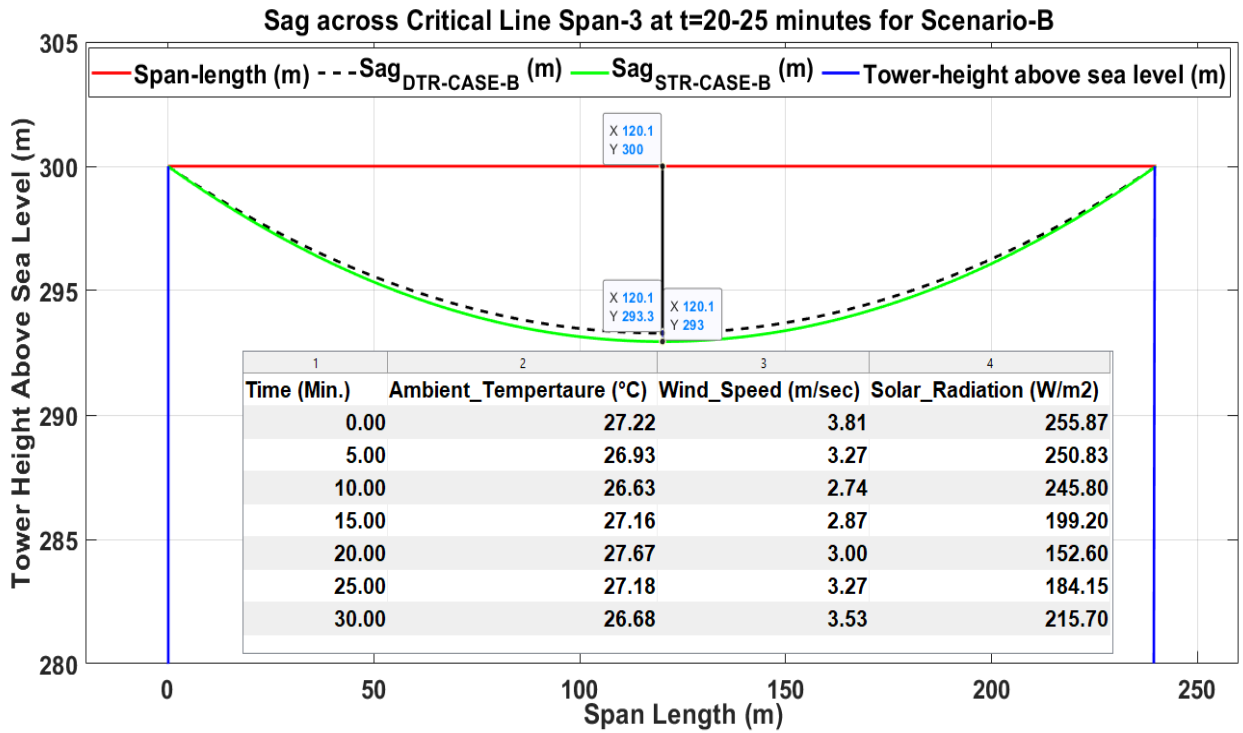


Fig. 8 Critical span-3 sagging when passing through flat terrain under t=20- 25 min

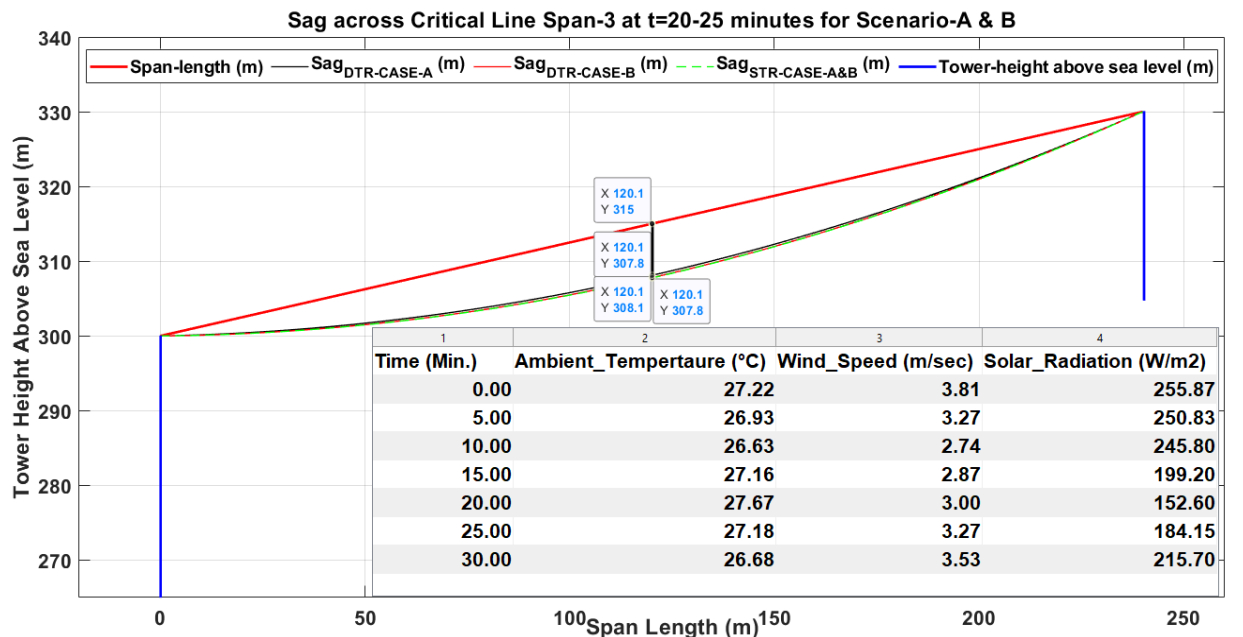


Fig. 9 Critical span-3 sagging when passing through non-flat terrain under t=20-25 min

6. Conclusion

This paper presents a novel technique to identify the critical spans across an overhead line operating under the DTR technique at the least computational cost. Optimal sensor placement used reference weather stations to determine the unknown weather elements across each span of the test line. The technique produced non-uniform segments, which

contained multiple critical and non-critical spans. Using the proposed critical-span identification technique, critical spans were identified based on weather and span-topography conditions.

The resulting critical spans were used to determine the thermal rating for the entire test line under static and real weather conditions. These spans were observed to have high sagging levels because they faced the worst weather and had the longest span lengths. These factors determined the global minimum of the line DTR to avoid ground clearance infringement across any line span, and thus control line loadability within allowable sag limits.

To validate the accuracy and computational efficiency of the proposed technique against the conventional technique, critical span identification using the conventional technique was carried out by computing the DTR across each span of the test overhead line, based on specified loadings and real weather conditions, to obtain the temperature and sag across each line span. The spans with the greatest sag were those with the highest conductor temperature and the longest span-length at the threshold of the MAT limit and were therefore identified as critical spans by the conventional technique.

The critical spans identified using the conventional technique were identical to those identified by the proposed technique. In the proposed technique, line temperature and sag across each individual span are not calculated; rather, the technique identifies spans as critical based on their surrounding weather conditions, topography and length. Based on the results obtained, the proposed technique is reliable and computationally cost-effective, and effective in differentiating critical and non-critical line spans across a non-uniformly segmented overhead line.

References

- [1] “Oncor’s pioneering transmission dynamic line rating (DLR) demonstration lays foundation for follow-on deployments,” U.S. Dept. Energy, MD, USA, 2014.
- [2] Final Report of Oncor-DOE Smart Grid Development Project fully documenting the DOE supported DLR project: https://www.smartgrid.gov/files/FTR_Final_Oncor_DE-OE0000320.pdf.
- [3] V. Cecchi, M. Knudson and K. Miu, "System Impacts of Temperature-Dependent Transmission Line Models," in *IEEE Transactions on Power Delivery*, vol. 28, no. 4, pp. 2300-2308, Oct. 2013. doi: 10.1109/TPWRD.2013.2276757.

-
- [4] V. Cecchi, A. S. Leger, K. Miu and C. O. Nwankpa, "Incorporating Temperature Variations Into Transmission-Line Models," in *IEEE Transactions on Power Delivery*, vol. 26, no. 4, pp. 2189-2196, Oct. 2011. doi: 10.1109/TPWRD.2011.2159520.
- [5] J. Teh and I. Cotton, "Critical span identification model for dynamic thermal rating system placement," in *IET Generation, Transmission & Distribution*, vol. 9, no. 16, pp. 2644-2652, 3 12 2015. doi: 10.1049/iet-gtd.2015.0601.
- [6] M. Matus *et al.*, "Identification of Critical Spans for Monitoring Systems in Dynamic Thermal Rating," in *IEEE Transactions on Power Delivery*, vol. 27, no. 2, pp. 1002-1009, April 2012. doi: 10.1109/TPWRD.2012.2185254.
- [7] J. W. Jerrell, W. Z. Black and T. J. Parker, "Critical span analysis of overhead conductors," in *IEEE Transactions on Power Delivery*, vol. 3, no. 4, pp. 1942-1950, Oct. 1988. doi: 10.1109/61.194004.
- [8] J. Wan *et al.*, "Determination of critical span in real time using proper orthogonal decomposition," *2013 Seventh International Conference on Sensing Technology (ICST)*, Wellington, 2013, pp. 816-821. doi: 10.1109/ICSensT.2013.6727765.
- [9] A. Hatibovics, "Determination of the lowest point of the conductor in inclined spans based on a known maximal sag of the parabola," *22nd International Conference and Exhibition on Electricity Distribution (CIRED 2013)*, Stockholm, 2013, pp. 1-4. doi: 10.1049/cp.2013.0583.
- [10] Talpur, Saifal, T. T. Lie, and R. Zamora. "Non-steady state electro-thermally coupled weather-dependent power flow technique for a geographically-traversed overhead-line capacity improvement." *Electric Power Systems Research* 177 (2019): 106017. doi: 10.1016/j.epsr.2019.106017.
- [11] IEEE Standard for Calculating the Current-Temperature Relationship of Bare Overhead Conductors," in *IEEE Std 738-2012 (Revision of IEEE Std 738-2006 - Incorporates IEEE Std 738-2012 Cor 1-2013)*, vol., no., pp.1-72, 23 Dec. 2013. doi: 10.1109/IEEESTD.2013.6692858.
- [12] Deb, Anjan K. *Powerline ampacity system: theory, modeling and applications*. CRC Press, 2017.
- [13] Morgan, Vincent T. "The thermal behaviour of electrical conductors." (Research Studies Press, 1997).
- [14] Ausgrid (2015) Network standard NS220. "Overhead design manual, NW000-S0092." Ausgrid.

-
- [15] National Institute of Water and Atmospheric Research (NIWA). [Online]. Available: <https://cliflo.niwa.co.nz/>. Accessed on 31st May 2019.
- [16] Küchenhoff, Helmut. "An exact algorithm for estimating breakpoints in segmented generalized linear models." (1996).
- [17] H. Jamali-Rad, A. Simonetto and G. Leus, "Sparsity-Aware Sensor Selection: Centralized and Distributed Algorithms," in *IEEE Signal Processing Letters*, vol. 21, no. 2, pp. 217-220, Feb. 2014. doi: 10.1109/LSP.2013.2297419.
- [18] C. Jiang, Y. C. Soh and H. Li, "Sensor Placement by Maximal Projection on Minimum Eigenspace for Linear Inverse Problems," in *IEEE Transactions on Signal Processing*, vol. 64, no. 21, pp. 5595-5610, 1 Nov.1, 2016. doi: 10.1109/TSP.2016.2573767.
- [19] Grant, Michael, Stephen Boyd, and Yinyu Ye. "CVX: Matlab software for disciplined convex programming (2008)." Web page and software available at <http://stanford.edu/~boyd/cvx> (2015).
- [20] Ryan, Sandra E., and Laurie S. Porth. "A tutorial on the piecewise regression approach applied to bedload transport data." Gen. Tech. Rep. RMRS-GTR-189. Fort Collins, CO: US Department of Agriculture, Forest Service, Rocky Mountain Research Station. 41 p. 189 (2007).
- [21] Morgan, V. T. "The current-carrying capacities of overhead-line conductors." (1978).
- [22] Dino, A., A. Ketley, and G. McDougall. "Dynamic transmission line rating: Technology review." *Hydro Tasmania Consulting* 30 (2009).
- [23] C. O. Boyse and N. G. Simpson, "The problem of conductor sagging on overhead transmission lines," in *Journal of the Institution of Electrical Engineers - Part II: Power Engineering*, vol. 91, no. 21, pp. 219-238, June 1944. doi: 10.1049/ji-2.1944.0029.
- [24] Muhr, Michael, et al. "Calculation of overhead line sags." *51st Internationales Wissenschaftliches Kolloquium*. Vol. 10. 2006.

Chapter 4

4.1 Introduction to Manuscript 3

This Manuscript addresses the techniques to enable the distribution transformer in order to achieve maximum capacity and maximum life expectancy. Under the proposed technique, the distribution transformer is loaded with a centralized battery energy storage system. The results are then compared with distribution transformer working without the battery energy storage system. The loading is considered in terms of electrifying an entire neighbourhood of 40 houses connected to a same DT, where each household consists of a single battery electric vehicle (BEV). The BEVs are charged under coordinated and uncoordinated charging scenarios, representing the BEV charging during off-peak hours and BEV charging during peak-hours, respectively. To improve the power transfer capacity, the distribution transformer is loaded under dynamically varying ambient temperature during two typical winter and summer months.

The Manuscript is published in the journal of *Energies* under the title “Maximum utilization of dynamic rating operated distribution transformer (DRoDT) with battery energy storage system: Analysis on impact from battery electric vehicles charging”. *Energies* 2020, vol. 13, 3411; doi:10.3390/3en13133411

4.2 Manuscript 3

Maximum utilization of dynamic rating operated distribution transformer (DRoDT) with battery energy storage system: Analysis on impact from battery electric vehicles charging

Saifal Talpur ^{1*}, Tek Tjing Lie ¹, Ramon Zamora ¹ and Bhaba Priyo Das²

1 School of Engineering, Computer and Mathematical Sciences, Auckland University of Technology, Auckland, New Zealand

2 ABB PGTR Hub (Asia), ABB Ltd. Singapore

Abstract

This paper investigates thermal overloading, voltage dips and insulation failure across a distribution transformer (DT) under residential and battery electric vehicle (BEV) loading. The objective of this paper is to discuss the charging impact of BEVs on voltage across consumer service points, life of paper insulation under varying ambient temperature (during winter and summer) with and without battery energy storage system (BESS). This paper contributes in two parts. First part deals with coordinated and

uncoordinated BEV charging scenarios. Second part deals with maximum DT utilization under dynamic rating operated DT (DRoDT) integration with BESS to flatten the peak load spikes, to obtain maximum DT utilization, to achieve the active and reactive power support and an enhanced DT lifespan. The obtained results indicate that when DT operates under the hybrid proposed technique, it attains maximum utilization, lower hot-spot temperature, enhanced lifespan, less degraded paper insulation and improved voltage across the consumer service points. The proposed technique is found effective in maintaining the loading across the distribution transformer within the nominal limits. Under this loading, the test DT is loaded below the nominal capacity. This operational loading across test DT is further facilitated with the help of within limits charging and discharging cycles of a centralized BESS. Under the proposed DRoDT integration with BESS, DT attains 25.9% more life when loaded with coordinated BEV charging in comparison to no BESS integration under the same loading scenario. The worst loading due to uncoordinated BEV charging also brings 51% increase in DT life when loaded under the proposed technique.

Keywords: *battery energy storage system; coordinated versus uncoordinated battery electric vehicles charging; distribution transformer; dynamic transformer rating; paper insulation*

NOMENCLATURE			
I_a, I_b, I_c	Phase load currents	k_a, k_b, k_c	Phase load factors
k_{11}	Thermal model constant	k_{unb}	Unbalanced load factor
$S_{T/F,base}$	DT nominal kVA	$S_{T/F,max}$	DT maximum kVA
$T_{ToT_{rise}}$	Top oil temperature rise	T_a	Ambient temperature
T_{ToT}	Top oil temperature	ΔT_{oi}	Top-oil temperature rise at start
T_{HST}	Winding hot-spot temperature	$\Delta T_{H_{rise/fall}}$	Hot-spot temperature rise/fall
ΔT_{oi}	Top-oil temperature rise at start	ΔT_{or}	Top-oil temperature rise in steady state
τ_0	Oil time constant	R	Ratio of load losses
DP_{start}	DP at start of DT loading	DP_{tend}	DP at end of DT loading at time t
A	Environmental factor	E_A	Activation energy
n	Number of loading interval	N	Total number of loading intervals
t_n	Step time of each loading interval	t_{exp}	Expected DT life
$E_{BESS,stored}$	Stored energy in BESS	η_{BESS}	BESS efficiency
$E_{nominal}$	BESS nominal energy	E_{losses}	Losses in BESS
$E_{BESS_Max_charge}$	BESS maximum charging	$E_{BESS_Min_discharge}$	BESS minimum discharging
$E_{BESS,extracted}$	Extracted energy from BESS	$E_{BESS,available}$	Available energy in BESS

1. Introduction

A rising demand in battery electric vehicles (BEVs) is becoming the major cause of under and over utilization of distribution transformers (DTs) in the low voltage (LV) distribution network. The BEV fleet has got the potential to underutilize DTs (loaded below the design rating) or overutilize the DTs (loaded above the design rating) based on their charging and demand profile. An uncoordinated BEV charging load integration with the base load will significantly raise hot spot temperature inside the windings, becoming an ultimate cause of insulation degradation through pyrolysis [1]. Additionally, due to aggregated BEV charging; generation, transmission and distribution network operators will face added complexity in securing and managing a reliable power flow in their networks [2]-[3].

The BEV charging can take place under both slow and fast charging modes. Slow charging can be further classified into coordinated and uncoordinated modes of charging. An uncoordinated BEV charging is the type of charging which does not only impact the DT insulation but also raises phase and line voltage drop across the residential loads in addition to reducing the system load factor [4]. Similarly, the authors in [4] have also demonstrated that uncoordinated BEV charging is responsible to significantly increase the peak load regardless the uncontrolled or non-resilient charging pattern. Despite causing insecurity in the network, the uncoordinated BEV charging is still widely adopted in contrast to smart BEV charging, mainly due to lack of communication infrastructures to enable demand response-based BEV charging [3]. Under uncoordinated BEV charging, vehicle is allowed to be charged when plugged. This type of charging causes load spikes which can cause DT overloading. Distribution transformer operating under maximum utilization can address uncoordinated BEV charging associated problems, provided it can handle the rising hot-spot temperature under no voltage violations, particularly at the end-most residential loads. As suggested in [5], the uncoordinated BEV charging can cause severe voltage violations and DT overloading leading to the likelihood of N-1 state.

The coordinated BEV charging method can reduce and/or eliminate congestion in the LV network besides delaying the costly asset upgrades. Hence, by providing the technical and economic benefits to distribution network operators (DNOs), the coordinated BEV charging mode is considered a better option over uncoordinated BEV charging. BEVs under coordinated BEV charging mode are not allowed to be charged at the plug-in time rather at the time defined by DNOs, usually, the off-peak time. The benefits associated

with delayed BEV charging are illustrated in [4] and [6]-[7], where authors in [4] have claimed that coordinated BEV charging based implementation will be able to improve asset efficiency, power quality and voltage regulation in the LV network. The coordinated BEV charging enables coordination between local and centralized control modes that is further used to provide effective branch congestion management required to deal with BEV charging based voltage drops and at the same time enables BEV participation in the electricity trading [6].

To obtain reliable electricity flow and efficient DT loading, increased BEV penetration trend needs to be addressed through efficient charging techniques useful for both users and the utilities. As an immediate asset to facilitate BEV charging, the DT efficiency and lifespan are heavily influenced by available battery capacity, current drawn, charger efficiency and the power limit of BEV chargers. The recent research work as published in [8]-[11] has suggested various viable techniques capable of addressing the LV network issues resulting from inefficient BEV charging. For instance, the optimized BEV charging schedule will offer shifting the charging load and simultaneously contributing to shaved load peaks [8]. Similarly, as suggested in [9], an integrated technique combining the day-ahead load planning with optimized smart charging can be effective towards minimizing the network congestion. In [10], a fuzzy logic control system is implemented to bring real-time communication between LV distribution system and BEVs to control the battery state of charge (SoC) based on electricity pricing. The implementation of incentive-based regulation as suggested in [11] will allow peak load shifting to minimize the network congestion.

The BEV penetration across the distribution transformers is mainly seen as an unbalanced load, causing harmonics [12], increased loss of life and reduced DT lifespan [13]. The techniques like demand response [14], demand response with dynamic rating [15], demand response in an intelligent grid [16] and the usage of battery storage in the LV network to provide active and reactive power balancing [17]-[18] are considered as potential means towards effective congestion management in the LV distribution network and to improve the DT lifespan. However, when DTs are loaded, particularly under uncoordinated BEV charging, voltage regulation and peak shaving amid improved DT life and costly asset upgrade deferral for DNOs become the major concerns for consumers as well as DNOs. The proposed dynamic rating operated distribution transformer (DRoDT)-battery energy storage system (BESS) technique can resolve consumer and the DNOs' issues by bringing the maximum DT utilization-based loading operation.

The remainder of this paper is organized as follows. Section 2 describes motivation behind the research work. Section 3 illustrates methodology of the proposed work. Section 4 describes the test system. Section 5 presents results and highlights the discussion. Section 6 summarizes findings of the paper in addition to presenting the future work.

2. Motivation

Residential load aggregation with BEV charging load is carried out to obtain maximum DT utilization, as beneficial for users as well as for DNOs in terms of reducing both losses and the upgrading costs. This work is inspired by [13] and [15]. In [13], the algorithm is designed to provide the maximum DT utilization under short-term emergency overloading. Similarly, the algorithm in [15] is designed to make sure T_{HST} remains under 110 °C based on demand response and dynamic thermal rating techniques. Regardless of optimal DT design, loading the DTs above their normal cyclic loading will likely cause the temporary weakening in the dielectric strength (of paper and oil) due to presence of gas bubbles when the temperature reaches 140°C or above [13]. The model can moreover be feasible under loss of supply to make sure that the DT loading duration is within the nominal DT limits [19]. Besides, the voltage regulation in [13] is investigated without considering the voltage drop due to impedance of the service cable. Similarly, the study has considered phase voltage regulation without analyzing the voltage drop across each household and/or the amount of voltage drop between the households nearest and farthest to the DT. Another drawback of the proposed algorithms in [13] and [15] is their load profile consideration for a single day instead of the entire seasonal based loading.

The seasonal-load profile can provide better estimate of the maximum peak demand and its impact on thermal loading as well as the total loss of life (LoL) of the DT as demonstrated in [20]. The algorithm in [15] proposes maximum DT utilization without considering the BEV charging load. Therefore, utilizing such approach under extensive BEV charging load will cause above the maximum DT utilization leading to excessive thermal loading for a longer duration, particularly in case of slow BEV charging, extending the DT's thermal overload time. Refs. [7] and [13] have considered loading the DT above normal cyclic loading to obtain maximum utilization. The studies, however, lack in examining the impact of DT'S thermal overloading on the voltage drop across each household, i.e., the thermal loading causing the voltage below the minimum specified can cause problems related to network reliability.

The work presented in [21]-[22] have demonstrated the BESS application in the LV network. The loading impact of BEV charging on the DT is reduced through the stored energy [21], further useful to increase hosting capacity and reduce congestion in the LV network [22]. A centralized BESS approach in [21]-[22] can relieve congestion in the LV network and increase the hosting capacity. The work, however, did not address the BESS charging/discharging impact on insulation and LoL. The voltage across each load point was also ignored under DT-BESS operation. The proposed approach in this paper is therefore designed to overcome the shortcomings of the above studies through following objectives:

- Minimizing the BEV charging impact on DT life
- Scheduling the charging and discharging of BESS during the low-price and high-price hours, respectively
- Flattening the load factor to obtain below the maximum limit [19]
- Maintaining voltage drop within nominal limits across each household
- Maximizing the paper insulation life

The hybrid DRoDT-BESS technique is therefore proposed in this paper to achieve the said objectives. The proposed technique is designed to not exceed of the test DT's temperature beyond 120 °C (design nominal [19]) during the winter season when the base load demand is comparatively higher than during summer. The weather-dependent DT thermal loading associated with electro-thermal coordination (ETC) between electrical and thermal parameters is carried out. Electrical parameter is the form of load factor (ratio of actual to base loads), whereas thermal parameter is the ambient temperature across the DT. The relationship based on coordination between electrical and thermal parameters can effectively determine the maximum DT capacity towards reliable transfer of excess electricity. For instance, a higher load factor under increased ambient temperature will limit the DT's hosting and thermal capacities and cause a rise in voltage dip across the load-points. Contrary to that, a reduced load-factor coupled with low ambient temperature will increase the DT's hosting and thermal capacities in addition to voltage surge across the load-points. In order to ensure an optimum DT operation to avoid these extreme conditions, this paper therefore introduces the hybrid technique capable of achieving the core objectives.

The constraints like surge in insulation degradation and voltage dips in result of increased DT loading can be considered as bottlenecks to optimal power flow through distribution feeders and the DTs, resulting in overutilization of DTs, higher LoL, lower power flow, increased congestion and costly upgrades. Contrary to that, load factor decrement can lead to voltage surges, causing underutilization of DTs. The DRoDT-BESS combination can bring DT loading within the limits by providing an optimum load sharing between DT and the BESS, DT capacity enhancement, optimal power flow in result of DT-BESS integration. The proposed technique can also be beneficial in case when DT goes out for maintenance and the stored energy in the centralised BESS can be used to improve the voltage across each phase (an added advantage over the decentralised BESS). BESS as a grid-booster together with DRoDT can mitigate voltage violations at each consumer service point. As mentioned in [14], voltage imbalance must be monitored at each consumer service point, not at the primary distribution level. This paper addresses this very issue by monitoring the voltage at each consumer service point before and after BESS implementation to analyze voltage deviation from the allowable range and the need for subsequent improvement.

Regarding BESS feasibility, a centralized 100 kW BESS at LV distribution network was used in this study. The BESS was installed at secondary side of the test DT to provide load sharing with test DT and contribute towards peak shaving and valley filling. In this study, BESS provided the optimal DT loading. To get a better idea about feasibility of the BESS, it is important to know the challenges and/or drawbacks that a BESS may bring in addition to offering such benefits. The benefits associated to BESS as per claimed in this study may outweigh the drawbacks associated with BESS. It is because, the importance of installing BESS in the LV network, particularly in this study is substantial, as helping the test DT towards fulfilling the load demands, mainly arising from BEVs. To make a fair judgment, the following points serve benefits as well as drawbacks associated with centralized BESS:

- Reduced electricity cost by 16.7% per house/day after centralized BESS installation [23]
- Substantial peak load reduction in the MV/LV substation due to utility owned BESS over distributed ownership of PV-battery system [24]
- Reinforcement deferral of a 10 kV cable in the distribution network

- Leading to cause high investment costs but enabling the reduced loading on DT and offering the voltage support [25]
- BESS as a possible solution to cope with drawbacks associated to DGs such as voltage fluctuations, reverse power flows and high capital costs [26]
- Lead acid batteries may face life reduction if operating under high temperature and reduced efficiency if operating under low temperature [27]

3. Methodology

In this paper, an LV network of 40 households with segregated base and BEV charging loads is designed. The loads are supplied electricity through a test DT and a BESS. The BESS at the time of charging through the test DT works as a load while under discharging mode, it works as a source. DT-BESS integration is considered to fulfil the active and reactive power demands such that the DT attains maximum utilization within normal loading while BESS operates within the optimal charging and discharging range (10%-90%). The BESS size selection is based on attaining the maximum DT utilization during off-peak and peak periods. This hybrid combination is implemented to maximize the test DT's utilization and bring an improvement in DT's life in addition to obtain within-limits voltage across each house under studied charging scenarios. To make this possible, the stored energy from the BESS is used at times of need. Additionally, the BESS charging and discharging range is selected carefully to avoid any under and/or over charging situation.

The test model is simulated under two charging scenarios to provide load-factor across each phase of the DT. The resulting load factors are used in Algorithm-1 to obtain resultant load-factor, top-oil temperature (in °C) and across windings temperature (in °C), degree of polymerization (DP) and estimated paper life during winter and summer months in the year 2018. The flow chart as shown in Fig. 1 illustrates the working principle of Algorithm-1. The purpose of the designed Algorithm-1 is twofold, i.e., to load test DT such that it operates and attains maximum loading throughout the entire loading operation. Load factor across each phase of the test DT is calculated through the phase current ratios as shown in (1) indicating non-identical load factors across all three phases of the test DT in case of different current flowing through each phase. The phase load factors are then used to find the unbalance load factor, representing the uneven load distribution through each phase of the test DT as shown in (2) [13]. T_{HST} is calculated

under exponential equations method as provided in [19] by using (3) and (4). An increment in is seen under rising as shown in (3). Similarly, a decrement in T_{HST} is seen under decreasing as shown in (4). Both rising and falling are then used with increasing and decreasing hot-spot to top-oil gradient to find T_{HST} as shown in (5).

$$k_a = \frac{I_{actual,a}}{I_{base}}, k_b = \frac{I_{actual,b}}{I_{base}}, k_c = \frac{I_{actual,c}}{I_{base}} \quad (1)$$

$$k_{unb} = \sqrt{\frac{(k_a^2 + k_b^2 + k_c^2)}{3}} \quad (2)$$

$$T_{ToT_{rise}} = (T_a + \Delta T_{oi}) + \left\{ \Delta T_{or} * \left[\frac{1+R*k_{unb}^2}{1+R} \right]^x - \Delta T_{oi} \right\} * \left(1 - e^{\frac{(-t)}{(k_{11}*\tau_0)}} \right) \quad (3)$$

$$T_{ToT_{fall}} = (T_a + \Delta T_{or}) * \left[\frac{1+R*k_{unb}^2}{1+R} \right]^x + \left\{ \Delta T_{oi} - \Delta T_{or} * \left[\frac{1+R*k_{unb}^2}{1+R} \right]^x \right\} * \left(e^{\frac{(-t)}{(k_{11}*\tau_0)}} \right) \quad (4)$$

$$T_{HST} = \left(T_{ToT_{rise/fall}} + \left(\Delta T_{H_{rise}} - \Delta T_{H_{fall}} \right) \right) \quad (5)$$

where I is the current in Amperes; k_a, k_b, k_c represent phase load factors in p.u.; ΔT_{oi} and ΔT_{or} are top-oil temperature rise at start and in steady state in degree K, respectively; k_{11} is thermal model constant; t is time variable in min; τ_0 is oil-time constant; R is ratio of load losses at rated current to losses at no-load current. Eq. 5 (Arrhenius formula) in [19] is used to find the change in degree of polymerization (DP) from initial $DP_{start}=1000$ (at the start of the DT loading) to the final $DP_{t_{end}}$ (at time t_{end}) as shown in (6) [19].

$$\frac{1}{DP_{t_{end}}} = \left(A * t_{end} * \exp\left(\frac{E_A}{R*T_{HST}}\right) \right) + \frac{1}{DP_{start}} \quad (6)$$

where $DP_{t_{end}}$ is found at $T_{HST,end}$. The other parameters considered are, environmental factor $A = 1.6 * 10^4$ in h^{-1} , gas constant $R = 8.314$ in $J \cdot K^{-1} \cdot mol^{-1}$ and activation energy $E_A = 86$ $kJ \cdot mol^{-1}$ for a thermally upgraded paper. The total loss of life (LoL) based on T_{HST} is calculated through (7) [19].

$$Loss_{life} = \sum_{n=1}^N \left(\exp\left(\frac{15000}{383} - \frac{15000}{(T_{HST}+273)}\right) \right) * t_n \quad (7)$$

where n is number of each loading interval, N is the total number of loading intervals, t_n is the step time of each loading interval, considered in hours. The expected DT life can be calculated through (8) [19].

$$t_{exp} = \frac{\left(\frac{1}{DP_{t_{end}}} - \frac{1}{DP_{start}} \right)}{(A * 24 * 365)} * \exp\left(\frac{E_A}{R * T_{HST,end}}\right) \quad (8)$$

Eq. 7 from [19] is used to find the total estimated DT life in years, where $DP_{t_{end}}$ is computed at $T_{HST,end}$. The proposed DRoDT-BESS technique as illustrated in Algorithm-1 and Fig. 1 is based on load sharing between DT and BESS to achieve:

- 1) accuracy in T_{ToT} and T_{HST} based calculations for accurate estimation of DP, LoL and the expected DT life-time
- 2) BESS charging during low-priced hours and discharging during high-priced hours
- 3) optimal load sharing between DT and BESS to obtain maximum DT operation within limits phase-rms voltage across each household
- 4) an optimal load flow to obtain reduced load peaks mainly during high-priced peak loading hours

Algorithm-1 considers both peak and off-peak periods, where peak period is from 17:00 to 21:00 and off-peak period is before 17:00 and after 21:00 hours. Load current (due to base and BEV loading) flowing through each phase of the test DT is obtained from the test system (see section IV) and is converted into respective load factors that further with the help of (2) are converted into the resultant load factor. The resultant load factor under varying ambient temperature is then used to find the hourly changes in T_{ToT} during winter and summer seasons. It is important to mention that T_{ToT} calculation in this paper is carried out by using the exponential equations method instead of the differential equation method from [19]. Under the combined DT-BESS operation, T_{ToT} is calculated by using the load factor as obtained after their load sharing. The coupling between thermal and electrical characteristics of the DT is therefore addressed in the context of electro-thermal coordination (ETC).

Based on the degree of coordination, an optimal DT loading can be obtained. For instance, a lower ambient temperature coupled with lower load factor will enhance the DT loading and will contribute to reduced congestion across the DTs [13]. Similarly, a higher ambient temperature at peak DT utilization will likely cause the DT to reach the thermal limit before the maximum specified [13]. A non-linear combination between ambient temperature and the load factor will also impact the optimal DT loading range. The optimal loading of the test DT in this paper is set at either DT achieving the maximum utilization or operating under normal loading limits as specified in [19]. To meet these criteria, the stored energy in BESS is used to fulfil the load-requirement while working in combination with the test DT. The DT loading limits at which BESS must feed-in to the loads via stored energy are set in accordance to the time-based load demand. For instance, during peak

loading period, when the DT load factor is equal to or above 0.73 p.u., and/or any load factor with corresponding T_a to cause T_{HST} between 80°C and 140°C during winter and summer seasons, the stored energy from the BESS is utilized. Similarly, during off-peak period, energy extraction from the BESS is based on either DT loading above 0.6 p.u or T_{HST} above 110°C as shown in Fig. 1. The proposed technique in addition to providing the active power support to flatten the load peaks also helps in regulating the voltage across each household within nominal limits ($\pm 6\%$) as per specified in [28].

Algorithm-1: proposed technique during BESS discharging

```

for ( $E_{BESS,stored} = (\eta_{BESS} * (E_{nominal} - E_{losses}))$ )
    ( $E_{BESS,Max\_charge} \geq E_{BESS,stored} \geq E_{BESS,Min\_discharge}$ )
     $t = (1:1:24)$ 
    for ( $t \geq 17$ ) && ( $t \leq 21$ )
        while [ $\{(k_{unb} * S_{T/F,base}) \rightarrow S_{T/F,max} \rightarrow (140^\circ < T_{HST})\}$ ] || ( $k_{unb} \geq 0.73$ )
            do ( $E_{BESS,extracted} = (E_{BESS,stored} - E_{BESS,available})$ )
                 $S_{T/F,max}|_{T_{a,min}}^{T_{a,max}} = [(P_{load}) - (E_{BESS,extracted})]$ 
                 $k_{unb} = \left(\frac{S_{T/F,max}}{S_{T/F,base}}\right)$ 
                ( $1.06 * V_{base}$ )  $\geq V_{a,b,c}^{actual} \geq (0.94 * V_{base})$ 
            end
        end
    end
    for ( $t \leq 17$ ) && ( $t > 21$ )
        while [ $(k_{unb} > 0.6) \rightarrow S_{T/F,max} \rightarrow (110^\circ < T_{HST})$ ]
            do ( $E_{BESS,extracted} = (E_{BESS,stored} - E_{BESS,available})$ )
                 $S_{T/F,max}|_{T_{a,min}}^{T_{a,max}} = [(P_{load}) - (E_{BESS,extracted})]$ 
                 $k_{unb} = \left(\frac{S_{T/F,max}}{S_{T/F,base}}\right)$ 
                ( $1.06 * V_{base}$ )  $\geq V_{a,b,c}^{actual} \geq (0.94 * V_{base})$ 
            end
        end
    end
end

```

Fig.1 indicates that the test DT supplies electricity to both residential load (including BEVs) and the BESS. However, the loading across test DT is reduced when BESS shares the load with the test DT. Load sharing with the help of BESS is a sub-optimal problem, where, the test DT is required to operate under maximum utilization. The parameter responsible for ensuring the maximum utilization of test DT is T_{HST} . The setting of T_{HST} is based on the loading time. During peak-loading period, T_{HST} must be below 140°C , and during off-peak loading, it must be below 110°C . This sub-optimal criterion is set to make sure the test DT operates under maximum utilization. When T_{HST} crosses the maximum limit of $140^{\circ}/110^{\circ}\text{C}$, BESS starts supplying the stored energy to the load until reaching the minimum discharge limit of 10%. Under both or any of those situations, the nominal voltage limit is also taken into account, which means after BESS sharing the load with the test DT, the voltage across all test DT phases is required to be within the nominal limit of $\pm 6\%$. Besides, as indicated in Fig.1, T_{HST} at which the test DT operates in the operation mode is used to find degree of polymerization, loss of life and the expected DT life with the help of the ambient and top oil temperatures under both the winter and the summer seasons in the simulation environment.

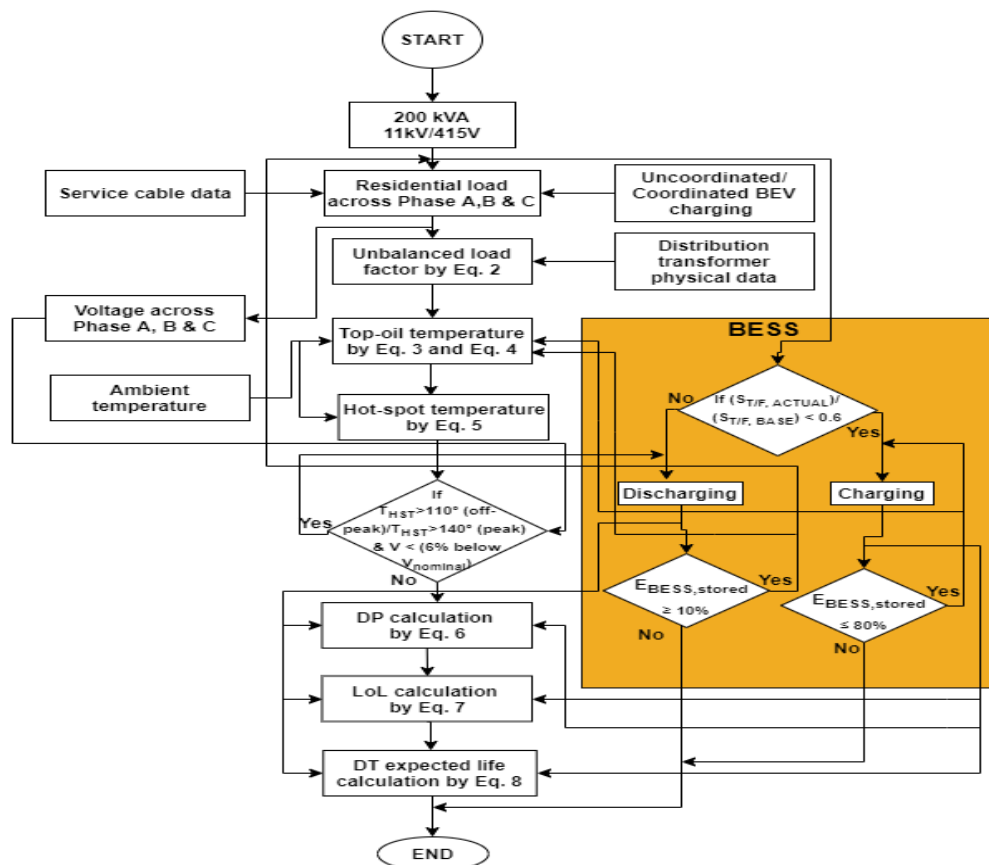


Fig. 1 Flow diagram of the proposed DRoDT-BESS technique

4. Test system

A test system developed in Simulink was used to carry out the design, modelling and simulation work in order to implement the proposed technique in the LV network. A neighborhood of 40 households, where each household has segregated base and BEV load, was connected to the secondary side of the test DT through XLPE service cable. An identical base load data as taken from [29] was used for each household in the entire neighborhood. The weather data for both winter and summer months was taken from [30]. The service cable was considered resistive-inductive type with data as shown in Table 1. A 50m distance was considered between two adjacent households. A complete model involving the test DT, BESS, base and the BEV loads is shown in Fig. 2.

Table 1
Service Cable Parameters

Type	XLPE Insulated/Single Core/Copper
Area	281 mm ²
Resistance (mΩ)	0.081 (at H-1), 52.71 (at H-14)
Reactance (mΩ)	0.082 (at H-1), 53.04 (at H-14)

BEVs used in the test system were 24 kWh Nissan Leaf, charged through 6.6 kW single-phase Level 2 AC chargers at 240 Vrms and 32 A rated charging current with additional parameters as shown in Table 2 under two charging scenarios, 1) coordinated and 2) uncoordinated. Under coordinated charging (controlled charging) scenario, all BEVs were charged during off-peak time, whereas under uncoordinated charging (uncontrolled charging) scenario, all BEVs were simultaneously charged during the peak loading time (plug-in time). Under uncoordinated charging scenario, as all BEVs were allowed charging at their fixed plugged-in time, voltage dip across each household was observed that increased with increase in length of the service cable with more voltage-drop across the farthest household than the household nearest to test DT. BEV charging as shown in Table 2 represents an unrealistic condition, where the aim was to get maximum DT loading period under the worst loading scenario and to find how much load BESS can share during the required maximum loading duration.

Table 2
BEV Parameters

Charging load power factor	0.9
Battery charging status	1 (SoC-100%), 0 (SoC-0%)
Initial battery SoC	0%
Charger load type	constant impedance

In terms of test DT connection, the primary side of the DT was connected to 11kV LV grid-side (primary side with phase-factors), considered as a slack-node at fixed input voltage ($|U|=1.0$ pu, $\delta=0^\circ$) to further restrict the BESS influence across the grid-side. An unbalance phase load consisting of 14 households across Phase-A and 13 households across each Phase-B and Phase-C was connected to 415 V secondary side of the test DT. Some important data used in thermal and electrical modeling of the test DT is shown in Table 3. The BESS used in the test system was considered 100 kW/200 kWh as a stationary centralized energy storage connected with the test DT.

Table 3
200 kVA Transformer Parameters

Number of phases	3
LV Voltage	415 V/50Hz
Cooling method	ONAN
Impedance	8%
Top oil temperature rise	55 K
Top oil temperature rise above ambient	60.95 K
Hot-spot to top-oil	23 K
Oil time constant	180
Winding time constant	4
Loss ratio	5
$k_{11}/k_{21}/k_{22}$	1.0/1.0/2.0

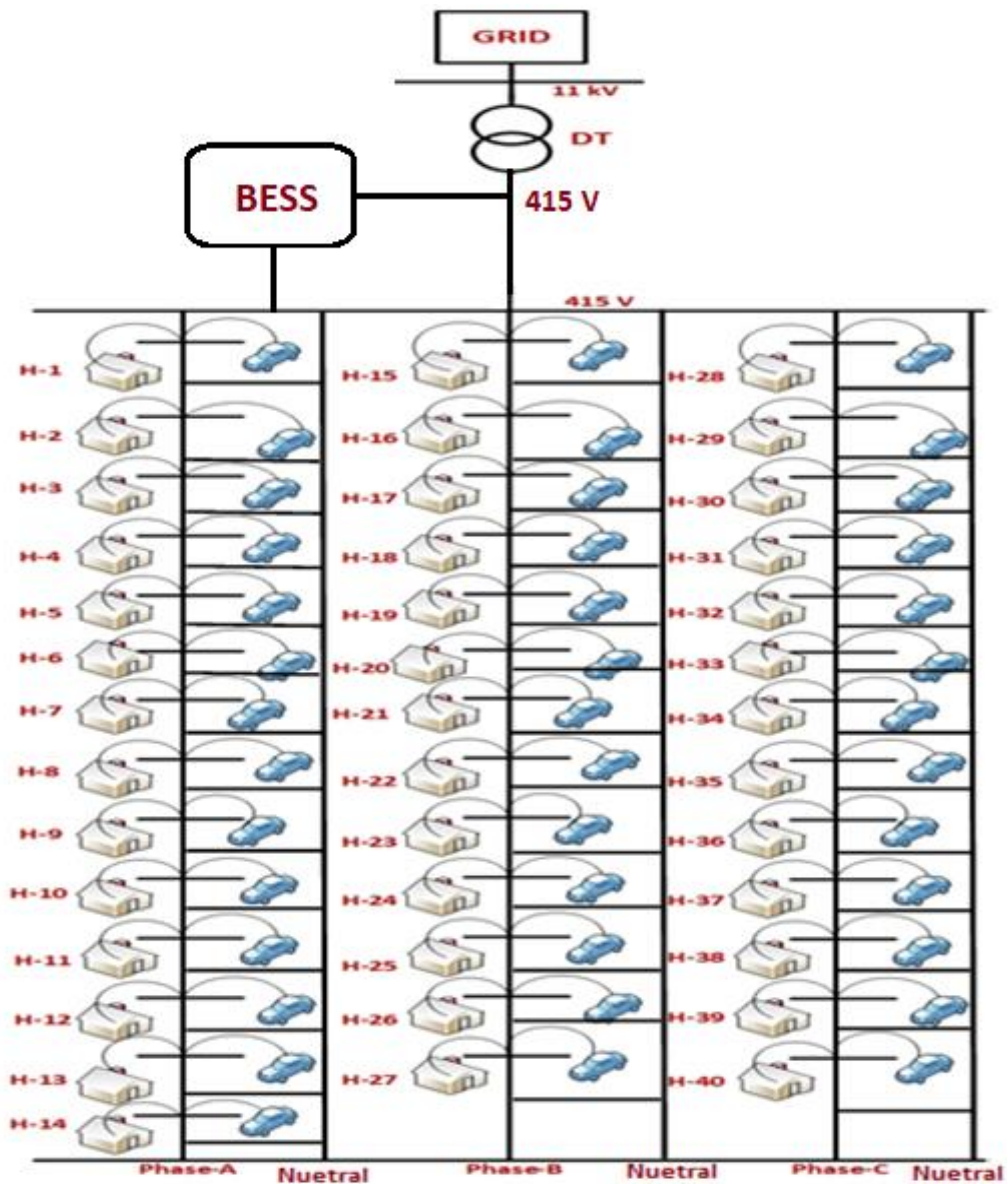


Fig. 2 Single line diagram of the modelled 40-house network

5. Results and Discussions

The results in the following scenarios indicate that in order to obtain maximum DT utilization, the DT must be operating under specific limits through its entire loading operation. These specific limits besides the load factor must also consider region-specific voltage regulation to facilitate an uninterrupted and reliable supply of electricity to consumers. Two weather scenarios are considered in this study, i.e. winter and summer. Weather data for both seasons was obtained from the location based in Henderson, New Zealand. Two month study was carried out in the simulations, where the month of July 2018 represented the winter season and January 2018 as the month in summer season.

5.1 DT Simulation Scenarios

A. Scenario 1: Uncoordinated BEV charging during winter

1) Without BESS

The results of this scenario as shown in Fig.3 represent uncoordinated BEV charging on electrical and thermal loading states across the test DT without BESS installation. The scenario represents BEV charging during peak-period. All 40 EVs are charged simultaneously at the time of being plugged. Hence, under this scenario, no delay in charging the vehicles is carried out. The simultaneous charging effect can therefore be seen causing congestion across the test DT in addition to voltage drop across each residential house nearest to and farthest from the test DT. A continuous hourly loading across the test DT for the whole month of July 2018 is seen to cause paper DP falling from 1000 to 233.5, slightly above the end of life threshold at 200.

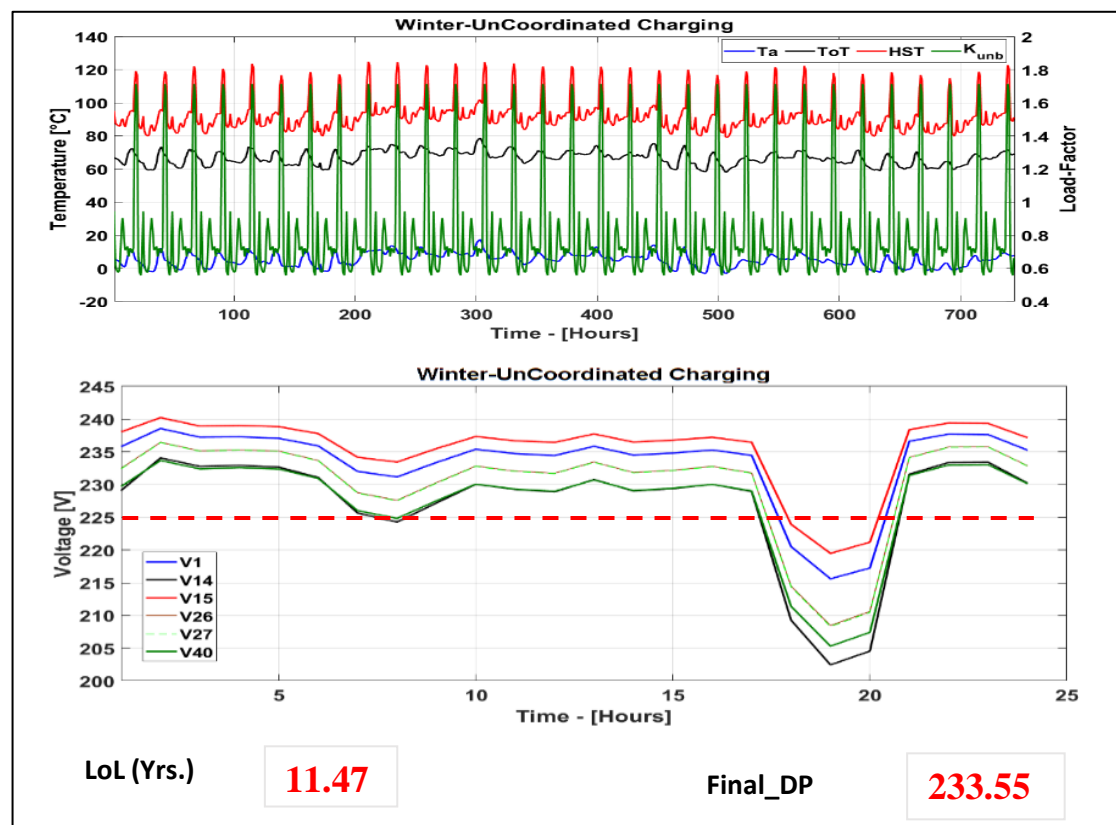


Fig. 3 Output under uncoordinated charging across selected households during winter without BESS

2) With BESS

Load sharing through BESS is obtained to relieve congestion across the test DT besides reducing the voltage dips across each household nearest to and farthest from the test DT as shown in Fig. 4. After BESS installation in the modelled LV network, 31.25% improvement in DP is obtained in comparison to the non-BESS installation under the same scenario. Similarly, 54.92% LoL of the test DT is decreased after BESS under the same weather and loading conditions.

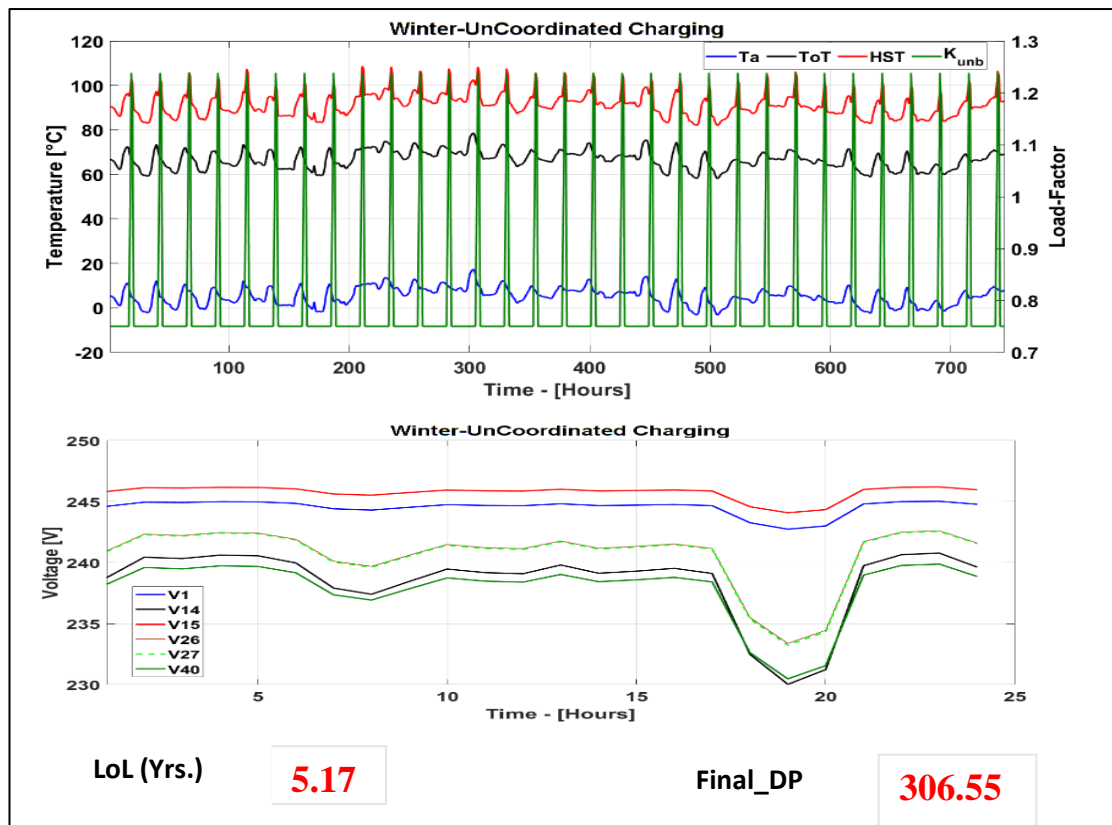


Fig. 4 Output under uncoordinated charging across selected households during winter with BESS

B. Scenario 2: Uncoordinated BEV charging during summer

1) Without BESS

Under this scenario, besides the BEV charging load, the ambient temperature is found to influence DT's thermal loading. A significant rise in the ambient temperature is observed to increase maximum T_{HST} by 11.56% and decrease DP by 10.85% in comparison to winter season under the identical residential and BEV charging load conditions as shown in Fig. 5.

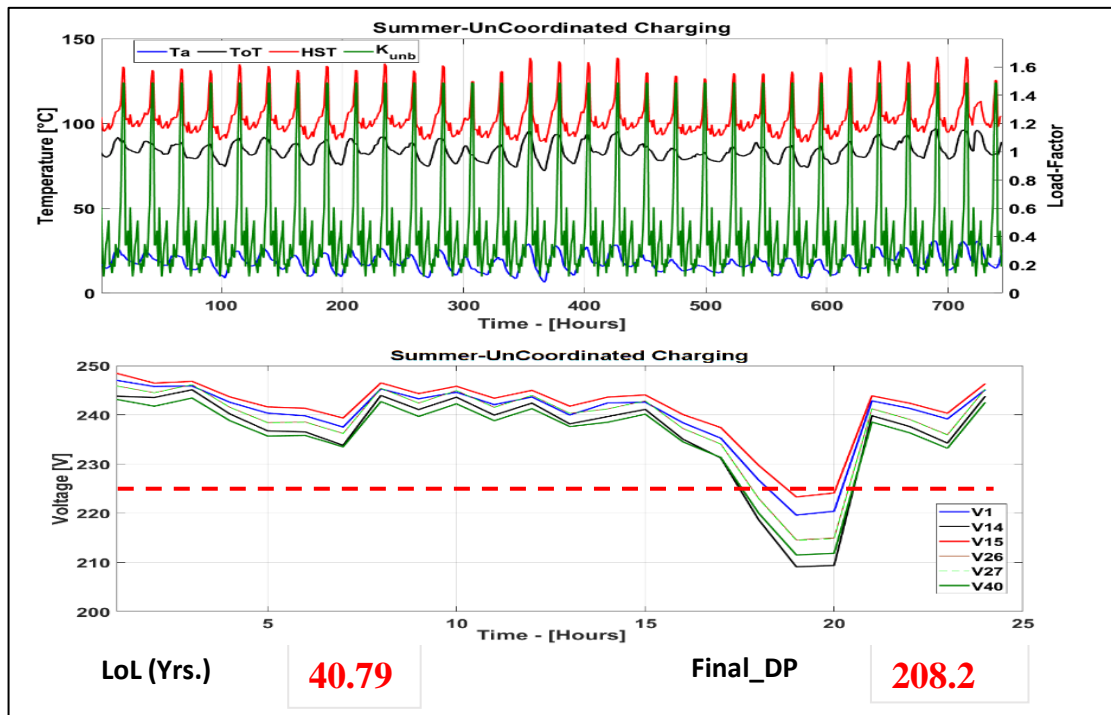


Fig. 5 Output under uncoordinated charging across selected households in summer without BESS

2) *With BESS*

This scenario represents load sharing through BESS along the test DT during summer. The results as shown in Fig. 6 indicate that the presence of BESS can effectively mitigate DT thermal overloading in comparison to the scenario carried out under the absence of BESS. The results further indicate that the hybrid technique is capable of reducing the T_{HST} to a certain extent throughout the entire loading duration.

C. *Scenario 3: Coordinated BEV charging during winter*

1) *Without BESS*

As shown in Fig. 7, the delay associated with coordinated BEV charging has the capability to protect test DT from thermal overloading but at the cost of voltage exceeding the nominal limit. For instance, the maximum voltage dip under this scenario across household-14 is observed 16.22% below the nominal limit as set under [28].

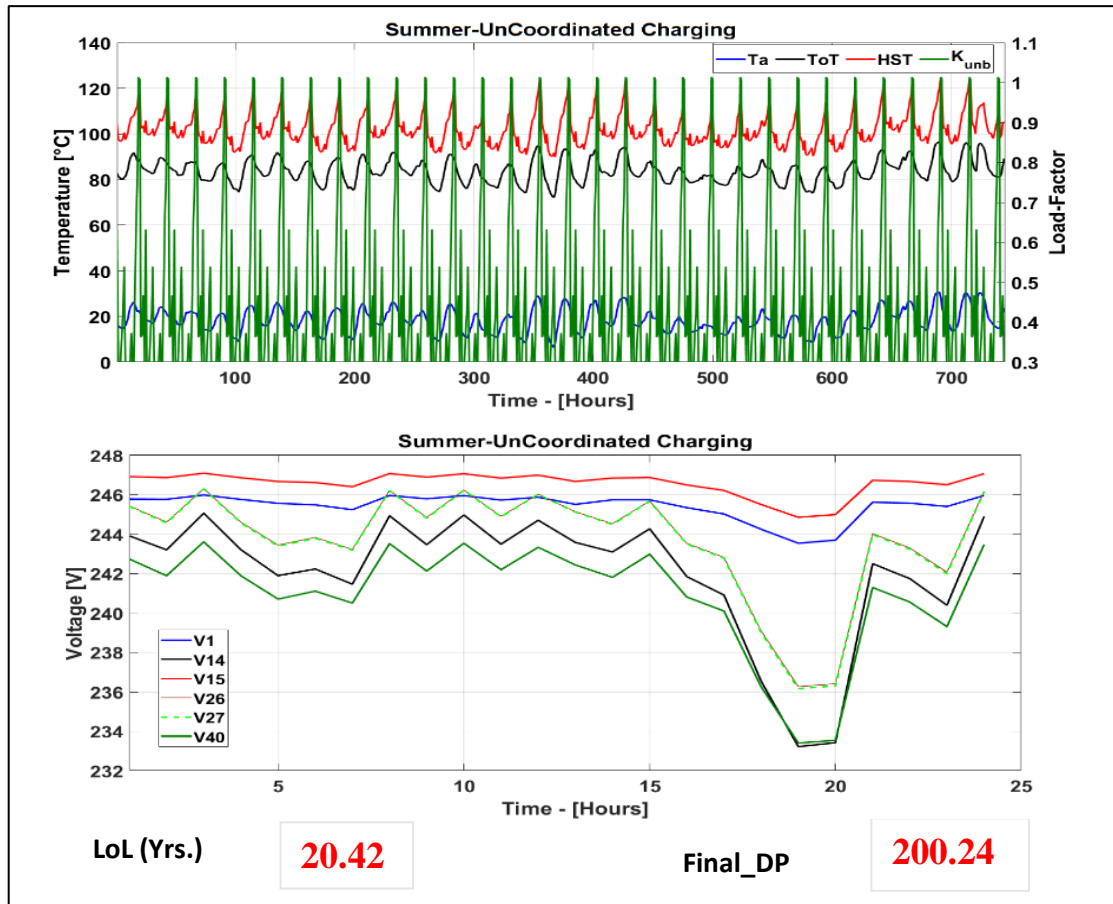


Fig. 6 Output under uncoordinated charging across selected households during summer with BESS

2) *With BESS*

As shown in Fig. 8, after BESS installation, not only the load peak is flattened but also 4.76% average rise in voltage is achieved across all load-points during 24 hours under the identical loading in comparison to the without BESS scenario under the same season.

D. *Scenario 4: Coordinated BEV charging during summer*

1) *Without BESS*

During summer, the test DT experiences high congestion, resulting in significant rise in T_{HST} and in voltage drop across each household as shown in Fig. 9. LoL of the test DT without BESS is observed 24.52% higher than the LoL with BESS.

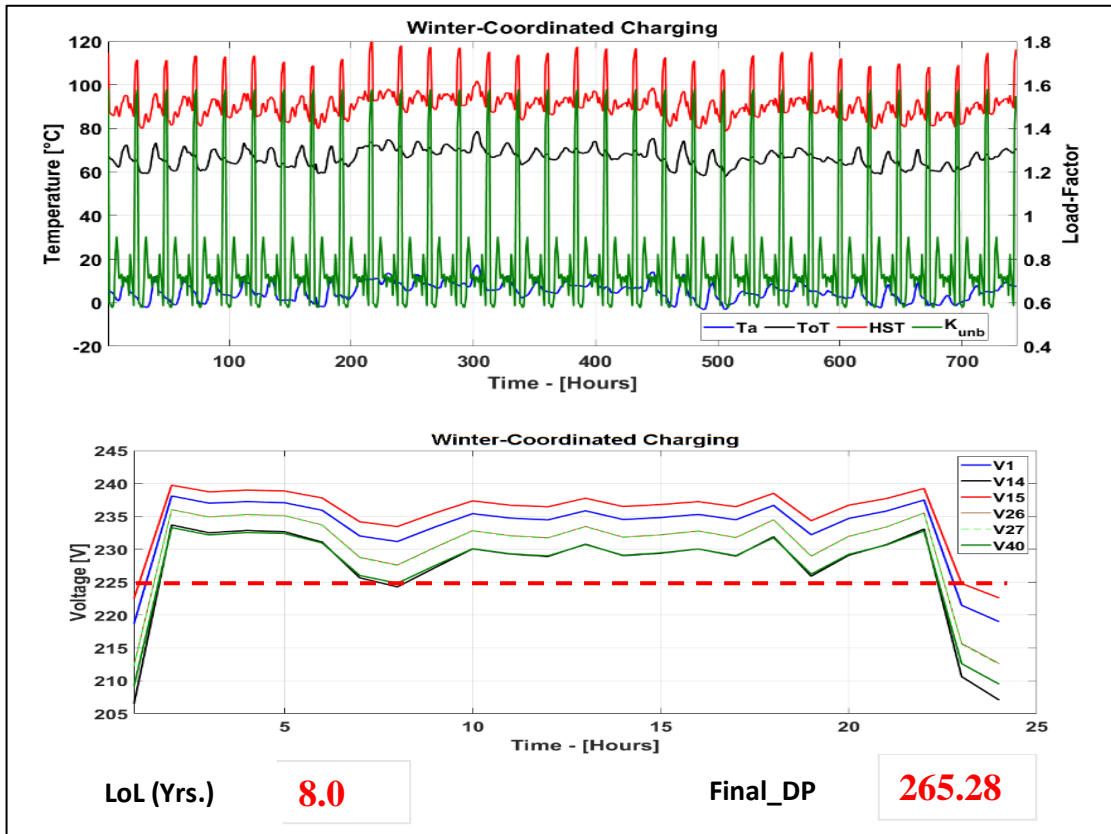


Fig. 7 Output under coordinated charging across selected households during winter without BESS

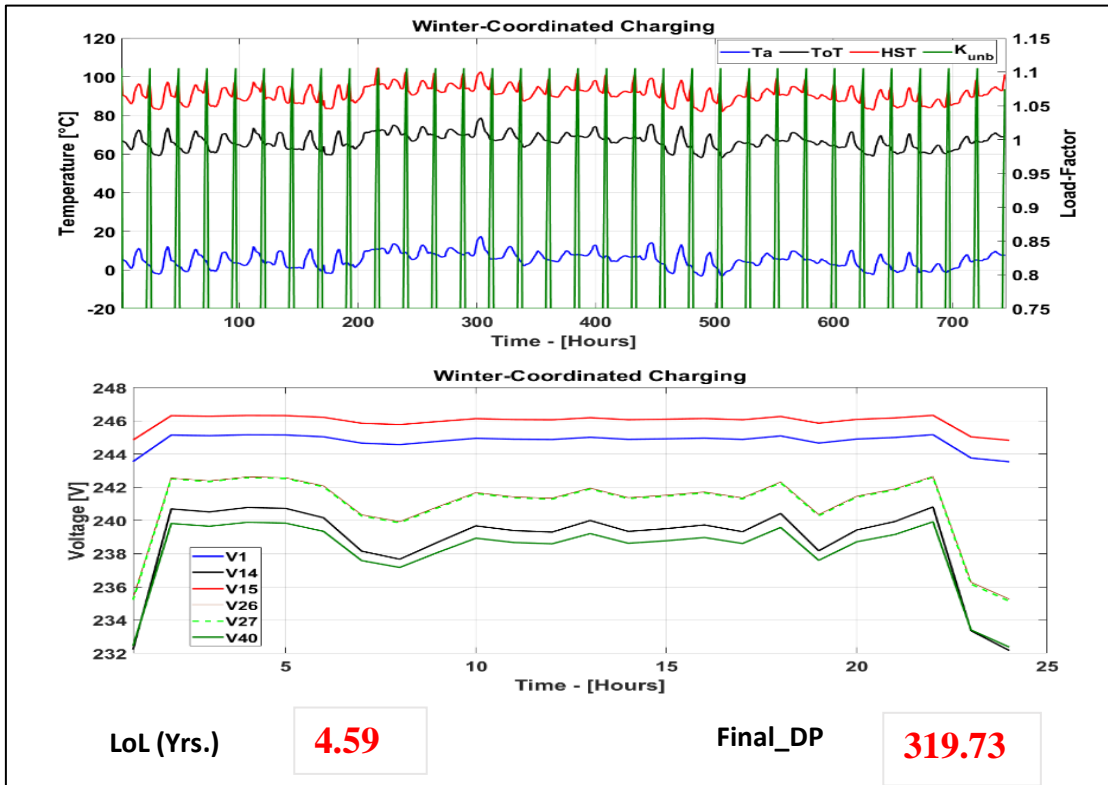


Fig. 8 Output under coordinated charging across selected households during winter with BESS

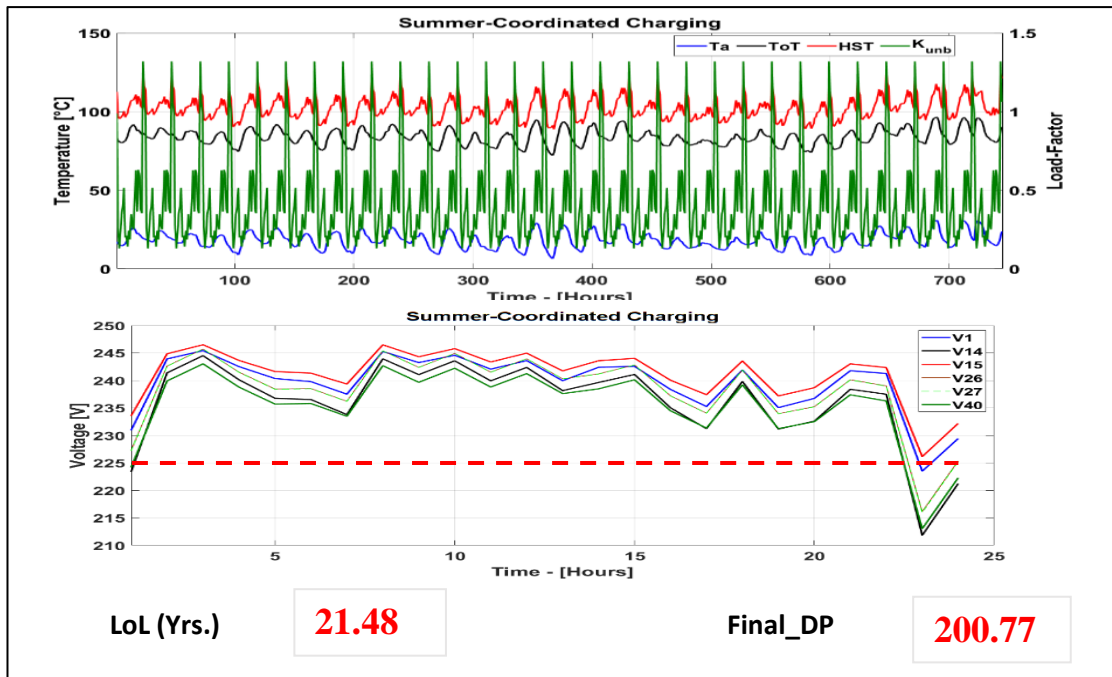


Fig. 9 Output under coordinated charging across selected households during summer without BESS

2) *With BESS*

To mitigate congestion by reducing the DT thermal overloading and improving the phase voltage across each household, BESS installation is carried out with the test DT.

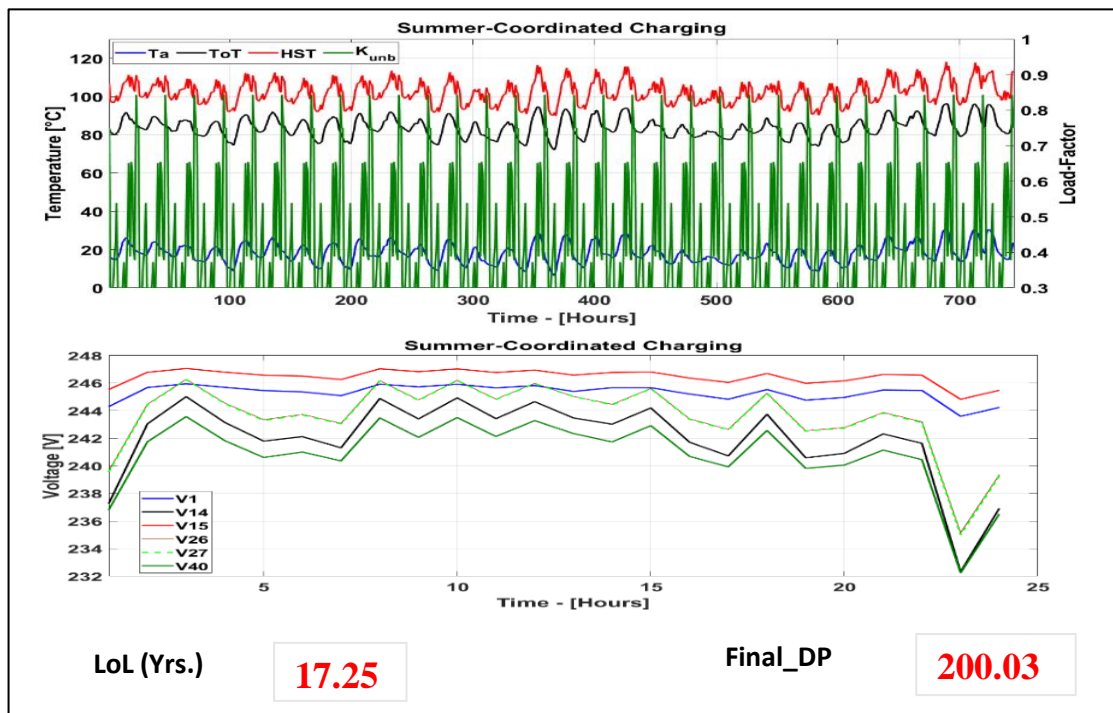


Fig. 10 Output under coordinated charging across selected households during summer with BESS

For instance, average voltage across all households during 24 hours of loading is observed 2.34% higher with BESS than without BESS under the same loading and weather conditions as shown in Fig. 10.

5.2 Centralized BESS integration

The integration of a centralized BESS with test DT is carried out to fulfil the load demand especially arising from BEV charging. BESS charging and discharging can be seen under nominal optimum range for all the studied scenarios as shown in Fig. 11. Fig.11 further indicates that BESS SoC remain between 10%-80% of the charging range. BESS integration during peak-loading period (under uncoordinated BEV charging) in winter resulted in optimal DT loading equivalent of 1.24 p.u. (i.e., well below the nominal cyclic loading [19] of the DT) with maximum T_{HST} obtained 108.7°C (below 120°C). The same scenario in summer has resulted in optimal DT loading of 1.01 p.u. with maximum T_{HST} obtained as 124.7°C (below maximum permissible 140°C [19]).

During winter, the test system under uncoordinated BEV charging without BESS resulted in 30% higher DT loading in comparison to coordinated BEV charging. Similarly, the test DT loading during winter under the proposed technique in result of uncoordinated BEV charging is found around 10% higher than under uncoordinated BEV charging. The results therefore indicate that BESS integration with DT can significantly reduce DT loading, particularly when DTs are faced with excess BEV penetration besides, it may improve DT life and provide voltage support in the LV network.

The proposed technique with BESS is further able to improve the voltage across each household by a significant margin. After BESS installation, average voltage across all households under scenario-1 is seen 4.64% higher than without BESS. Similarly, the average voltage dip across the same households under scenario-2 with BESS is seen 2.27% lower than found without BESS. Scenario-3 and scenario-4 are also observed with improved voltage across each household after BESS installation.

For instance, before the BESS installation, the average voltage drop during 24 hours of loading between household-1 and household-14 under scenario-3 and scenario-4 is obtained 2.61% and 1.43%, respectively, that is then reduced to 2.45% and 1.37%, respectively, after the BESS installation.

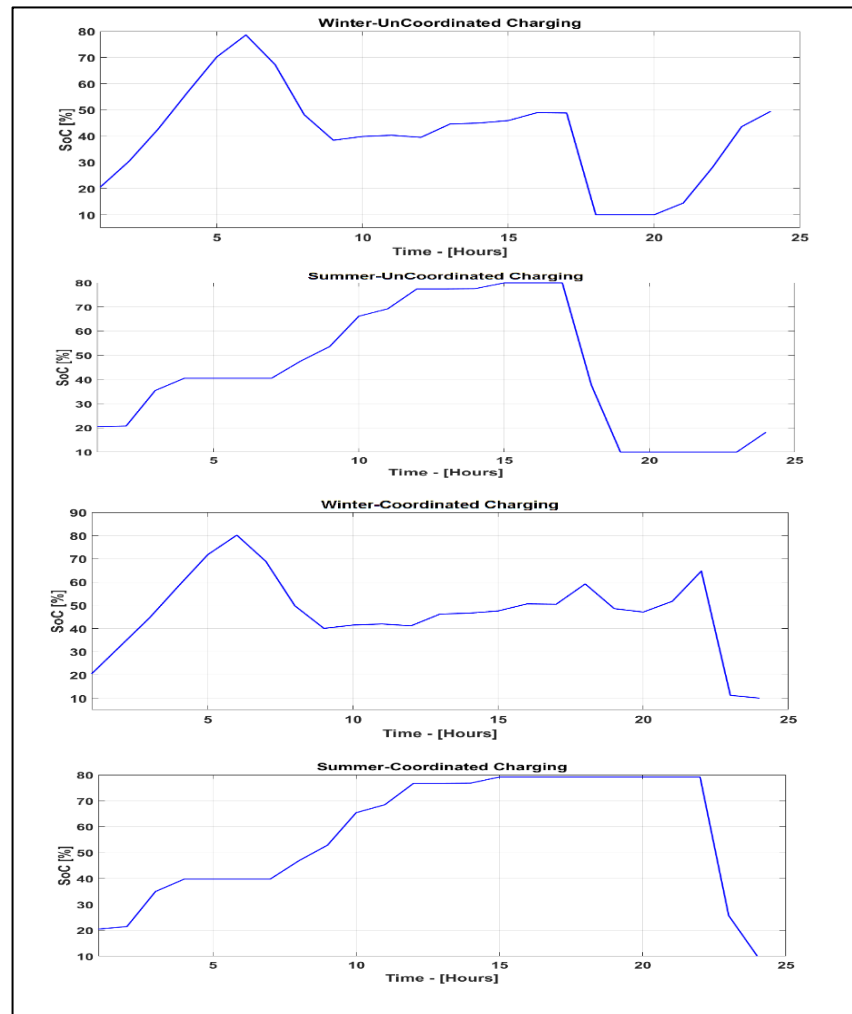


Fig.11 BESS state of charge (SoC) under multiple simulated scenarios

6. Conclusions and Future work

In this paper, an integrated DRoDT-BESS technique is presented, which is unique in its “designing for maximum utilization” concept. The obtained results indicate the capability of the proposed technique in reducing the congestion, DT thermal loading and voltage dips under studied BEV charging scenarios and different weather conditions. The objectives, like, optimal DT loading, optimum DT utilization under non-cyclic loading, accuracy regarding the T_{TOT} calculation, minimized DT thermal loading, optimal power flow, reduced congestion and voltage within the nominal limits are achieved with the help of the proposed technique. Under the proposed technique, the minimized congestion and thermal loading took place due to optimal timing associated with BESS charging/discharging cycles. BESS charging was carried out during off-peak period,

whereas the discharging took place during peak-periods and/or at the times of DT thermal loading beyond non-cyclic loading, to benefit both end-consumers and the DNOs. For the end-consumers, the benefits like 1) reliable active power flow by avoiding the risk of load-shedding (through minimized DT overloading), 2) voltage within limits and 3) reduced electricity price were obtained.

For the DNOs, the benefits like 1) longer DT life, 2) deferral of costly grid upgrades and 3) no additional support required in terms of reactive power were obtained. After considering the fluctuation of ambient temperature and the BESS integration, the proposed technique is found useful in significantly reducing the test DT's loss of life by 11.21% during winter when loaded under coordinated BEV charging compared to loaded under uncoordinated BEV charging. The loss of life reduction in summer under coordinated BEV charging is observed 15.52% lower than observed under uncoordinated BEV charging.

The technical and economic challenges associated to BESS raise concerns on feasibility of the BESS. It is therefore important to take into account these issues before operational usage of a BESS. Additionally, temperature variation, degradation and loss of life of the BESS are important parameters for better evaluation of the BESS feasibility. Their careful analysis and study will lead to decide the application of BESS in the LV network. These factors further lying out of the focus of the paper are therefore recommended as a future work.

References

- [1] A. D. Hilshey, P. Rezaei, P. D. H. Hines and J. Frolik, "Electric vehicle charging: Transformer impacts and smart, decentralized solutions," 2012 IEEE Power and Energy Society General Meeting, San Diego, CA, 2012, pp. 1-8. doi: 10.1109/PESGM.2012.6345472
- [2] Muratori, Matteo. "Impact of uncoordinated plug-in electric vehicle charging on residential power demand." *Nature Energy* 3.3 (2018): 193.
- [3] R. Jarvis and P. Moses, "Smart Grid Congestion Caused by Plug-in Electric Vehicle Charging," 2019 IEEE Texas Power and Energy Conference (TPEC), College Station, TX, USA, 2019, pp. 1-5.
- [4] E. Sortomme, M. M. Hindi, S. D. J. MacPherson and S. S. Venkata, "Coordinated Charging of Plug-In Hybrid Electric Vehicles to Minimize Distribution System Losses," in *IEEE Transactions on Smart Grid*, vol. 2, no. 1, pp. 198-205, March 2011.

-
- [5] E. Akhavan-Rezai, M. F. Shaaban, E. F. El-Saadany and A. Zidan, "Uncoordinated charging impacts of electric vehicles on electric distribution grids: Normal and fast charging comparison," 2012 IEEE Power and Energy Society General Meeting, San Diego, CA, 2012, pp. 1-7. doi: 10.1109/PESGM.2012.6345583
- [6] J. A. P. Lopes, F. J. Soares and P. M. R. Almeida, "Integration of Electric Vehicles in the Electric Power System," in *Proceedings of the IEEE*, vol. 99, no. 1, pp. 168-183, Jan. 2011.
- [7] C. Z. El-Bayeh, I. Mougharbel, D. Asber, M. Saad, A. Chandra and S. Lefebvre, "Novel Approach for Optimizing the Transformer's Critical Power Limit," in *IEEE Access*, vol. 6, pp. 55870-55882, 2018. doi: 10.1109/ACCESS.2018.2873077
- [8] Y. Wi, J. Lee and S. Joo, "Electric vehicle charging method for smart homes/buildings with a photovoltaic system," in *IEEE Transactions on Consumer Electronics*, vol. 59, no. 2, pp. 323-328, May 2013. doi: 10.1109/TCE.2013.6531113
- [9] N. G. Paterakis, O. Erdinç, A. G. Bakirtzis and J. P. S. Catalão, "Optimal Household Appliances Scheduling Under Day-Ahead Pricing and Load-Shaping Demand Response Strategies," in *IEEE Transactions on Industrial Informatics*, vol. 11, no. 6, pp. 1509-1519, Dec. 2015. doi: 10.1109/TII.2015.2438534
- [10] H. S. Salama, S. M. Said, I. Vokony and B. Hartmann, "Impact of Different Plug-in Electric Vehicle Categories on Distribution Systems," 2019 7th International Istanbul Smart Grids and Cities Congress and Fair (ICSG), Istanbul, Turkey, 2019, pp. 109-113. doi: 10.1109/SGCF.2019.8782335
- [11] E. Veldman and R. A. Verzijlbergh, "Distribution Grid Impacts of Smart Electric Vehicle Charging From Different Perspectives," in *IEEE Transactions on Smart Grid*, vol. 6, no. 1, pp. 333-342, Jan. 2015.
- [12] B. Das, T. S. Jalal and F. J. S. McFadden, "Comparison and extension of IEC thermal models for dynamic rating of distribution transformers," 2016 IEEE International Conference on Power System Technology (POWERCON), Wollongong, NSW, 2016, pp. 1-8. doi: 10.1109/POWERCON.2016.7753896
- [13] M. Bunn, B. P. Das, B. Seet and C. Baguley, "Empirical Design Method for Distribution Transformer Utilization Optimization," in *IEEE Transactions on Power Delivery*, vol. 34, no. 4, pp. 1803-1813, Aug. 2019.
- [14] J. Medina, N. Muller and I. Roytelman, "Demand Response and Distribution Grid Operations: Opportunities and Challenges," in *IEEE Transactions on Smart Grid*, vol. 1, no. 2, pp. 193-198, Sept. 2010.

-
- [15] M. Humayun, A. Safdarian, M. Z. Degefa and M. Lehtonen, "Demand Response for Operational Life Extension and Efficient Capacity Utilization of Power Transformers During Contingencies," in *IEEE Transactions on Power Systems*, vol. 30, no. 4, pp. 2160-2169, July 2015.
- [16] S. Shao, M. Pipattanasomporn and S. Rahman, "Demand Response as a Load Shaping Tool in an Intelligent Grid With Electric Vehicles," in *IEEE Transactions on Smart Grid*, vol. 2, no. 4, pp. 624-631, Dec. 2011. doi: 10.1109/TSG.2011.2164583
- [17] Y. P. Gusev and P. V. Subbotin, "Using Battery Energy Storage Systems for Load Balancing and Reactive Power Compensation in Distribution Grids," 2019 International Conference on Industrial Engineering, Applications and Manufacturing (ICIEAM), Sochi, Russia, 2019, pp. 1-5.
- [18] L. Viernstein, R. Witzmann and J. Przibylla, "Grid voltage level spanning operational strategies for battery energy storage systems in distribution grids," 2016 IEEE Electrical Power and Energy Conference (EPEC), Ottawa, ON, 2016, pp. 1-6.
- [19] Power Transformers—Part 7: Loading Guide for Mineral-Oil-Immersed Power Transformers, IEC Standard 60076-7:2018, 2018.
- [20] K. C. Schneider and R. F. Hoad, "Initial transformer sizing for single-phase residential load," in *IEEE Transactions on Power Delivery*, vol. 7, no. 4, pp. 2074-2081, Oct. 1992. doi: 10.1109/61.157012
- [21] Kröger, David, et al. "Scheduled charging of electric vehicles and the increase of hosting capacity by a stationary energy storage." (2019).
- [22] Specht, Lukas, et al. "Autonomous and cost-efficient operation of a stationary battery energy storage in low voltage networks." (2019).
- [23] Z. Qiao and J. Yang, "Comparison of centralised and distributed battery energy storage systems in LV distribution networks on operational optimisation and financial benefits," in *The Journal of Engineering*, vol. 2017, no. 13, pp. 1671-1675, 2017, doi: 10.1049/joe.2017.0616.
- [24] M. Z. Degefa, H. Sæle, J. A. Foosnaes and E. Thorshaug, "Seasonally variant deployment of electric battery storage systems in active distribution networks," in *CIREED - Open Access Proceedings Journal*, vol. 2017, no. 1, pp. 1975-1979, 10 2017, doi: 10.1049/oap-cired.2017.0757.
- [25] S. Nykamp, T. Rott, N. Dettke and S. Kueppers, "The project "ElChe" Wettringen: storage as an alternative to grid reinforcements - experiences, benefits and challenges

from a DSO point of," International ETG Congress 2015; Die Energiewende - Blueprints for the new energy age, Bonn, Germany, 2015, pp. 1-6.

[26] J. L. Lorente, X. A. Liu, R. Best and D. J. Morrow, "Energy storage allocation in power networks – A state-of-the-art review," 2018 53rd International Universities Power Engineering Conference (UPEC), Glasgow, 2018, pp. 1-6, doi: 10.1109/UPEC.2018.8542106.

[27] Divya, K. C., and Jacob Østergaard. "Battery energy storage technology for power systems—An overview." *Electric power systems research* 79.4 (2009): 511-520.

[28] Electrical Installations—Known as the Australian/New Zealand Wiring Rules, AS/NZS 3000:2018, 2018.

[29] BRANZ. [online]. Available: https://www.branz.co.nz/cms_show_download.php?id=9d566b918fccd025f0d7d979e9e6d5df71b1101b/. Accessed on 3rd October 2019.

[30] National Institute of Water and Atmospheric Research (NIWA). [Online]. Available: <https://cliflo.niwa.co.nz/>. Accessed on 3rd October 2019.

Chapter 5

5.1 Introduction to Manuscript 4

This Manuscript presents the concept of demand response to obtain maximum loading capacity across a distribution transformer. The scope of the Manuscript spans over improved capacity of the distribution transformer in order to reduce congestion, minimize overloading and provide effective voltage regulation without any capital expenditure involved. The use of demand response technique and smart BEV charging method towards maximum loading across the distribution transformer are examined in detail in the Manuscript. The proposed technique is moreover found effective in reducing the DT loading and regulating the voltage during entire loading duration.

This manuscript is accepted for publication in “IEEE-ISGT Europe 2020 Conference under the title “Application of demand response and smart battery electric vehicles charging for capacity utilization of the distribution transformer.”

5.2 Manuscript 4

Application of demand response and smart battery electric vehicles charging for capacity utilization of the distribution transformer

Saifal Talpur, T. T. Lie and R. Zamora

Corresponding author email: saifal.talpur@aut.ac.nz

Abstract

This paper deals with managing the load across distribution transformer through demand response and smart battery electric vehicle (BEV) charging techniques. A neighborhood of 40 households connected across a 200-kVA distribution transformer is investigated in this paper. Each house is provided with a single BEV. Residential and BEV loads across each house are managed through time of use and non-time of use demand response-based techniques, managed under shifting the load based on unit pricing. To implement demand response technique, appliances in each household are classified as shiftable and non-shiftable. Operating time of shiftable appliances is controlled to attain the required peak shaving. The load levelling is effective in minimizing the transformer loading obtained under time-variant unit pricing used to control both residential and BEV charging load. This paper investigates electrical loading of the distribution transformer under residential and BEV charging load.

Keywords— demand response, shiftable and non-shiftable appliances, smart versus dumb battery electric vehicle charging, distribution transformer, optimal power flow

1. Introduction

Demand response is a load control method used to respond to energy consumption at appliance levels to control loading stress across distribution transformers (DTs) and avoid congestion in the low voltage (LV) network. An effective load control under demand response is achieved through load shifting. Load shifting requires shifting the load of certain appliances without affecting the consumer's comfort and at the same time obtaining the peak shaving. Peak shaving is required when load across distribution transformers exceeds their nominal loading. In order to achieve peak shaving at no impact on user's comfort level, residential load is divided into shiftable and non-shiftable appliances. Shiftable appliances are the type of appliances whose load is shifted for certain amount of time. The load across non-shiftable appliances is kept constant irrespective of transformer loading.

An extensive research work related to appliance-based demand response has been carried out in [1]-[5]. For instance, [4] has investigated peak load shaving through vehicle to house energy transfer based on demand side management. Peak load shaving through scheduling based residential distributed energy storage system is introduced in [5]. Similarly, the study related to minimizing the transformer load and ageing is carried out in [6]-[9] for the purpose of improving the life cycle under demand response and particle swarm optimization techniques to relieve the charging burden [8]. Application of demand response to mitigate congestion in the low voltage distribution network [9] in addition to reduced thermal overloading of distribution transformers [10] are investigated extensively. Demand response can lead to reduced unit pricing for residential, commercial and industrial consumers as well. Literatures [11]-[13] provide solutions to minimize the electricity costs in the wider consumer network.

A growing trend towards battery electric vehicles (BEVs) usage imposes an additional loading on distribution transformers that need to be addressed through smart load reduction techniques, like demand response. The work in [14]-[16] is dedicated towards managing the BEV loading through applying the demand response. BEV charging in residential premises is considered flexible towards shifting the charging time in accordance to consumer's choice. The traditional charging techniques in [17]-[19] offer flexibility in terms of load shifting based on unit price, the proposed algorithm also offers

an efficient solution for charging owners (residential customers) and Distribution System Operators (DSOs). Benefits provided to charging owners are efficient charging operation and reduced billing costs. DSOs avail from peak shaving that can reduce congestion in their network. Residential charging is mainly offered under AC source that is considered cumbersome but effective in relieving the congestion across the low voltage distribution network assets, for instance distribution transformers. The residential load peak during the peak hours can affect the charging flexibility, hence implementing the efficient demand response techniques can provide peak shaving. A smart AC charging method can reduce electrical, thermal and mechanical stresses across distribution transformers. In addition, it is able to minimize feeder losses, regulate voltage, and manage effective thermal overload and convenient charging facility.

2. Background

After reducing the stress across distribution transformers in result of excess BEV charging load, this paper proposes to implement demand response across residential and BEV charging loads. Using the coordinated BEV charging towards effective relief across distribution transformers [20]-[23] and flattening the load peak across residential load are widely recognized methods. Using the stored energy from centralized [24]-[25] and/or decentralized battery storages [26] to support the active power during transformer overloading is used to lessen the burden across distribution transformers. Distribution transformers are considered optimally loaded under load factor below the nominal maximum [27]. When loaded above the nominal loading, they may face reduced life and becoming the cause of excessive voltage drop across service points; factors leading to affect stable electricity supply to consumers. The goal of this paper is to offer following benefits by introducing an effective residential and BEV load management technique to minimize electrical and thermal stresses across distribution transformer in the LV distribution network:

- Flexible and effective BEV charging
- Regulated voltage at each load point
- Reduced transformer loading and congestion

Under the proposed technique, residential and BEV loads are treated as separate loads, where residential load is controlled through load shifting mechanism and BEV load is controlled under voltage and time of use (ToU) based pricing model. Load aggregation

of residential and BEV loads are carried out to determine peak loading across the distribution transformer. A three-phase 11kV/400V transformer with nominal capacity of 200 kVA is used in this paper, referred as a test transformer with physical dimensions as shown in Table I. The transformer is connected to 40 households through XLPE cable with physical data as mentioned in Table II. Each household is moreover equipped with a single 40 kWh Nissan Leaf charged through 7.4 kW Level-2 AC charger under 230V (rms) with physical dimensions as mentioned in Table III. Transformer loading is divided into electrical and thermal loadings, where electrical loading corresponds to the load factor derived from the load across each phase of the distribution transformer. Thermal loading is derived from electrical loading in the form of temperature changes across transformer oil and copper windings.

3. Proposed Model

Under the proposed model, residential and BEV loads were treated separately. Residential load was controlled through demand response, while BEV loading was controlled under smart and dumb charging techniques as shown in Fig. 1. A neighborhood of 40 households was simulated, where each household was considered having single BEV. Residential loading was carried under-price-based demand response technique (implemented through linear optimization) while BEV loading was carried under smart charging technique. The difference between both techniques is their characteristics in handling the type of load. In the demand response based technique, total residential load across each household was divided into two groups, namely shiftable load and non-shiftable load. Under shiftable load, consumers were allowed to adjust the timing of appliance loading (irrespective of unit-pricing), whereas under non-shiftable load, no change in operational timing of appliance loading was allowed. Tables IV and V provide operational timing and maximum kW rating of appliances as obtained from [28] and [29] under shiftable and non-shiftable loading categories, respectively.

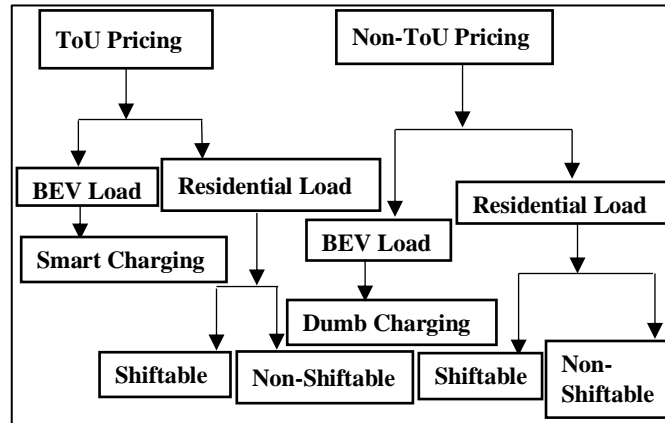


Fig.1 Load classification tree

Table I
Distribution Transformer Data

Number of phases	3
LV Voltage	415 V/50Hz
Cooling method	ONAN
Impedance	8%

Table II
Service Cable Parameters

Type	XLPE Insulated/Single Core/Copper
Area	281 mm ²
Resistance (mΩ)	0.081 (at H-1 from DT), 52.71 (at H-14 from DT)
Reactance (mΩ)	0.082 (at H-1 from DT), 53.04 (at H-14 from DT)

Table III
BEV Parameters

Charging load power factor	0.9
Charger efficiency	0.9
Battery charging status	1 (SoC-100%), 0 (SoC-0%)
Initial battery SoC	0%
Charger load type	constant impedance

Table IV
Max. rating and operating time of shiftable appliances

Appliance(s)	Max. Rating (kW)	On-Time	Off-Time
Dishwasher	1.8	16.00	20.00
Laundry machine	2.0	7.00	8.00
Clothing dryer	1.5	20.00	21.00
Water Heater	2.4	19.00	22.00
Storage			
Clothing iron	1.1	21.00	22.00

A. Unit pricing based demand response across the residential load

Under this category, load shifting was carried based on time-variant and time-invariant pricing models without affecting the consumer's comfort. Time variant unit pricing was named ToU pricing model, whereas, time-invariant unit pricing was named non-ToU pricing model.

i. ToU pricing model

The objective of time dependent pricing model was to obtain an efficient load control management with flattened load peaks, minimized congestion in the LV network and reduced transformer ageing. In this model, pricing curve as shown in Fig.3 was divided into three pricing zones, specifically: above average, average and below average. Under above average unit pricing, shiftable load in each household in the entire neighborhood was considered off-loaded. Similarly, under average and below average unit pricing, shiftable load was considered on-loaded.

ii. Non-ToU pricing model

Under non-ToU pricing model, changes in load consumptions were considered independent of unit pricing as flat unit pricing was considered for residential load in each household in the entire neighborhood for the entire day.

iii. Mathematical modelling

Mathematical modeling is carried for residential and BEV loading. The residential load modeling was based on optimizing the demand of shiftable loads with respect to unit pricing. Equation (1) presents the concept of load demand in a typical house, where load optimization was carried out across shiftable appliances through controlling the operating time of individual appliances to minimize the aggregated load demand. Peak shaving during peak hours was used to achieve an optimal DT loading. In order to achieve peak shaving, the load demand from shiftable appliances was reduced during peak hours, further shown in (2) from [30].

$$P_T = \left[\sum_{t_S \in T}^{S \in P} S + \sum_{t_{NS} \in T}^{NS \in P} NS \right] \gg \min \left(\sum_{t_S \in T}^{S \in P} S \right), T = [1, 2 \dots 24]$$

$$\text{s.t., } S_{\text{aggregated}} \leq P_T, NS_{\text{aggregated}} \leq (P_T - S_{\text{aggregated}}) \quad (1)$$

where, S represents the aggregated load of shiftable appliances in kW and NS represents aggregated load of non-shiftable appliances in kW. P is the sum of aggregated and non-aggregated loads in kW.

$$\left[\left((x_{i,t} \in \{0,1\} \forall (i,t)) \cdot \left(\sum_{t=1}^h D_{1,t} \right) \right) \right] = (Z_{i,t}) \forall (i,t) \quad (2)$$

where, x is a control variable, t is time interval in hours with number of operating intervals Z for appliance i over the allowable operation D for any h duration. Equation (3) from [30] represents a simplified optimal load modelling of non-shiftable appliances. Non-shiftable load as shown in Table V was not shifted over the period of time.

$$C.L = \sum_{t=1}^h C_t L_t$$

where, C is the unit cost in NZD per kwh, L is the shiftbale load in kW over time interval t in hours.

Table V

Max. rating and operating time of non-shiftable appliances

Appliance(s)	Max. Rating (kW)	On-Time (hr)	Off-Time (hr)
Lighting	0.15	16.00	24.00
Refrigerator	0.10	00.00	24.00
Electric stove	2.40	17.00	19.00
TV	0.08	12.00	24.00
Computer	0.06	12.00	24.00
Coffee maker	1.20	06.00 16.00	10.00 20.00
Vacuum cleaner	1.0	20.00	22.00
Cell phone charger	0.14	17.00	24.00
Router	0.01	00.00	24.00
Microwave	0.75	07.00	09.00
Toaster	1.20	08.00	09.00
Hair dryer	1.60	21.00	22.00

B. BEV charging

i. Introduction

BEV charging can take place through AC and DC energy sources. The AC charging is comparatively slower but impose a less burden on DTs in comparison to DC charging. In this study, BEV charging was categorized into smart and dumb charging methods, where

smart charging method was designed to be efficient by causing less burden on the distribution transformer. Contrary to that, dumb charging method was considered as a traditional charging technique irrespective of loading across the distribution transformer.

ii. Mathematical modelling

Mathematical modeling of smart BEV charging was carried under (4)-(6). Equation (4) involves rated charging current $I_{charger}$ equivalent of 32 A at 0.9 lagging power factor $p.f$ with charger efficiency η of 0.9 at 230 V input voltage V_{input} . Input voltage is the voltage across each BEV by considering that all BEVs in each household are connected at the time, the subject BEV is being plugged. The charging power from (4) is used in (5) to find stored energy at time t . It is further considered that in (5), input voltage is calculated based on the assumption that all BEVs are connected in each household except BEV in the subject household. The procedure is repeated for each BEV in the entire neighborhood of 40 households.

$$P_{in} = (V_{input} * I_{charger} * p.f) \quad (4)$$

$$E_{stored,t} = (P_{in} * time_t) \quad (5)$$

Equation (6) represents final stored energy $E_{stored,final}$ at hour $t + n$ from $E_{stored,t}$ starting at t , where, t is the arrival time and $t + n$ is the departure time of each BEV. Energy is stored during each hour until battery in each BEV is fully charged.

$$E_{stored,final} = (E_{stored,t}) + \dots + (E_{stored,t+n}) \quad (6)$$

Based on a pre-condition, all BEVs are required as fully charged before 7 am. Total charging time $time_{charging,total}$ as shown in (7) represents the accumulated hourly time for a single BEV from plugged-in to plugged-out. For simplicity, plugged-in time is termed as arrival time $time_t$ of the BEV, while plugged-out time $time_{t+n}$ is termed as a departure time of the BEV.

$$time_{charging,total} = time_t + time_{t+1} + \dots + time_{t+n} \quad (7)$$

To consider a worst loading scenario across the DT, state of charge (SoC) of each BEV during plug-in time was considered 0%. Further, it was also considered that each BEV must be fully charged storing 40 kWh (maximum battery capacity) of electricity before plugged-out. A detailed overview of both battery charging strategies is mentioned in the later sections.

iii. *Types*

a. *Smart BEV charging*

In this paper, smart charging was integrated with demand response to provide active and reactive power support to lessen the burden on the distribution transformer. Algorithm-1 determines the procedure carried out for smart charging technique.

Algorithm-1: proposed technique for smart BEV charging

```

for ( $V_{input} > V_{max} || V_{input} < V_{min}$ )
    ( $P_{in} = (V_{input} * I_{charger} * p.f)$ )
    for  $t = (1:1:31)$ 
        if ( $t \geq 7 \&\& (t \leq 11) || (t \geq 17) \&\& (t \leq 21) || (t \geq 21)$ )
             $E_{stored,t} = (P_{in} * t)$ 
             $E_{stored,final} = (E_{stored,t}) + \dots + (E_{stored,t+n})$ 
        end
    end
end

```

The timing as shown in Algorithm-1 represents the peak loading time during which BEV is not allowed charging even being plugged and therefore depends on the stored energy. Similarly, BEV is not allowed charging during out of limits input voltage as shown in Algorithm-1. This smart BEV charging mechanism is therefore categorized under the following ToU and voltage models.

1) *ToU pricing model*

Under ToU pricing model, BEV charging is allowed during the time when unit price is below 19.2 NZcents/kwh as shown in Fig. 3. Under this model, BEV charging is not allowed during peak-hours when unit price is above the average (~19.14 NZD/kWh). The unit pricing belongs to residential consumer's network in New Zealand and is obtained from [31]. Fig. 3 shows the time-dependent changes in unit pricing, where below average unit pricing is found during early morning and late nights, average unit pricing is found just before and after peak hours and above average unit pricing is found during peak hours. This pricing scheme benefits BEV owners in terms of lower electricity bills and at the same timing benefiting the DSO in terms of reduced stress across their assets. By

considering the factors like voltage limits and ToU pricing, smart charging offers benefits to both consumers and the DSO.

2) Voltage model

Under this factor, BEV charging is based on considering the voltage at charging connection point in each household in the entire neighbourhood. Voltage is checked against nominal voltage limits recommended as $\pm 6\%$ as set under NZ standard [32]. In case of out of limit voltages, charging is delayed until voltage reaches the nominal limits. Voltage across each service point is checked for the entire duration a BEV remains connected. The lower the voltage across the charging point, the longer the time a BEV takes to be fully charged and vice versa. Based on voltage consideration, BEV connected at the end of service point takes longer time in being fully charged than a BEV connected at the beginning of the service point due to higher voltage drop. Under voltage adopted scheme, the time to fully charge a BEV has dependence on the supply voltage. Based on (2), the higher the input voltage, the lower the time to fully charge any BEV. Similarly, according to (3), a lower input voltage requires a longer charging time for any BEV to be fully charged.

b. Dumb BEV charging

This method of charging was applied across BEVs without voltage and pricing considerations. BEVs under this charging method were allowed charging at the time of plugged in. This method is useful when BEV owners want their BEVs to be charged without any delay. Due to no voltage and ToU considerations, charging load under this method may cause excess load peaks.

4. Test System

A test system comprising 40 households as shown in Fig. 2 was developed in Simulink. Each household was equipped with residential and BEV loads. Each household was connected through resistive-inductive type XLPE service cable with data as mentioned in Table II. Additionally, 50m distance was considered between two adjacent households. A complete model comprising the DT, residential and BEV loads is shown in Fig. 2. Primary side of the DT was connected to 11kV LV grid-side, considered as a slack-node at fixed input voltage ($|U|=1.0$ pu, $\delta=0^\circ$) to further restrict the BESS influence across the grid-side. An unbalance phase load consisting of 14 households across Phase-A and 13 households across each Phase-B and Phase-C was connected to 415 V secondary side of the test DT. Transformer loading and voltage across households at each phase of the test DT are calculated under Scenario-A and Scenario-B. Scenario-A represents ToU pricing

model with smart BEV charging, while Scenario-B represents non-ToU pricing model with dumb BEV charging.

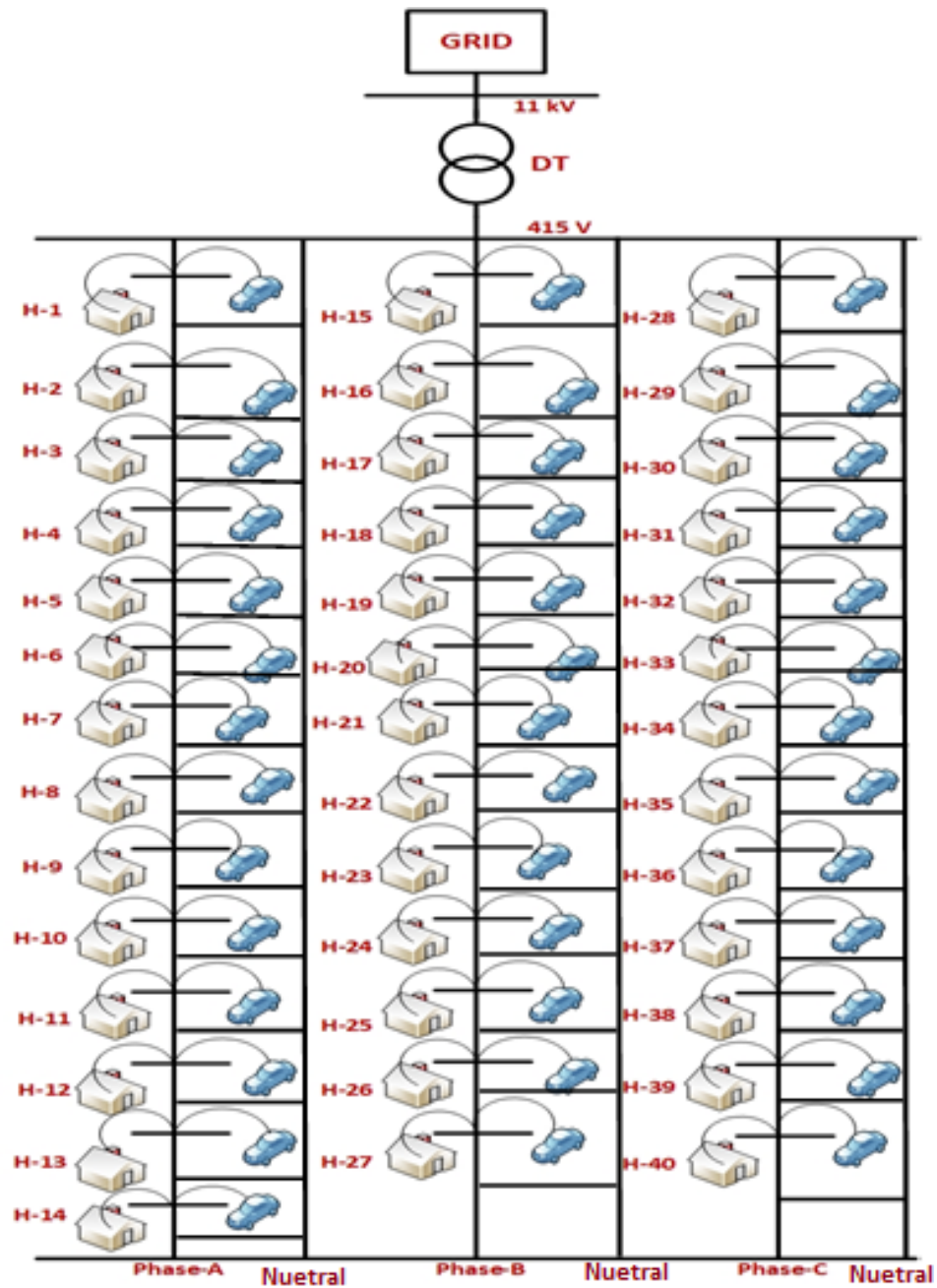


Fig. 2 Single line diagram of 3-phase 4 wire test system

i. Scenario-A

Under this Scenario, voltage across each household is found under $\pm 6\%$ of the nominal voltage limits. Moreover, the Scenario provides maximum capacity across the test DT, where voltage dip is followed by increase in transformer utilization as shown in

Fig. 3. The figure also shows that based on demand response and smart BEV charging, consumers consume electricity during off-peak hours due to lower unit pricing, hence load levelling through peak shaving is achieved. This leads to obtaining an overall objective, which is to minimize electrical and thermal stresses across the test DT.

ii. Scenario-B

Under this Scenario, voltage across households nearest and farthest from the test DT is found out of limits but the DT loading is found within the capacity limits. The results of this Scenario are shown in Fig. 4, indicating that rise in transformer loading reduces voltage across each household. The figure shows increased DT loading during peak hours due to flat unit pricing for the entire day, hence consumers consume electricity mainly during peak hours when leaving for work or returning from the work. Besides, it can be seen in Fig. 4 that minimum voltage limits across the observed household terminals are out of nominal limits, whereas maximum voltage limits are within the nominal limits.

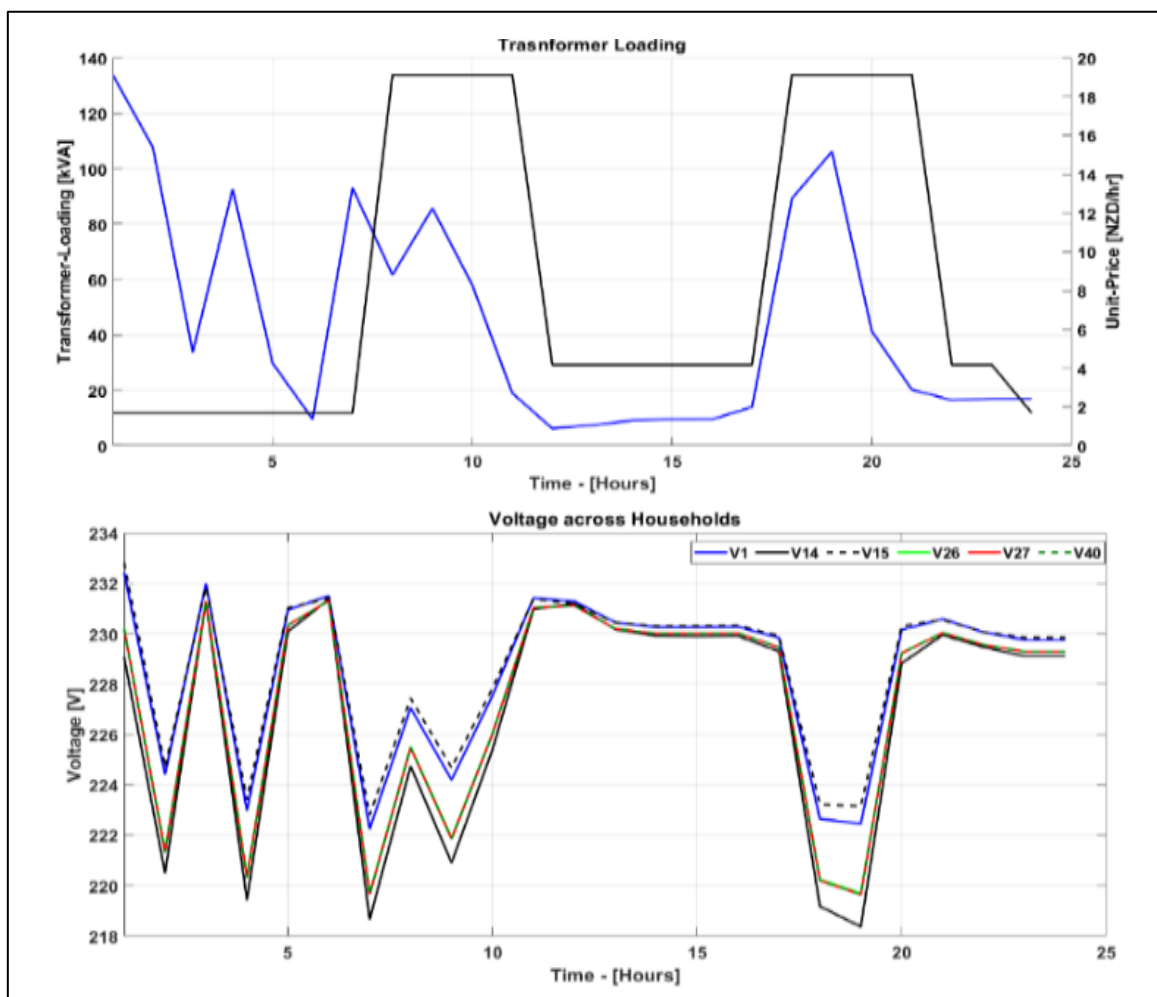


Fig. 3 Transformer loading and voltages in result of residential and BEV load modelling under ToU pricing model

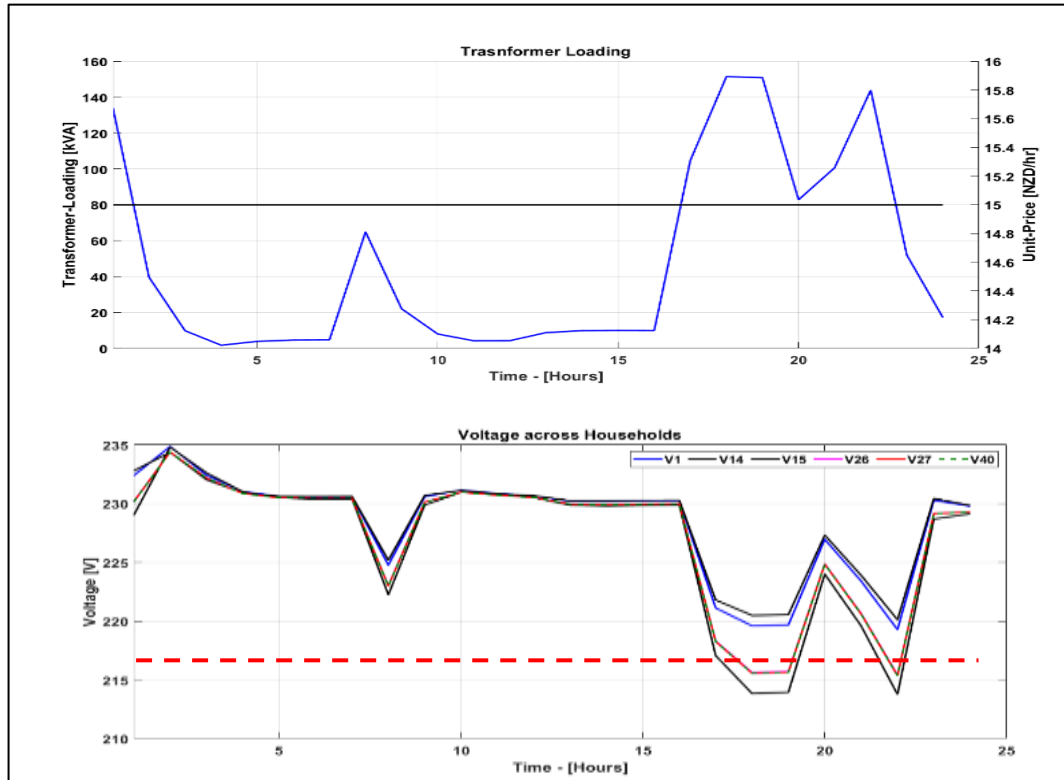


Fig. 4 Transformer loading and voltages in result of residential and BEV load modelling under non-ToU pricing model

5. Conclusion

This study has presented the application of demand response and smart BEV charging techniques in alleviating the electrical loading across the distribution transformer. In this paper, residential and BEV loads are treated as separate load entities, where residential load is controlled through demand response and BEV load is controlled through unit pricing adjustments. To validate the effectiveness of the proposed techniques, a swapping mechanism is adopted. Under this mechanism, residential load is controlled through variations in unit pricing, whereas BEV load is controlled through keeping the unit pricing as constant. The results are thereafter validated under both scenarios. The smart BEV charging approach as controlled through unit-pricing and terminal voltage is more effective in active and reactive power support to each household across the DT in comparison to dumb charging approach. The ability of smart charging approach towards sensing the load across distribution transformer before allowing the charging is more effective in reducing the transformer loading.

References

- [1] Y. Liu, L. Xiao, G. Yao and S. Bu, "Pricing-Based Demand Response for a Smart Home with Various Types of Household Appliances Considering Customer Satisfaction," in *IEEE Access*, vol. 7, pp. 86463-86472, 2019.
- [2] Y. Wang, H. Liang and V. Dinavahi, "Two-stage stochastic demand response in smart grid considering random appliance usage patterns," in *IET Generation, Transmission & Distribution*, vol. 12, no. 18, pp. 4163-4171, 16 10 2018.
- [3] Jordehi, A. Rezaee. "Optimisation of demand response in electric power systems, a review." *Renewable and Sustainable Energy Reviews* 103 (2019): 308-319.
- [4] L. Zhao and V. Aravinthan, "Strategies of residential peak shaving with integration of demand response and V2H," *2013 IEEE PES Asia-Pacific Power and Energy Engineering Conference (APPEEC)*, Kowloon, 2013, pp. 1-5.
- [5] Barzkar, Arash, and Seyed Mohammad Hassan Hosseini. "A novel peak load shaving algorithm via real-time battery scheduling for residential distributed energy storage systems." *International Journal of Energy Research* 42.7 (2018): 2400-2416.
- [6] N. G. Paterakis, I. N. Pappi, O. Erdinç, R. Godina, E. M. G. Rodrigues and J. P. S. Catalão, "Consideration of the Impacts of a Smart Neighborhood Load on Transformer Aging," in *IEEE Transactions on Smart Grid*, vol. 7, no. 6, pp. 2793-2802, Nov. 2016.
- [7] S. N. G. Gouriseti, H. Kirkham and D. Sivaraman, "A review of transformer aging and control strategies," *2017 North American Power Symposium (NAPS)*, Morgantown, WV, 2017, pp. 1-6.
- [8] Y. Yao and W. Gao, "Relieving the pressure of electric vehicle battery charging on distribution transformer via particle swarm optimization method," *2014 North American Power Symposium (NAPS)*, Pullman, WA, 2014, pp. 1-5.
- [9] A. N. M. M. Haque, M. T. Rahman, P. H. Nguyen and F. W. Bliet, "Smart curtailment for congestion management in LV distribution network," *2016 IEEE Power and Energy Society General Meeting (PESGM)*, Boston, MA, 2016, pp. 1-5.
- [10] Haque, A. N. M. M., et al. "Demand response for real-time congestion management incorporating dynamic thermal overloading cost." *Sustainable Energy, Grids and Networks* 10 (2017): 65-74.
- [11] M. Muratori and G. Rizzoni, "Residential Demand Response: Dynamic Energy Management and Time-Varying Electricity Pricing," in *IEEE Transactions on Power Systems*, vol. 31, no. 2, pp. 1108-1117, March 2016.Kk

-
- [12] Yan, Xing, et al. "A review on price-driven residential demand response." *Renewable and Sustainable Energy Reviews* 96 (2018): 411-419.
- [13] Ma, Kai, et al. "Residential power scheduling for demand response in smart grid." *International Journal of Electrical Power & Energy Systems* 78 (2016): 320-325.
- [14] López, M. A., et al. "Demand-side management in smart grid operation considering electric vehicles load shifting and vehicle-to-grid support." *International Journal of Electrical Power & Energy Systems* 64 (2015): 689-698.
- [15] A. Soares, Á. Gomes, C. H. Antunes and C. Oliveira, "A Customized Evolutionary Algorithm for Multiobjective Management of Residential Energy Resources," in *IEEE Transactions on Industrial Informatics*, vol. 13, no. 2, pp. 492-501, April 2017.
- [16] Ghazvini, Mohammad Ali Fotouhi, et al. "Demand response implementation in smart households." *Energy and buildings* 143 (2017): 129-148.
- [17] I. S. Bayram, M. Ismail, M. Abdallah, K. Qaraqe and E. Serpedin, "A pricing-based load shifting framework for EV fast charging stations," *2014 IEEE International Conference on Smart Grid Communications (SmartGridComm)*, Venice, 2014, pp. 680-685.
- [18] Wang, Baocheng, et al. "An EV Charging Scheduling Mechanism Based on Price Negotiation." *Future Internet* 10.5 (2018): 40.
- [19] B. Wang, B. Hu, C. Qiu, P. Chu and R. Gadh, "EV charging algorithm implementation with user price preference," *2015 IEEE Power & Energy Society Innovative Smart Grid Technologies Conference (ISGT)*, Washington, DC, 2015, pp. 1-5.
- [20] E. Sortomme, M. M. Hindi, S. D. J. MacPherson and S. S. Venkata, "Coordinated Charging of Plug-In Hybrid Electric Vehicles to Minimize Distribution System Losses," in *IEEE Transactions on Smart Grid*, vol. 2, no. 1, pp. 198-205, March 2011.
- [21] Jhala, Kumarsinh. *Coordinated electric vehicle charging with renewable energy sources*. Diss. Kansas State University, 2015.
- [22] S. Zou, Z. Ma, X. Liu and I. Hiskens, "An Efficient Game for Coordinating Electric Vehicle Charging," in *IEEE Transactions on Automatic Control*, vol. 62, no. 5, pp. 2374-2389, May 2017.
- [23] J. Wang, G. R. Bharati, S. Paudyal, O. Ceylan, B. P. Bhattarai and K. S. Myers, "Coordinated Electric Vehicle Charging With Reactive Power Support to Distribution Grids," in *IEEE Transactions on Industrial Informatics*, vol. 15, no. 1, pp. 54-63, Jan. 2019.

-
- [24] A. Nag and R. J. Haddad, "A novel centralized storage model for distributed photovoltaic generation systems," *2017 IEEE International Conference on Smart Grid Communications (SmartGridComm)*, Dresden, 2017, pp. 122-127.
- [25] T. Debela and A. Bhattacharya, "Design and analysis of a DC/AC microgrid with centralized battery energy storage system," *IECON 2017 - 43rd Annual Conference of the IEEE Industrial Electronics Society*, Beijing, 2017, pp. 8779-8784.
- [26] K. Worthmann, C. M. Kellett, P. Braun, L. Grüne and S. R. Weller, "Distributed and Decentralized Control of Residential Energy Systems Incorporating Battery Storage," in *IEEE Transactions on Smart Grid*, vol. 6, no. 4, pp. 1914-1923, July 2015.
- [27] M. Humayun, A. Safdarian, M. Z. Degefa and M. Lehtonen, "Demand Response for Operational Life Extension and Efficient Capacity Utilization of Power Transformers During Contingencies," in *IEEE Transactions on Power Systems*, vol. 30, no. 4, pp. 2160-2169, July 2015.
- [28] Powershop [Online]. Available: <https://www.powershop.co.nz/assets/DownloadableResources/63c48ace03/Appliances-and-their-power-usage.pdf>.
- [29] Origin Energy [Online]. Available: https://www.originenergy.com.au/content/dam/origin/residential/docs/home-products/hot-water/Dux_Electric_Storage_80-400L.pdf. Accessed on 20th May 2020.
- [30] Entriken, R., Hu, R. L., Skorupski, R., & Ye, Y. (2015). A Mathematical Formulation for Optimal Load Shifting of Electricity Demand. vol. X, no. X, 1-46.
- [31] Electra [Online]. Available: <https://electra.co.nz/prices/>. Accessed on 27th November 2019.
- [32] Electrical Installations—Known as the Australian/New Zealand Wiring Rules, AS/NZS 3000:2018, 2018.

Chapter 6

6.1 Conclusions

Maximum capacity utilization was obtained across overhead line and distribution transformer in a simulation environment. Proof of concept was carried out by undertaking the worst loading scenarios. In case of an overhead line, MV network and in case of a distribution transformer, LV network was considered. For validation, results from the proposed techniques were validated with results obtained under conventional techniques. The work presented in this thesis mainly aimed at proposing the techniques capable of increasing the power transfer capacity of overhead line and distribution transformer assets. The goal was to achieve maximum asset utilization to curtail thermal bottlenecks in case of overhead lines and reduce thermal and electrical loadings in case of distribution transformers. Following highlights the goals as achieved in this thesis:

- development of a weather-dependent electro-thermal power flow technique to minimize congestion in the overhead transmission network
- identification of thermal bottlenecks under space and time dependent constraints to find the actual power transfer capacity of overhead lines
- integration of dynamic transformer ratings with battery energy storage system for optimal transformer loading and voltage regulation across each end user under worst battery electric vehicles loading
- integration of dynamic transformer ratings with demand response and smart battery electric vehicles charging for optimal transformer loading and voltage regulation across each end user under worst battery electric vehicles loading

The results from each task were published in the peer-reviewed manuscripts, where each manuscript was based on addressing a research question. The summary of results as obtained under each manuscript is furthermore highlighted in the following segments.

The methodology proposed in ‘Manuscript-1’ was used to obtain maximum optimal loading across overhead lines under electro-thermally coupled dynamic weather-dependent line rating. The ETC based line rating technique as proposed in ‘Manuscript-1’ (ETC-DWLR) was performed under cyclical loading, where short-term overloading of an overhead line was investigated under dynamic weather conditions. The ETC-DWLR technique, when compared with ETC-SWLR and conventional DLR techniques was

found efficient in minimizing the line congestion and avoiding any load-shedding situations. The calculated power flow through the subject overhead line showed that the proposed technique is capable of mitigating the congestion from the electricity network by allowing an excess power transfer under safety constraints. Additionally, in ‘Manuscript-1’, sensitivity analysis was carried out to estimate line temperature related changes with respect to changes in the ambient conditions, with obtained results showing higher sensitivity between wind speed and the line temperature. The study also investigated the presence of critical spans (passing through flat and non-flat terrains) and the impact of corresponding weather and loading conditions on line’s AC resistance and bus voltage magnitude through the designed line-modeling tool.

‘Manuscript-2’ was based on developing the technique for identification of critical spans across an overhead line, passing through a multi-geographical region at the least computational cost. In this manuscript, optimal sensor placement was carried out to determine the unknown weather elements across each span of the test/subject overhead line. The technique resulted in non-uniform segments, each containing a set of critical and non-critical line spans. Using the proposed critical-span identification technique, critical spans were identified under weather and span-topography based conditions. The resulting critical spans were used to determine the thermal rating for the entire test line under static and real weather conditions. Additionally, it was found that under the same line loading, critical spans faced comparatively higher sagging levels than non-critical line spans due to facing the worst weather and possessing the longer span lengths. These factors further determined the global minimum thermal loadability of the test line to find the minimum of maximum line current such that no ground clearance infringement is obtained across any line span, hence controlling the line loadability within the allowable sag limits.

Furthermore, for validation, accuracy and computational efficiency of the proposed technique were compared with obtained under conventional technique. In result, critical spans identified under the proposed technique were found identical to those identified under the conventional technique. In the proposed technique, spans were classified as critical and non-critical under the judgment of weather conditions and the span-topography, i.e., the spans with comparatively worst weather conditions by exhibiting higher ambient temperature, lower wind speed and higher solar radiation were categorized as critical. Based on this judgment, the technique termed these spans as critical spans. Thereafter, temperature and sag across each line span was calculated to

validate the results from the proposed technique, which furthermore proved the accuracy of the proposed technique in addition to achieving to higher computational efficiency.

In ‘Manuscript-3’, the goal was to increase the thermal capacity of a distribution transformer to accommodate excess BEV charging load. To address this issue, an integrated DRoDT-BESS technique was proposed, which was unique in “designing the distribution transformer for maximum optimal utilization”. The obtained results validated the capability of the proposed technique in increasing the thermal loadability of the distribution transformer and regulated voltage for end-users under multiple BEV charging scenarios and weather conditions. The objectives, like, optimal DT loading, maximum DT utilization, accuracy regarding the T_{Tot} calculation, minimized thermal stress and voltage within the nominal limits were achieved with the help of the proposed technique.

Under the proposed technique, the stored energy from the BESS was used to flatten and shifting the load peaks. The proposed model was found useful for both end-consumers and the DNOs. For end-consumers, the associated benefits like 1) transfer of required active power to avoid the risk of load-shedding, 2) voltage within limits and 3) reduced electricity price were obtained. For the DNOs, benefits like 1) longer DT life, 2) deferral of costly grid upgrades and 3) no reactive power requirement were obtained.

To avoid technical and economic challenges associated with BESS and achieving the goal of improved thermal loadability of the distribution transformer, a relatively different technique was proposed in ‘Manuscript-4’. Under the proposed technique, the application of demand response and smart BEV charging were carried out with dynamic transformer rating. Furthermore, residential and BEV loads were treated as separate load models, where residential load was controlled through demand response and BEV load was controlled through unit pricing adjustments. To validate the effectiveness of the proposed techniques, a swapping mechanism was adopted. Under this mechanism, residential load was controlled through variations in unit pricing, whereas BEV load was controlled through keeping the unit pricing as constant. The results were thereafter validated under both scenarios. The manuscript introduced two approaches for BEV charging, represented as smart BEV charging and dumb BEV charging. Smart BEV charging approach as controlled through unit-pricing and terminal voltage was found more effective in providing the active power and voltage supports to each household across the test DT in comparison to the dumb charging approach. The ability of smart charging approach towards sensing the load across distribution transformer before allowing the BEV charging was found effective in reducing the transformer loading. Dumb charging on the

other hand was found incapable of sensing the transformer load before allowing the BEV charging, hence was found causing voltage dips (raising with distance of households from the DT).

6.2 Future work

The work carried out in this PhD project was based on objectives related to obtaining the ‘maximum optimal asset utilization’ across overhead transmission lines and distribution transformers. The results obtained in Chapter 2, Chapter 3, Chapter 4 and Chapter 5 of the thesis can be extended to address the issues that were left unaddressed. Hence, the work presented in this thesis is extendable to carry out the future research work. A brief summary of possible future contributions with respect to the research questions as addressed in the individual manuscripts is mentioned as below:

Future work in **Chapter 2** can be extended towards applying the ETC technique for a combined asset management model involving the power transformers and overhead lines. In result, the controlled power flow during power injection and power distribution can be used to obtain the optimal capacity limits without changing the relay settings.

Future work in **Chapter 3** can be extended towards involving the real weather conditions from field sensors, placed at optimal locations across OHLs based on the proposed technique to identify the set of critical spans under each loading interval. The work can also consider the impact of weather parameters on the line loadings, particularly when weather dynamics are faster and more transient in nature than line loading dynamics.

Future work in **Chapter 4** can be extended to involve the application of distributed generation and fast EV charging. To improve condition monitoring, dissolved gas analysis (DGA) can be incorporated in the proposed model to provide condition monitoring under maximum loading based capacity utilization of the distribution transformers.

Future work in **Chapter 5** can be extended to consider BEV charging impact in the real-networks, where the combined impact from DTs, feeders, and cables can be carried out to validate the effectiveness of an integrated demand response and smart charging based approach. Additionally, the distributed energy resources can be incorporated in the integrated network, where with the help of optimization and machine-learning techniques, optimum results can be obtained to suit the requirements of prosumers, aggregators and distribution network operators.